

Reservoir compaction in shallow gas reservoirs

The impact of production-induced reservoir compaction on the recovery of gas from shallow reservoirs

Marloes Jongerius

Technische Universiteit Delft

RESERVOIR COMPACTION IN SHALLOW GAS RESERVOIRS

THE IMPACT OF PRODUCTION-INDUCED
RESERVOIR COMPACTION ON THE RECOVERY OF GAS FROM SHALLOW RESERVOIRS

by

Marloes Jongerius

in partial fulfillment of the requirements for the degree of

Master of Science
in Petroleum Engineering and Geoscience

at the Delft University of Technology,
to be defended publicly on Tuesday September 15, 2016 at 09:30 AM.

Supervisor:	Prof. dr. ir. J. D. Jansen,	TU Delft
Thesis committee:	Dr. A. Barnhoorn,	TU Delft
	Dr. H.A. Abels	TU Delft
	Dr. M. Gutierrez-Neri	EBN

ABSTRACT

Compaction occurs in many consolidated hydrocarbon reservoirs and is responsible for both improvement and loss of recovery. This study assesses the effects of rock compaction and the consequences on the production and recovery in unconsolidated shallow gas reservoir a topic of which little is known.

The compaction behaviour in unconsolidated to weakly-consolidated reservoirs is studied by compiling a large data set from published laboratory experiments data. Analysis of the data set indicates that the initial porosity, the pre-consolidation stress and the degree of consolidation of the reservoir formation are the main controlling parameters on the rock compressibility.

To account for compaction in unconsolidated sands, a set of equations describing plastic deformation is derived from the equations describing linear elastic compressibility. The pore volume reduction and permeability reduction calculated based on these equations tend to over predict the effects of compaction when compared to measured data. Empirical relationships are derived for pore volume and permeability reduction based on compaction behaviour trends which can be applied to unconsolidated reservoirs.

With these derived empirical trends compaction is simulated on shallow gas reservoirs. A simplified reservoir model is built capturing the main characteristic of shallow gas reservoirs in the Netherlands. The integration of the effects of compaction within the simulations is done by incorporating the range observed in the pressure-dependent rock characteristics i.e. pore volume (porosity) and permeability. The assumption of a constant reservoir compressibility leads to an uncertainty in the recovery factor of up to 10% when compared to the pressure-dependent assumption.

Two effects of pore volume reduction are visible in P/Z plots (mass balance plots) of compaction-sensitive gas reservoirs: 1) the P/Z line decreases more gradually than when no pore volume reduction occurs, 2) P/Z line deflects downwards with ongoing production and deviates from the straight-line. The higher the pore volume reduction, the more pronounced is this bending of the P/Z -line. The effect of permeability reduction is not visible on the shape of the P/Z plot.

In all cases, it is observed that the effect of reservoir compaction is, with respect to the no-compaction case, positive for the recovery of gas. The predicted recoveries show differences which can amount up to 20% additional recovery. For a typical shallow gas reservoir of 1 BCM, these difference translate to a potential underestimation of 0.2 Bcm of gas produced.

ACKNOWLEDGMENTS

This research would not have been possible without the help of others, therefore I would like to thank those who contributed to my research process.

First of all I would like to thank EBN for providing the data, software applications, office facilities and a great working environment. From EBN I would like to thank especially my supervisor Mariene for helping me getting acquainted with the problem and your support, suggestions and feedback. Further I would like to thank Marc for his help and valuable explanations on geomechanics.

From the Delft University of Technology I would like to thank my supervisors Jan Dirk Jansen and Auke Barnhoorn for their time, valuable feedback and suggestions.

Furthermore I would like to thank Schlumberger for the availability of the software and the software support on every detailed question.

Finally, I would like to give a special thanks to my colleague-interns. For the listening-ear, the feedback and the good laughs we had. And last but not least I would like to thank my family and friends for their support throughout my study period.

CONTENTS

1	Introduction	1
1.1	Dutch shallow gas reservoirs	2
1.2	Problem statement	2
1.3	Study goals	3
1.4	Workflow	3
2	Theoretical background	5
2.1	Gas behavior	5
2.2	Reservoir rock compaction	6
2.2.1	Stress redistribution	6
2.2.2	Rock Compressibility	7
2.2.3	Geomechanical behaviour	7
2.2.4	Consolidated sandstone	8
2.2.5	Weakly consolidated to unconsolidated sandstone	9
2.2.6	Uncertainties in experimental rock compaction data	10
2.2.7	Geological characteristics	10
2.2.8	Impact on the flow parameters	12
2.3	Reservoir Simulation	13
3	Rock Compaction database	15
3.1	Methodology	15
3.1.1	Data conversion	16
3.1.2	Assumptions	16
3.1.3	Equations	17
3.1.4	Stress regime	22
3.2	Results	24
3.2.1	Rock compaction trends	24
3.2.2	Impact of data conversion: Experimental & Calculated data	26
3.2.3	Trends observed related to geological characteristics	28
3.3	Discussion	39
4	Reservoir Simulations	45
4.1	Methodology	45
4.1.1	Reservoir Characterization: Dutch Shallow gas fields	45
4.1.2	Model Definition	46
4.1.3	Simulation	47
4.2	Results	51
4.2.1	Rock compaction trends	51
4.2.2	Impact of data conversion: Experimental & Calculated data	54
4.2.3	Pressure-dependent pore compressibility	56
4.2.4	Trends related to geological characteristics	57
4.3	Discussion	59
5	Recommendations	65
6	Conclusions	67
A	Appendix: Glossary	69
B	Appendix: Rock compaction database	71
C	Appendix: Unit conversion	75

D Appendix: Reservoir simulation: Trend detail	77
Bibliography	81

1

INTRODUCTION

Production-induced compaction occurs in many reservoirs and it is responsible for both improvement and/or loss of recovery and a number of field operations problems [11] [6] [12]. Since a number of years multiple shallow gas fields are produced in the Netherlands and various fields pending under development (figure 1.1). Recent analysis carried out in one of these shallow gas fields show a change in reservoir performance that could not be explained by only taking into account the standard production mechanisms. The observed change in performance could be the result of reservoir compaction, leading potentially to an uncertainty in the ultimate recovery with respect to the initial approximations. Compaction in unconsolidated gas reservoirs has been loosely described in literature as a potential source of compaction drive due to pore volume reduction, but could also be a potential source of productivity decline mainly due to permeability reduction.

Shallow gas reservoirs are, in this study, defined as gas reservoirs in weakly to unconsolidated, low pressure sandstone formations [1]. These reservoirs produce in general from formations at a depth of 400-800 mbsl. Due to the unconventional shallow depth of these reservoirs, the gas in the reservoir is at low temperature and pressure. Where the rock compressibility is in conventional reservoirs a factor 10^3 lower than the gas compressibility and thus has a negligible impact, however for the highly compressible weakly to unconsolidated formations the rock compressibility cannot be neglected (figure 1.2).

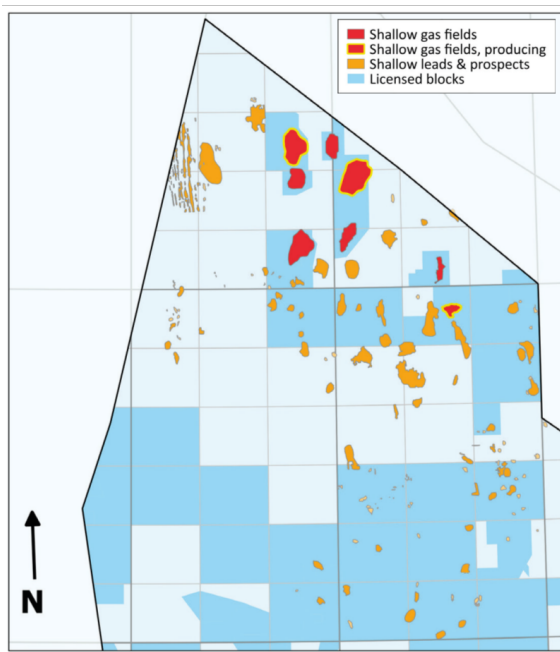


Figure 1.1: Shallow gas leads, prospects and field in the Northern Dutch offshore [1]

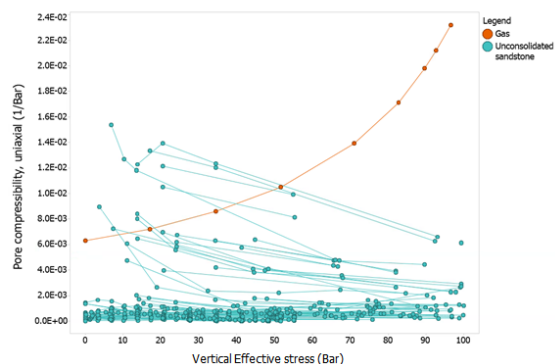


Figure 1.2: Gas compressibility (orange) compared to the pore compressibility of weakly to unconsolidated sandstone of all samples used in the data set

1.1. DUTCH SHALLOW GAS RESERVOIRS

Since the early seventies the presence of shallow gas in the Dutch part of the North Sea has been recognized. The first Dutch offshore shallow gas field came on stream in 2007 [1]. Nowadays the Netherlands has multiple shallow gas fields in production and various fields pending for development. These shallow gas fields are in general located in unconsolidated Tertiary formations. The defined shallow gas leads are mainly based on bright amplitudes are caused by anomalous acoustic impedance in gas bearing reservoirs. The reservoirs often consist of multiple stacked low-relief anticlinal reservoir above salt domes. The predicted recovery factor for these reservoirs (ranging from 1-8 Bcm of gas-initially-in-place) is around 60-80% mainly depending on the moment of water breakthrough [1].

1.2. PROBLEM STATEMENT

A decline of fluid pressure, driven by the withdrawal of fluid from a reservoir, results in a change in volume of both the reservoir fluids and the reservoir rock [13]. The production-induced decrease of the pore pressures triggers a stress redistribution, in which the effective stresses increases. The increase of effective stresses in a depleting sandstone reservoir triggers a combination of elastic and inelastic deformation mechanisms, and affects the volume of the reservoir rock [14].

In the first stage of pressure redistribution the increasing effective stresses work in weakly to unconsolidated sandstone, as a cementing material by compressing the sand grains with each other (in absence of cementing material) [15]. With on-going production and a pressure decrease, the effective stress on the grains increases until the yield strength is exceeded and grain movement is initiated. The sand grains will hold each other by their apparent cohesion (friction), until the effective stress tensor overcomes the frictional forces at the critical pressure [15], which is the onset of plastic deformation [7]. The two main mechanisms of deformation in a granular medium are: 1) re-arrangement of the position and orientation of the grains relative to each other by slippage and rotation of the grains, 2) deformation of the grains themselves [16]. The grain movement is associated with an increase in the pore compressibility of the material [17]. This 'repacking' can induce, mostly irrecoverable, reductions in porosity and permeability [6].

Unconsolidated sandstones have unique uncertainties in the material behaviour [9]. Another difficulty lies in the translation from the experimental rock compressibility data to in-situ rock compressibility [18]. Little is known about the error resulting from simplifications used in compaction experiments and the data conversion for weakly to unconsolidated sandstone. It is often assumed that compressibility is fairly constant with stress. However the compressibility of a reservoir is varied with stress and rock type and thus will change as fluids are withdrawn from the reservoir and the effective stresses are increased [17] [19].

The volume reduction of the bulk rock of a reservoir is accompanied by a change in the pore volume of the rock. Due to the decrease of available pore space for an equal gas volume, the gas present in the pore volume will be compressed. As pressure is an indicator for potential energy available to drive the flow towards the well, the gas is here driven by the compaction process towards the well (compaction drive). This makes that a proper integration of rock compressibility is important for reserves estimation, determination of drive energies and overall reservoir development plans [19]. To date no proper integration of the compaction-related reservoir characteristics is done for unconsolidated reservoirs, as often the only rock mechanical data included in a reservoir simulator is the rock compressibility [20]. For a proper coupling of fluid-flow simulation and the geomechanical behavior all relevant rock characteristics should be incorporated and updated during the simulation. Incorporating both production-induced porosity and permeability changes to a simple simulation model can result in significant variations in the predicted reservoir productivity [6].

The phenomenon of rock compaction in unconsolidated reservoirs and the impact on the relevant rock characteristics is not yet fully understood, neither what the consequences may be for gas recovery. The authors whom studied the compressibility of weakly to unconsolidated sandstone often did not perform reservoir simulations. The impact of a proper integration of the variable compressibility and the relevant characteristics on production from the compacting reservoir is thus not assessed. Neither is the impact of a lack of knowledge on the relevant processes and characteristics is not understood.

1.3. STUDY GOALS

The objective of this study is to assess and evaluate the potential effect (positive or detrimental) of reservoir compaction in the ultimate recovery in shallow gas reservoirs. Increased knowledge on the main parameters controlling the reservoir compaction will lead to better understanding of the potential effects. Furthermore the impact of rock compaction on the reservoir performance is not yet fully understood. A variation in ultimate recovery can have a significant impact on the development decision for these small fields.

The study objectives are as follows:

- To understand the relevant mechanism occurring during compaction in weakly to unconsolidated sandstone and to define the rock characteristics controlling rock compaction
- To gain better insight into the effects of rock compaction on the porosity and permeability of unconsolidated shallow reservoirs
- To assess the impact of reservoir compaction on the recovery of gas from shallow reservoirs
- To to better understand the effects of reservoir compaction during field production
- To assess the uncertainty related to (a lack of) data on rock compressibility in shallow gas reservoirs

1.4. WORKFLOW

This study is divided into two parts. To assess the significance of compaction in the production of a weakly to unconsolidated reservoir, a good knowledge of the potential formation compressibility is required [6]. The lack of data on the Dutch shallow unconsolidated gas reservoirs limits the incorporation of the effects of compaction. To get a better understanding of compaction behaviour in weakly to unconsolidated reservoirs and to assess the potential formation compressibility of the Dutch shallow gas reservoirs, a literature-based rock compaction data set is gathered in which the experimental results of various authors are compared and analyzed. For the analysis a number of subsets based on trends of compaction behaviour within the dataset or geological characteristics, are defined.

A numerical reservoir simulator has been used to study the effect of rock compaction on the production behaviour of a weakly to unconsolidated shallow gas reservoir. A simplified reservoir model has been constructed in Petrel. The square tank model is based on a simplified representation of an average Dutch shallow gas reservoir. The skeleton of the generic model is filled with the reservoir characteristics as defined based on the simplified representation. The dataset and defined subsets form the basis of the reservoir simulations. Scenario's based on the defined trends on the pressure-dependent rock characteristics (pore volume and permeability) are the input of the simulations. The output of these scenarios is represented by the production rate, the reservoir pressure, the cumulative gas production and the material balance based plot of the pressure over the gas compressibility coefficient (p/z) versus the cumulative gas production (G_p). Eclipse 100 is used for the reservoir simulations.

2

THEORETICAL BACKGROUND

2.1. GAS BEHAVIOR

Due to the shallow depth of the shallow gas reservoirs, the gas in the reservoir is at relative low temperature and pressure. The most accurate way to determine the relevant properties of a gas sample is by a laboratory analysis. However in the absence of this data, one can use theoretical correlations for an estimation of the fluid properties [10].

The behaviour of an ideal gas can be described by an Equation of State, describing the relation between the occupied volume by the gas and the pressure and temperature [10]. The assumption of ideal behaviour is not valid for gasses at pressures and temperatures that deviate from ideal of standard conditions, a correction then must be made to account for the deviation from ideal behaviour [21]. This could be done by including a 'z factor', the compressibility factor, which corrects the ideal gas EOS, and allows for descriptions of a real gas [10]. At low pressure and the conditions on ideal gas behaviour are more likely to be met; the molecules are relatively far apart. At low pressures the compressibility factor thus can be approached by a value of 1 [21].

The equation of state for a gas can be given by [22]:

$$(2.1) \quad pV = znRT$$

The gas compressibility (C_g) can be given by [22]:

$$(2.2) \quad C_g = \frac{1}{p} - \frac{1}{z} \frac{\delta z}{\delta p}$$

Where p is the pressure of the gas (Pa), V is the volume occupied by the gas (m^3), z is the compressibility factor (-), n is the amount of substance of gas, R is the universal gas constant ($J \cdot mol \cdot K^{-1}$) and T is the absolute temperature (K).

Flow in a reservoir is driven by the pressure difference available over the flow path. A certain amount of energy is required to overcome the resistance to flow through the rock, which is manifested in a pressure decrease in the direction of flow towards the well [21]. This pressure drop depends on the gas flow rate, fluid properties and rock properties [21]. To be able to predict the production rate, the amount of gas initially in place (GIIP) and how much of it can be recovered (i.e. the recovery factor), requires the ability to relate volumes of gas existing in the reservoir to reservoir pressure [21]. In a closed reservoir, flow occurs due to expansion of the fluid [21]. In a gas reservoir this is the main driving mechanism of flow towards the wellbore.

2.2. RESERVOIR ROCK COMPACTION

Reservoir compaction related to the withdrawal of fluid from a reservoir occurs in most reservoirs during exploitation [23][13]. Compaction is stated as the process in which the compressive strength of the rock is exceeded and irreversible plastic deformation occurs [18][24]. The term “compressibility” is usually reserved for poroelastic, reversible deformation [24], but is as well used to quantify the relationship between the pressure exerted on a body and its resulting change in its volume (elastic and plastic) [25].

2.2.1. STRESS REDISTRIBUTION

In the period after formation of the reservoir, partitioning of the overburden stress will have attained a metastable equilibrium the related processes of deformation of the rock structure and the generation of pressures in the pore fluid [2][8]. In this equilibrium the total overburden is carried partly by the reservoir rock and partly by the reservoir pore (fluid) pressure (figure 2.1). The pore fluid is acting in the pore spaces between the mineral grains and the rock structure and presses out against the overburden (vertical) and the horizontal reservoir stress [19][16].

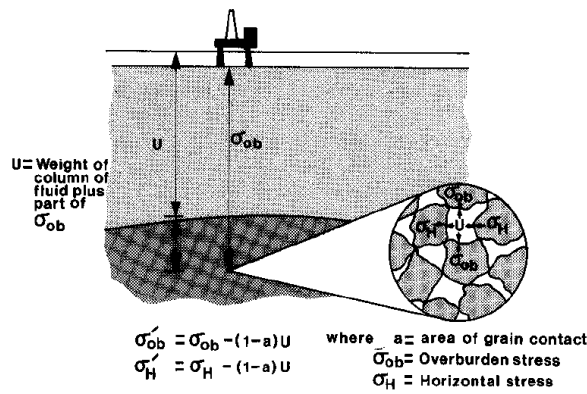


Figure 2.1: Stress distribution within a hydrocarbon reservoir at hydrostatic pressure [2]

During production of the reservoir fluids a certain amount of energy is necessary to overcome the resistance to flow through the rock [21]. This process can cause a considerable drop of the reservoir pressure, in the direction of flow toward the well. [16][21]. Meanwhile, the weight of the overburden (layers on top of the reservoir) remains constant. Consequently a larger part of this overburden load has to be carried by the rock skeleton [16]. The stress on the rock structure (i.e. the effective stresses) increases [20]. This stress re-distribution could induce significant compaction of the reservoir [26] by triggering a combination of elastic and inelastic deformation mechanisms such as elastic (Hertzian) grain contact spreading, micro-crack growth and closure, cement breakage, grain rotation and sliding, as well as crystal plastic deformation in clay and mica grains [14]. Their relative importance depends on micro structure, grain and fluid composition, porosity, stress, stress path (loading history), pore pressure and temperature [14]. The reservoir rock will be compressed (compacted) until a new equilibrium is reached [16].

The producing reservoir remains physically connected to the rock surrounding it [14]. During production, a the portion of the overburden weight is transferred from the reservoir pore fluid to the reservoir rock matrix and a part is transferred to the geological media laterally exterior to the reservoir ('sideburden'). The ability to transfer the overburden load to the sideburden depends on the strength, or rigidity, of the overburden. [27] However, an often used assumption to approximate the stress path followed by a reservoir, in the mechanical description of deformation, is the assumption of uni-axial strain during deformation. As the fluids are withdrawn from the reservoir, it is assumed to only compact one-dimensional in the vertical direction [28]. This assumption is valid if the vertical extent of the reservoir is small compared to its lateral extent [19]. Although field observations have confirmed that stress state evolutions could be more complex and rarely satisfy purely uni-axial conditions [7], it is stated to be a useful assumptions in simplifying the problem. It allows for the approach of the rock properties by uni-axial lab measurements.

2.2.2. ROCK COMPRESSIBILITY

The amount of compression as result of the pressure redistribution within the reservoir may be expressed in the quantity names 'Compressibility' which represent the change in volume per unit pressure change. The compressibility expresses the easiness of the material to deform as a result of a change in the stress equilibrium.

Compressibility (C) [25]:

$$(2.3) \quad C = -\frac{1}{V} \frac{dV}{dP}$$

Since both pore and bulk volume are varied during compression, there are two different compressibility's associated with a porous rock.

Pore compressibility (C_p) [25]:

$$(2.4) \quad C_p = -\frac{1}{V_p} \frac{dV_p}{dP}$$

Bulk compressibility (C_b) [25]:

$$(2.5) \quad C_b = -\frac{1}{V_b} \frac{dV_b}{dP}$$

Where V_p is the pore rock volume (m^3) and V_b is the bulk rock volume (m^3).

2.2.3. GEOMECHANICAL BEHAVIOUR

A model describing the geomechanical behaviour of the reservoir is useful for better understanding and prediction of compaction in a reservoir, during production.

The effective stress development in a depleting sandstone reservoir triggers a combination of elastic and inelastic deformation mechanisms. Where inelastic deformation can be time-independent (plastic) or time-dependent (viscous), In most cases a combination of both processes occur at the same time [14]. The deformation process is often approached by only describing the elastic behavior of the reservoir ('Poroelastic theory'). In which the elastic contact theory is used to calculate the approach of the spheres to each other as pressure is applied; this Hertzian contact model is valid only for the elastic range [29]. The Poroelastic theory is a simplification of the real deformational behavior and does not fully describe the process. A shortcoming of Poroelastic theory is that most depleting reservoirs undergo both elastic and inelastic deformation [6]. Furthermore it cannot explain the compaction behavior beyond the critical pressure; the Poroelastic theory fails to take into consideration the grain rotation and grain crushing mechanisms [29].

A combination of elastic and plastic mechanisms and associated responses is gathered under the 'Elasto-Plastic model', and gives a more complete description of the relevant mechanism. Often the current stress regime in the reservoir is lower than the maximum experienced during the geological history (the preconsolidation stress), the initial deformation will then be dominated by elastic behaviour with a clear transition to plastic deformation. In reservoirs for which the initial stress state is close to or at the preconsolidation stress, the elastic behaviour will be absent in the laboratory and cannot be detected in the experimental data [23].

The transition from elastic to plastic behaviour can also be described by incorporating 'End caps' in the representation of the deformation process. End caps represent the locus of points with the same volumetric plastic strain [6]; their shape depends on the material properties and the failure criterion model chosen. If the sample is stressed beyond the end cap, inelastic deformation will occur and the sample will compact and become stronger. The "hardening" of the sample leads to an expansion of the end cap associated with the decrease in porosity [6]. Compaction and grain rearrangement (and eventually grain crushing and pore collapse) are idem the dominant deformation modes once the formation is loaded beyond the end caps [6].

There often seems to be a misunderstanding as to the complexity of compaction in unconsolidated materials [30]. As stated by Schutjens [14] inelastic deformation can be time-independent (plastic) or time-dependent (viscous), and in many cases a combination of both processes occur at the same time.

Creep (time-dependent/viscous) is often a dominant deformation mechanism, but is typically ignored in the deformation description of the material. The magnitude of the creep is the most significant in poorly sorted, clay rich unconsolidated core samples [19]. The underestimation of the influence of creep of deformation could be explained by the relaxation rates, which are quite slow on the laboratory scale, but still considerably faster than typical reservoir drawdown rates [11]. For weakly to unconsolidated sandstone reservoirs in which viscous deformation could be significant, experiments that capture this phenomenon should be used [6].

2.2.4. CONSOLIDATED SANDSTONE

Most research comprising compaction, has been done on the effects of compaction in conventional consolidated reservoirs. Compaction in unconsolidated gas reservoirs has only been loosely described in literature and is not yet fully understood.

According to Yale [19] ‘consolidated sandstones have undergone significant diagenesis and have their grains well cemented and dropping a sample on the floor does not cause it to disintegrate’. The unconsolidated character of a sample is by Yale [19] described as ‘samples as those which fall apart completely after drying and/or cleaning with porosities between 27% and 40%’. But there is no clear overruling distinction between the concepts of unconsolidated and consolidated rocks. There appears to be a “transition zone” in compressibility’s between unconsolidated and consolidated rocks as evidenced by measurements made in numerous laboratory studies, where rock is found to be somewhat cemented intergranularly, but yields its elastic properties early in any loading cycle [31].

The difference between deformation of consolidated and unconsolidated materials is in general within the cement present in the consolidated rock. In a natural consolidated sandstone, there are both grain-grain and grain-intergranular material-grain contacts (figure 2.2) [32], where in a purely unconsolidated material only grain-grain contacts are present. So as the degree of cementation decreases, there is a gradual transition in the deformation behavior from elastic to plastic associated with the gradual transition in the character of the grain contacts [13].

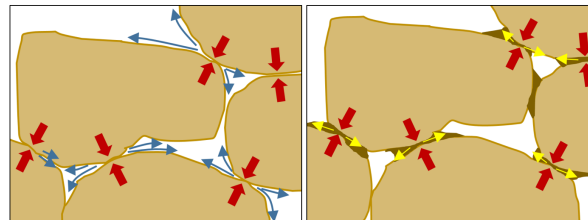


Figure 2.2: Right: Stress distribution in a compacting unconsolidated sandstone reservoir, where the deformation processes are controlled by the frictional forces. Left: Compacting consolidated sandstone where the cement and long grain-to-grain contacts control the deformation processes.

The deformation at these two kind of contacts is not the same for a given pressure on the rock [32]. At the beginning of the deformation the effective stress is firmly located in the cementation resistance [2]. As is also confirmed by Dvorkin [33], whom found that intergranular cement may strongly affect stress distribution at the grain contacts. Where for an unconsolidated material it could be assumed that mean pressure at the time of pore collapse coincides with pre-consolidation pressure [15]. The intergranular cementation can delay pore collapse to some extent to a critical pressure above the pre-consolidation pressure. Due to this characteristic the stress-strain curve is found to noticeably differ from that for the non-cemented aggregate with solely grain-to-grain contact (figure 2.3) [33]. As the consolidated material progressively fails, the effective stress it is transferred directly to frictional resistance, or the pore pressure increases [2]. Eventually, the frictional term becomes dominant [2] and the deformational mechanism becomes roughly equal to deformational processes in unconsolidated material.

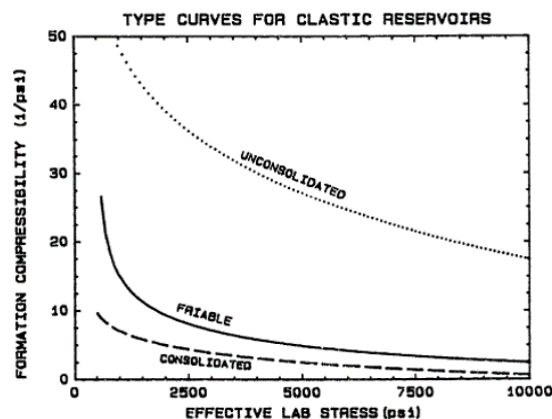


Figure 2.3: Generalized curves showing the order of difference between the rock compressibility of consolidated and unconsolidated sandstone [3]

2.2.5. WEAKLY CONSOLIDATED TO UNCONSOLIDATED SANDSTONE

The inelastic properties of the reservoir are especially important for unconsolidated rock [6]. As stated before the consolidated material, in which the matrix structure is well defined, cemented and continuous, is better prepared to support the overburden than the one that is loosely sorted, non-cemented, and non-continuous (unconsolidated) [31]. The unconsolidated reservoirs thus behave differently than their well-cemented counterpart [6].

Pressure depletion associated with hydrocarbon production rapidly induces large strain deformational behavior in unconsolidated materials [6][28]. Once the increasing effective stresses reaches the mechanical failure limit (critical pressure), plastic deformation such as grain rearrangement (and eventually grain crushing and pore collapse) occurs.

In the first stage of pressure distribution the confining pressure works as a cementing material by compressing the sand grain to each other (in absence of cementing material). Upon contact, sand grains will hold each other by their apparent cohesion (friction) [15]. If the shear force at the contact point (a component of the increasing effective stress) exceeds the maximum friction force [16] sliding starts to occur at the contact points (grain-grain contact). The mechanical compaction for low stresses in a weakly to unconsolidated medium mainly results from slippage and rotation of grains [16], which change their position and orientation but not their shape [30][9]. Due to the changes or orientation and position of individual grains, the material could be packed into a different configuration [17]. The repacking can induce marked reductions in porosity and permeability, which are mostly irrecoverable [6].

There is a lack of studies on the stability and possible stages and/or configurations as can be found in grain packings. Although Weltje [34](2011) states that a sphere is considered stable if it has at least three contacting spheres and the plane through the center points of those spheres lies below its center of mass. Further it is necessary that the contacting spheres are evenly spaced around its center.

An assumption often made is that pore compressibility is fairly constant with stress. Though the compressibility of a reservoir is varying with pressure and rock type and thus will continually change as fluids are withdrawn and the grain pressure increases [17][19]. As the effective stress increases and the yield strength is exceeded, the pore volume compressibility increases [11]. With a further increases in applied stress, the compressibility peaks at a relatively high value and then begins to diminish. The sample stiffens, this hardening results from both the rearrangement in the grain packing and the gradual deformation of squeezing of ductile material between hard grains and into the intergranular space. As the sample stiffens it regains the ability to support additional shear stress and there is a gradual change from deformation accommodated by grain boundary sliding, to elastic straining of the individual grains [2] and more of the load is now taken up by the rock skeleton [11][2]. The related rate of pore space reduction reaches likewise its maximum during the transition from the wholly plastic behavior to this stiffening phase of the deformation [2]. As the pore space substantially is decreased, this is accompanied by closure of the pore throats as the grain packing is reconfigured, resulting in an overall decrease in permeability [2].

2.2.6. UNCERTAINTIES IN EXPERIMENTAL ROCK COMPACTION DATA

The unconsolidated character of the studied shallow gas reservoirs creates unique uncertainties in experimental rock mechanics data and the parameters needed in reservoir simulation [9]. The most important uncertainties that should be taken into account in assessing experimental data on weakly to unconsolidated sandstone samples are briefly discussed:

I. Core recovery

Laboratory measurements are sensitive to grain disturbance, originated during sample recovering [5]. The experimentally obtained compressibility's are likely to be lower than actual in-situ rock compressibility values. The error caused by the recovering of the core/drilling is unclear and cannot be defined.

II. Testing method

The various testing methods, used to determine the effect of an increase in effective stress on the rock characteristics, all have their own set of assumptions and according errors. In comparing different compressibility tests and converting them to subsurface rates, there will be an uncertainty as result of the chosen testing method.

For repeated loading tests the dependency of the compressibility on previous loading cycles should be taken into account. First-cycle compaction is always large and the samples always exhibit mechanical hysteresis. In the second and subsequent cycles, hysteresis is almost eliminated and compaction of the samples is nearly reversible [9]. For the studied very weakly consolidated or unconsolidated sandstone the uniaxial compressibility measured during the first and the second laboratory loading cycle can differ by a factor of five [16]. Further, different rates of applied stresses (laboratory as opposed to geologic settings) cause materials to compact differently. In the subsurface the compaction occurs in a creep relaxed state, whereas in the laboratory strains accumulate, which is thought to result in additional grain breakage [30]. For example creep associated with the deformation of unconsolidated rocks can cause compressibility tests run at high rates of pressure increase to be invalid [19].

III. Assumptions in formula

There is not one valid method on translation of experimental rock mechanics data (measured as function of effective stress) to in-situ data. For each method assumptions are done to be able to calculate various properties. Little is known about the errors resulting from this simplifications [18].

IV. Core characteristics

The core characteristics are often taken in a range or are determined in a different way per article.

2.2.7. GEOLOGICAL CHARACTERISTICS

Several studies can be found in literature that aim to compare samples of different unconsolidated sandstones to define the influence of certain characteristics on compressibility.

The variations in rock compressibility can be large and are mainly controlled by variations in geological age and sand morphology [11]. Which can be specified as the framework mineralogy, clay content, texture (grain size and sorting), stress history and incipient overgrowth cements (figure 2.4) [4] [24].

Stress History / Pre-consolidation stress

The burial history, and according stress history is a main control on the compressibility [4]. In general, for sands of similar mineralogy and texture, as maximum effective stress (i.e. the preconsolidation stress) increases, the magnitude of the compressibility curve decreases and the peak compressibility occurs at higher depletion stress [4].

Cement / Level of Consolidation

The rigidity of the framework is controlled by the elastic response of the material, as caused by the elastic characteristics of the cement. As mentioned, overgrowth cements are stiffening the sand framework [4]. Incipient overgrowth cement, even when present in very small volumes, enhance the rigidity of the framework [4].

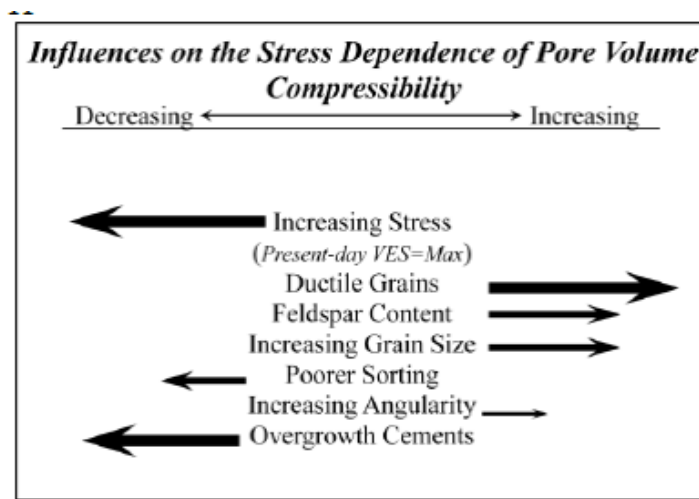


Figure 2.4: Important controls on the pore compressibility of unconsolidated sandstone [4].

Grain size

A strong correlation between the degree of sorting (range of present grain sizes) and compressibility can be found [19]. For an unimodal sorting, an increase in grain size, gives an increase in the maximum compressibility [4][30]. The increase in grain size implies an increase of the effects of friction and adhesion [] (Weltje, 2013), as can be explained by the correlation between grain size and grain shape. Related to the nature of the sediment, smaller grains are often more angular, which causes an increase in friction and it can decrease the efficiency of the stacking. A multimodal sorting gives a broadening of the compressibility peak [4].

Moreover, the effect of sorting on the variability of the flow characteristics should be recognized. The range of the residual porosity is independent of grain size for unimodal and narrow grain-size distribution (good sorting) but it depends strongly on the grain shape and grain-size distribution for multimodal grain-size distributions (poor sorting) [24]. The permeability is likewise dependent on the degree of sorting; an increase in the amount of fine/ductile grains, gives rise to a higher decrease of the flow characteristics (add: source). Grain size is of second order influence on compressibility when compared to stress history or framework mineralogy [4].

Grain shape

The shape of the grain, in particular the angularity, is of influence on the compaction process, although this effect is small [30]. With increasing control of the frictional forces in the deformational process, the role that texture plays in determining material response to increasing pressure increases [28]. However, the reduction of the pore volume and permeability could have a different dependence on the grain shape. The optimal grain configuration for a certain stress regime depends on the optimal configuration possible for a certain combination of present grain shapes.

Ductile grains

The presence of ductile grains (clay) increases the compressibility, as clay clasts are extremely soft [30] (Myers, 2014). As the volume of ductile grains increases the peak of the compressibility curve occurs at progressively lower stresses, and the magnitude of the peak compressibility increases [4].

Mineralogy

Observations as done by Fatt [32] point to a possible relation between the observed compressibility and the composition of sandstone. The elasticity of the minerals determine the elastic compressibility of the rock and where yield strength of the available minerals is controlling in the potential of grain crushing/breaking. For Feldspar or Carbonate lithic fragments it is found that the peak compressibility can be observed at a lower stress level [4][30].

Correlation

The geology related rock characteristics are not autonomous, there exists a correlation between several characteristics as all the characteristics are related to the depositional environment, the sediment source and the time of burial.

The time of burial incorporates the range of possible preconsolidation stresses as a rock could have experienced. Sandstone with a long period of burial and a high preconsolidation stress is often characterized by predominantly long grain contacts; and has little, if any, load-bearing ductile material [11]. The relative low initial compressibility of this samples, continues to decrease monotonically with increasing effective stress. Relative younger sand, typically still has point-grain contacts instead of long grain contacts, and still has a significant amount of loadbearing ductile material, which results in a somewhat higher initial compressibility. For this rock type softening continues with increasing effective stress to some maximum value of compressibility, which may be several times larger than the initial value of either end member [11].

2.2.8. IMPACT ON THE FLOW PARAMETERS

Understanding the relation between the deformational mechanisms and the associated change in rock properties is important for the understanding and prediction of the production behaviour of the compacting reservoir and the ultimate recovery. Furthermore from a reservoir management point of view, compaction-induced changes in porosity and permeability need to be understood and modeled in order to optimize the drilling, completion and production strategy as a function of time and reservoir fluid pressure [14].

Porosity

As defined compaction is the process in which the compressive strength of the rock is exceeded and plastic deformation occurs, this process results in irreversible reduction of porosity and permeability [23]. It is often attempted to predict the relation between deformation and the resulting porosity reduction. A number of authors developed a method to predicting porosity from other rock characteristics such as the grain-size distribution or the rock compressibility, however these attempts had only limited success [9] [24] [6] [35].

It has been found that the rate of pore space reduction reaches its maximum during the transition from plastic behavior to this stiffening phase of deformation [2].

Permeability

More than porosity, permeability is a representative parameter for the ability of the material to transmit fluids. For high-permeability weakly cemented sandstone, a large reduction in permeability is triggered by the onset of shear-enhanced compaction once the sample is loaded beyond the critical pressure, the sample moves from the elastic domain into the plastic deformation domain [6][36]. During the transition from plastic behavior to the stiffening phase of deformation, the pore space is substantially decreased, accompanied by closure of the pore throats, blocking some of the pathways for fluid migration, resulting in an overall decrease in permeability [2][6].

The change in permeability as a function of pressure does not follow the simple trend observed for the porosity reduction; a small change in the porosity can be accompanied by a large decrease in permeability [6][9]. The reduction of permeability can be as high as 70% of the original permeability for a 10% change in porosity [6].

An empirical porosity-permeability relation to apply i.e. on well log data is often derived from core data representing the 'average' relation between porosity and permeability. But since unconsolidated and friable cores are expensive to retrieve and test, it is desirable to have an acceptable correlation between porosity and permeability [9]. Several attempts are done in literature, all with their own advantages and disadvantages.

A well-known, standard empirical relation between porosity and permeability for unconsolidated sand is given by Kozeny-Carman [37]. The Kozeny-Carman relation relates porosity and tortuosity to permeability. A relation exists between tortuosity variations in different samples which correlate with variations in sediment source (grain shape, roundness, surface texture and orientation), geological age and the depth of burial [11]. Incorporating this information within the Carman-Kozeny relation helps in predicting the permeability for unknown formations. However, as plastic deformation begins, permeability reduction is more drastic than the Kozeny-Carman relationship predicts [6].

2.3. RESERVOIR SIMULATION

The rate and degree of production-induced pore-pressure reduction depends on the permeability distribution, the location of the production wells, and the production rate [13]. The pore pressure dissipation is highly dependent on rock compressibility, dissipation of the pore pressure is faster for more rigid rocks than for more compressible rocks [20]. Where on the other hand, as stated by Fatt [32], for low pressures are the compressibility's are rather sensitive function of pressure.

The total compressibility of the system (C_t) is described by [10]:

$$(2.6) \quad C_t = C_g + C_p$$

The produced gas volume (at reservoir conditions) (ΔV_{prod}) then can be expressed as [25]:

$$(2.7) \quad \Delta V_{prod} = -V_p(C_g + C_p) \cdot \Delta P$$

For unconsolidated reservoirs a proper integration of the formation compressibility is important for an accurate estimation of the reserves, the determination of drive energies, and the overall reservoir development plan [19]. The usage of compressibility values in the mass balance equation (MBE) which are significantly lower than those which exist in the reservoir could for example suggest a strong water drive where one does not exist [19].

An accurate simulation model should include a integration of the formation compressibility [38]. Moreover, for a proper coupling of fluid-flow simulation and the geomechanical behavior all relevant rock characteristics should be incorporated and updated during the simulation[20]. Incorporation of both production-induced porosity and permeability variations to a simple simulation model can result in significant variations in the predicted reservoir productivity [6]. Coupled simulation shows that plastic deformation significantly increases the compaction drive energy of the reservoir due to the extra drive energy on the pore structure [3]. The effects of the decrease in permeability, especially near the wellbore in high drawdown wells, are often not modelled in standard reservoir simulation [3].

3

ROCK COMPACTION DATABASE

3.1. METHODOLOGY

To assess the significance of reservoir compaction in the production history of a reservoir, a good knowledge of the formation compressibility is required [14]. A literature-based rock compaction data set has been created with data from 92 oedometer tests on 53 samples, 70 axial compression tests on 35 samples and 137 uniaxial confined compression tests on 100 samples reported in literature. A table with all the datasets used can be found in Appendix B.

The experimental data is utilized to examine and clarify the effect of compaction on unconsolidated sandstone. As Mattax [9] stated; it seems desirable to have readily available a complete set of test results for comparison with other data or to use in the absence of formation data. The studied literature data, consists mainly of unconsolidated sample, retrieved from depths ranging from four kilometer to subsurface.

The data as reported in literature, is retrieved by usage of a digital graph digitizer [39]. This process allows data recovery from figures of a diverse character. The variable nature of the data set gives need to normalization of the data set before on is able to analyze and examine the data. The defined equations are used to convert the data set to one format. The chosen quantities are the vertical effective stress (Bar), the pore volume compressibility (1/Bar), the relative change in pore volume (-) and the relative change in permeability (-).

The variable nature of the data set gives also difficulties in normalization of the data set. The sample recovering of an unconsolidated sample is subject to difficulties due to the unstable nature of the sample and gives rise to an uncertainty in the experimental data as is presented in literature. This uncertainty should be taken into account when the compaction behaviour of the different samples are compared. Further, the experimental data on the compressibility of the samples comes from both oedometer tests and triaxial tests. In the oedometer test the sample is subjected to laterally constrained vertical loading. In the triaxial test the sample is subjected to equal all-around pressure [25]; the data should be corrected for the impact of the different stress paths on the sample.

A number of subsets, based on trends of compaction behaviour within the dataset or geological characteristics, is formed. The examination of the data set is done with the help of analysis software (Spotfire). It is aimed to clarify with these subsets the geological processes enhancing compaction and trends describing compaction behaviour.

3.1.1. DATA CONVERSION

Conversion of the data is necessary to incorporate the literature reported data of various nature into a database with one format for the reported quantities. This was done with the help of the following equations. The equations are derived from equations describing linear elastic behaviour, where any of the pore volume compressibility could be determined in the laboratory and the equations can be used to determine the required parameter. To define the equations for the unconsolidated plastic behaviour, assumptions are made. Plasticity will result in other volumetric behaviour than poro-elastic theory predicts based on macroscopic strain measurements. However, here it is assumed that the equations are valid to describe the behaviour in shallow (low effective stresses) unconsolidated reservoirs.

The reported quantities to represent the deformation as a result of compression are: strain (volumetric and axial), porosity, permeability, bulk compressibility (uniaxial and triaxial) and pore compressibility (uniaxial and triaxial). For plastic behaviour one should input a table of pore volume changes versus the reservoir pressure. This makes it necessary to determine the change in pore volume reduction and the change in permeability reduction for each of the samples. The equations are ordered based on the following workflow, where for each quantity various formula are presented.

- 1) The stresses and according effective stresses in the reservoir are determined, to determine the range of vertical effective stresses that are representative for the studied reservoir.
- 2) The standard input of a reservoir simulator is the pore volume compressibility. Based on the assumption of uniaxial strain the uniaxial pore volume compressibility is required.
- 3) The pore volume variation is used to describe the effects of compaction on the rock undergoing plastic deformation.
- 4) The permeability variation describes the effect of compaction on flow through the rock.

3.1.2. ASSUMPTIONS

I. Uniaxial Strain

The reservoir deforms under uniaxial strain. This gives that during depletion of the reservoir, there will be no lateral deformation.

In reality the deformation is coupled to the stress path, but modelling shows that the assumption of uniaxial strain is a powerful tool (Hettema, 2016, personal communication) [28].

II. Biot-Willis

The grain compressibility (C_s) is negligible: a) with respect to the bulk compressibility, b) with respect to the low pressures in the reservoir (Hettema, 2016, personal communication). Within the equation of [25] the grain compressibility can be set to zero. This equation than can be simplified to:

$$\begin{aligned}
 C_s &= C_b(1 - \alpha) \\
 0 &= C_b(1 - \alpha) \\
 0 &= (1 - \alpha) \\
 \alpha &= 1
 \end{aligned}
 \tag{3.1}$$

This gives that the Biot-Willis constant (α) is approximated as 1 for an unconsolidated sandstone. The validation of this assumptions is confirmed by the results of Zoback [25] (figure 3.1).

III. Creep

The creep occurring in unconsolidated sandstones [5] is neglected since there is no consistency yet in literature on the impact and time scale at which creep is occurring.

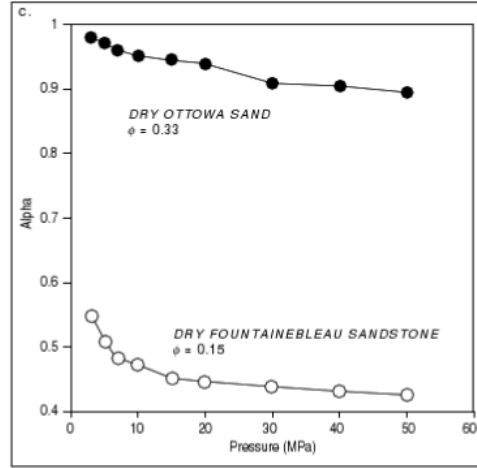


Figure 3.1: Difference in the Biot-Willis constant between consolidated and unconsolidated sand, where a clear difference can be seen between the values found for unconsolidated and consolidated sandstone. The unconsolidated sandstone has a Biot-Willis constant of approximately one [5].

3.1.3. EQUATIONS

RESERVOIR STRESSES

Stress state

The pore pressure is for the Dutch shallow gas reservoirs equal to the hydrostatic pressure. The hydrostatic pressure (P) can be determined as a function of the depth, the water density and the gravitational constant [5].

$$(3.2) \quad P = \rho_w \cdot g \cdot h$$

Where P is the pore pressure (Bar), ρ_w is the water density (kg/m^3), g is the gravitational constant ($\text{m}^3/\text{kg} \cdot \text{s}^2$) and h is the height of the water column (\approx reservoir depth) (m).

The vertical stress (S_v) is equal to the overburden stress and is given by [5]:

$$(3.3) \quad S_v = \rho_b \cdot g \cdot h$$

Where ρ_b is the bulk rock density (kg/m^3).

The horizontal stresses (S_h and S_H) are unknown, but can be approximated with the formula used to determine the stress path and horizontal effective stress (further in this study).

The mean stress represent the average stress in the reservoir and is given by [14]:

$$(3.4) \quad S_m = \frac{S_v + S_h + S_H}{3}$$

Stress path

The stress ratio (K) represents the ratio between the horizontal effective stress and the vertical effective stress [40]. With the help of the Biot-Willis assumption this can be simplified to:

$$(3.5) \quad K = \frac{\sigma_h}{\sigma_v} = \frac{S_h - P}{S_v - P}$$

Where σ_v is the vertical effective stress (Bar) and σ_h is the horizontal effective stress (Bar)

The initial stress ratio (K_0) can be rewritten as function of the Poisson ratio, where the Poisson ratio should be $0.2 < \nu < 0.3$ (Hettema, personal communication) [40]:

$$(3.6) \quad K_0 = \frac{\nu}{1 - \nu}$$

Where ν is the Poisson ratio (-).

The average stress path (γ) is defined as the mean effective stress divided by the pore pressure [40]:

$$(3.7) \quad \gamma = \frac{2}{3} \alpha (1 - K)$$

$$(3.8) \quad \gamma = \frac{2}{3} \cdot (1 - K)$$

Where α is the Biot-Willis constant (-).

Effective stress

The vertical effective stress (σ_v) represent the stress that is effectively exerted on the grain contacts; and is the difference between the vertical stress and the counteracting pore pressure [38]. With the Biot-Willis assumption ($\alpha = 1$) this can be written as:

$$(3.9) \quad \sigma_v = S_v - \alpha P$$

Since the horizontal stress is (often) not known, the initial stress ratio 3.6 can be used to determine the horizontal effective stress (σ_h):

$$(3.10) \quad \sigma_h = S_h - \alpha P$$

$$(3.11) \quad \sigma_h = K \cdot \sigma_v$$

$$(3.12) \quad \sigma_h = \frac{\nu}{1 - \nu} \cdot \sigma_v$$

The mean effective stress (σ_m) is represented by the difference between the mean stress and the pore pressure [38]. The mean effective stress can be rewritten by implementing equation 3.12 for the horizontal effective stress and equation 3.9 for the vertical effective stress:

$$(3.13) \quad \sigma_m = \frac{S_v + S_h + S_H}{3} - \alpha P$$

and since:

$$(3.14) \quad S_h = S_H$$

The mean effective stress then can be rewritten as:

$$(3.15) \quad \sigma_m = \frac{S_v + 2 \cdot S_h}{3} - \alpha P$$

$$(3.16) \quad \sigma_m = \frac{\sigma_v + 2 \cdot \sigma_v \cdot K}{3}$$

$$(3.17) \quad \sigma_m = \frac{1 + 2 \cdot K}{3} \cdot \sigma_v$$

The mean effective stress can furthermore be linked to the pore pressure by combining equation 3.24 with equation 3.26.

$$(3.18) \quad \frac{\sigma_m}{K_{b,h}} = -(\alpha - \gamma) \cdot \frac{\Delta P}{K_b}$$

$$(3.19) \quad \sigma_m = -(\alpha - \gamma) \cdot \Delta P$$

Where K_b is the bulk modulus (-).

By incorporating equation (3.7) for the stress path, the equation can be rewritten as

$$(3.20) \quad \sigma_m = -\left(\alpha - \left(\frac{2}{3} \cdot \alpha \cdot (1 - K)\right)\right) \cdot \Delta P$$

With α is 1 (assumption 2), this can be rewritten as:

$$(3.21) \quad \sigma_m = \frac{1 - 2K}{3} \cdot \Delta P$$

STRAIN

The volumetric strain (ϵ_v) represents the bulk deformation of the sample [40]. With the help of the Biot-Willis assumption, which states that the grain compressibility is assumed to be negligible compared to the bulk compressibility, the equation can be simplified to a function of only pore volume variation.

$$(3.22) \quad \epsilon_v = -\phi \cdot \frac{\Delta V_p}{V_p} + \frac{\sigma_m - \phi \cdot P}{K_s}$$

$$(3.23) \quad \epsilon_v = -\phi \cdot \frac{\Delta V_p}{V_p}$$

Where K_s is the grain compressibility (Bar) and ϕ is the porosity

Since the volumetric strain is given by change in the pore volume, equation 3.22 can be redefined with the help of equation 3.28. This can be rewritten to function of the (hydrostatic) bulk compressibility.

$$(3.24) \quad \epsilon_v = \frac{\Delta \sigma_m}{K_b}$$

$$(3.25) \quad \epsilon_v = C_{bc,H} \cdot \Delta \sigma_m$$

Where K_b is the bulk modulus (Bar)

The volumetric strain can also be defined as function of stress path, pore compressibility and the bulk modulus [40].

$$(3.26) \quad \Delta \epsilon_v = -(\alpha - \gamma) \cdot \frac{\Delta P}{K_{b,H}}$$

The axial strain is equal to the volumetric strain if the radial strain approaches zero. Then based on equation 3.23 it can be expressed as:

$$(3.27) \quad \Delta \epsilon_a = \frac{\Delta L}{L} = -\phi \cdot \frac{\Delta V_p}{V_p}$$

Where L is the vertical length of the sample or reservoir (m).

ROCK COMPRESSIBILITY

The modulus (K) is a function of the change in pressure per unit of volume change, it represents the stiffness of the material. The modulus of a material can be given by [25]:

$$(3.28) \quad K = -V \frac{dP}{dV}$$

The compressibility is the inverse of the bulk modulus and gives the change in volume per unit of pressure change [25].

$$(3.29) \quad C = \frac{1}{K} = -\frac{1}{V} \cdot \frac{dV}{dP}$$

Hydrostatic compression test

For an hydrostatic compression test the strain is volumetric and the effective stress change is the mean effective stress. By rewriting equation 3.29 and equation 3.23 the hydrostatic bulk compressibility ($C_{b,H}$) can be expressed as:

$$(3.30) \quad C_{b,H} = \frac{\epsilon_v}{\Delta\sigma_m}$$

The hydrostatic bulk compressibility can be defined as the function of the porosity change [38]. With the help of equation 3.21 it can be rewritten as function of the mean effective stress.

$$(3.31) \quad C_{b,H} = \frac{\Delta\phi}{(\phi_{ref} + \Delta\phi - \alpha) \cdot \Delta P}$$

$$(3.32) \quad C_{b,H} = \frac{\Delta\phi}{(\phi_{ref} + \Delta\phi - 1) \cdot \sigma_m \cdot \frac{3}{1-2K}}$$

Φ_{ref} is the porosity at the start of compaction (-) $\Delta\phi$ is the difference between ϕ and ϕ_{ref} (-)

The hydrostatic pore compressibility ($C_{p,H}$) can be derived from the bulk compressibility by correcting for the initial porosity of the sample [38]. With usage of the Biot-Willis assumption ($\alpha=1$), the equation can be simplified.

$$(3.33) \quad C_{p,H} = \frac{C_{b,H}}{\phi_{ref}} \cdot (\alpha - \phi_{ref} \cdot (1 - \alpha))$$

$$(3.34) \quad C_{p,H} = \frac{C_{b,H}}{\phi_{ref}}$$

Uniaxial compression test

The uniaxial bulk compressibility ($C_{b,k}$) is a function of the axial strain and the change in vertical effective stress (or likewise the axial effective stress).

$$(3.35) \quad C_{b,k} = \frac{\Delta\epsilon_A}{\Delta\sigma_v}$$

The uniaxial pore compressibility ($C_{p,k}$) can be determined as function of the uniaxial bulk compressibility (equation 3.29 combined with equation 3.23) or the hydrostatic pore compressibility [38].

$$(3.36) \quad C_{p,k} = \frac{C_{b,k}}{\phi_{ref}}$$

$$(3.37) \quad C_{p,k} = C_{p,H} \cdot \frac{1+2K}{3}$$

PORE VOLUME REDUCTION

The change in pore volume is a function of the variation in pore volume with respect to the initial pore volume of the material [40].

$$(3.38) \quad V_p/V_{p,ref} = 1 - \frac{\Delta V_p}{V_{p,ref}}$$

With equation 3.23 and equation 3.27 this can be rewritten as a function of axial strain (anisotropic compression) or volumetric strain (hydrostatic strain) [40].

Hydrostatic compression test

$$(3.39) \quad V_p/V_{p,ref} = 1 - \frac{\epsilon_v}{\phi_{ref}}$$

Uniaxial compression test

$$(3.40) \quad V_p/V_{p,ref} = 1 - \frac{\epsilon_A}{\phi_{ref}}$$

The pore volume reduction can furthermore be defined as a function of porosity [40]. This can be simplified based on the assumption Biot-Willis assumption which gives negligible grain compressibility ($K_s \rightarrow \infty$):

$$(3.41) \quad V_p/V_{p,ref} = 1 - \frac{\phi - \phi_{ref}}{\phi_{ref} \cdot (1 - \phi_{ref})} - \frac{\sigma_m - \phi_{ref}}{K_s \cdot (1 - \phi_{ref})}$$

$$(3.42) \quad V_p/V_{p,ref} = 1 - \frac{\phi - \phi_{ref}}{\phi_{ref} \cdot (1 - \phi_{ref})}$$

The normalized pore volume reduction can furthermore be defined as a function of the compressibility of the material.

Hydrostatic compression test

By combining equation 3.23, equation 3.39 and equation 3.29 one can write:

$$(3.43) \quad V_p/V_{p,ref} = 1 - \frac{\Delta\sigma_m}{K_b \cdot \phi_{ref}}$$

$$(3.44) \quad V_p/V_{p,ref} = 1 - \frac{\Delta\sigma_m \cdot C_{b,H}}{\phi_{ref}}$$

$$(3.45) \quad V_p/V_{p,ref} = 1 - \Delta\sigma_m \cdot C_{p,H}$$

Uniaxial compression test

With the help of equation 3.40, equation 3.28 and equation 3.29 one can write:

$$(3.46) \quad V_p/V_{p,ref} = 1 - \frac{\Delta\sigma_v}{K_b \cdot \phi_{ref}}$$

$$(3.47) \quad V_p/V_{p,ref} = 1 - \frac{\Delta\sigma_v \cdot C_{b,k}}{\phi_{ref}}$$

$$(3.48) \quad V_p/V_{p,ref} = 1 + C_p \cdot \Delta P$$

$$(3.49) \quad V_p/V_{p,ref} = 1 - \Delta\sigma_v \cdot C_{p,k}$$

PERMEABILITY REDUCTION**Kozeny-Carman**

Kozeny-Carman can be used to express the permeability as a function of porosity. However, since for the studied data there is often no other data on the rock characteristics available than the porosity, simplified version of the equation is necessary.

Option I: Chan [6] defined a modified version of the Kozeny-Carman relationship to determine the permeability change (k/k_i).

$$(3.50) \quad k/k_i = \left(\frac{\phi - \phi_c}{\phi_{ref} - \phi_c}\right)^3 \cdot \left(\frac{1 + \phi_c - \phi_{ref}}{1 + \phi_c - \phi}\right)^2$$

Where ϕ_c is the percolation porosity (-), which ranges from 0 to 0.05 for most cases [6]. The percolation porosity is set to 0.01 in this study.

Option II: Hettema (2016, personal communication) determined the following simplified representation of Kozeny-Carman. This option is used as the standard option in this study.

$$(3.51) \quad k/k_i = \left(\frac{\phi}{\phi_{ref}}\right)^3 \cdot \left(\frac{1 - \phi_{ref}}{1 - \phi}\right)^2$$

Transmissibility

The variation in permeability can likewise be expressed as a variation in transmissibility. The change in transmissibility is defined as the ratio between the changed transmissibility and the initial transmissibility (T/T_{ref}). Transmissibility is a function of permeability, viscosity, surface area and the thickness [17], in which the permeability is the only varying parameter during compression. The transmissibility reduction then can be simplified to:

$$(3.52) \quad T/T_{ref} = \frac{k/\mu \cdot A/d}{k_{ref}/\mu_{ref} \cdot A/d} \approx \frac{k}{k_{ref}}$$

Where T is the transmissibility (-) and T_{ref} is the transmissibility at the start of compaction (-), k is the permeability (mD), k_{ref} is the permeability to which the varying permeability is compared (mD), μ is the viscosity (Pa·s), μ_{ref} is the viscosity to which the varying viscosity is compared (Pa·s), A is the surface through which the fluid flows (m²), and d is the length of the flow through this surface (m).

VOID RATIO

The void ratio (e) is an often used quantity in soil mechanics related to porosity [41]:

$$(3.53) \quad e = \frac{V_s}{V_b}$$

$$(3.54) \quad \phi = \frac{e}{1+e}$$

Where V_s is the volume of the (solid) grains (m³).

3.1.4. STRESS REGIME

The shallow depth of the reservoirs results in a low temperature and low (hydrostatic) pressure. There is almost no overpressure due to the limited strength of the seal in the shallow subsurface [42].

Here, the stresses in the reservoir are approximated in order to determine the change in vertical effective stress as is taking place in the reservoir using equation 3.3 (figure 3.2). The overburden gradient is taken from [43] and approximately equal to 2,2 g/cm³. The hydrostatic pressure gradient is set to 1.1 g/cm³. Equation 3.2, 3.3 and 3.12 are used to determine the horizontal stress, based on the assumption that the Poisons ratio of an unconsolidated sandstone can be approximated by a value between 0.2 and 0.3.

The effective stresses are defined by equation 3.9 and equation 3.10 and thus can be calculated for the reservoir based on the assumptions for the overburden gradient and the hydrostatic gradient. As the pore pressure decreases during production, with a constant overburden stress, the effective stresses increase. The change in vertical effective stresses for shallow gas reservoirs at hydrostatic pressure up to 800 m range from 40 bar to 90 bar (figure 3.3). This range is used to determine the valid data range of the experimental rock compaction data presented in literature.

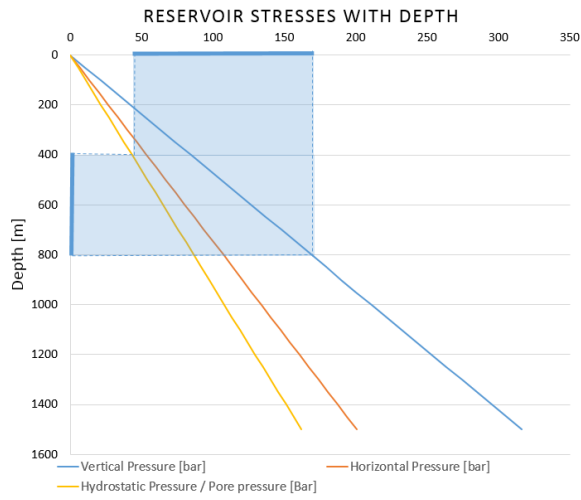


Figure 3.2: Relation between depth and stress for the Dutch shallow gas reservoirs

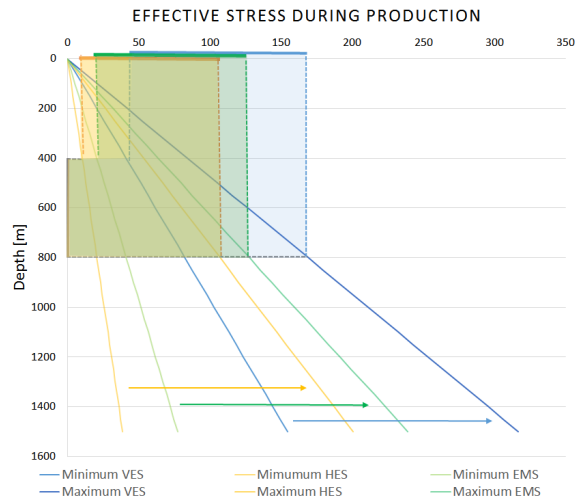


Figure 3.3: Relation between depth and the vertical effective stress during production of the Dutch shallow gas reservoirs, in which the gas pressure is roughly equal to the hydrostatic pressure.

3.2. RESULTS

The literature-based rock compaction data set consists of more than 200 samples (see appendix B). The pore compressibility of the samples ranges from $9\text{e-}5 \text{ bar}^{-1}$ to $1.54\text{e-}2 \text{ bar}^{-1}$ (figure 3.5a). The decrease in pore volume reaches a maximum of 70% (figure 3.5b), whereas the maximum permeability reduction is about 95% (figure 3.5c).

3.2.1. ROCK COMPACTION TRENDS

Three compaction behaviour trends representing the main behaviour observed in the datasets are defined. These trends are solely based on the empirical behaviour and not on an understanding of the mechanisms causing the trends in the response.

The trends are classified as low, medium and high, which represent a low, medium and high pore volume reduction and subsequent permeability reduction obtained using the simplified Carman-Kozeny relationship. Results are shown in figure 3.4 and table 3.1.

Six empirical relations are derived that represent the three defined trends.

$$\begin{aligned} \text{Trend Low: } V_p/V_{p,ref} &= 3 \cdot 10^{-6} x^2 - 0.0011x + 0.9999 \\ k/k_{ref} &= 9 \cdot 10^{-6} x^2 - 0.0028x + 1.0011 \end{aligned}$$

$$\begin{aligned} \text{Trend Mid: } V_p/V_{p,ref} &= -5 \cdot 10^{-8} x^2 + 3 \cdot 10^5 x^2 - 0.005x + 1.0035 \\ k/k_{ref} &= -2 \cdot 10^{-7} x^3 + 0.0001x^2 - 0.0126x + 1.006 \end{aligned}$$

$$\begin{aligned} \text{Trend High: } V_p/V_{p,ref} &= -5 \cdot 10^{-7} x^3 + 0.0001x^2 - 0.0125x + 1.0043 \\ k/k_{ref} &= -2 \cdot 10^3 x^3 + 0.0004x^2 - 0.0282x + 1.0037 \end{aligned}$$

Trend	Pore volume reduction			Permeability reduction		
	Min (Experim. data)	Max* (Experim. data)	Empirical relation*	Min (Experim. data)	Max* (Experim. data)	Empirical relation*
Low	0%	11%	8%	0%	27%	18%
Mid	11%	33%	23%	27%	65%	49%
High	33%	62%	50%	65%	88%	81%

*Maximum reduction at a Vertical effective stress of 100 Bar

Table 3.1: Minimum, maximum and empirically-predicted compaction-induced pore volume and permeability reduction for the three defined trends.

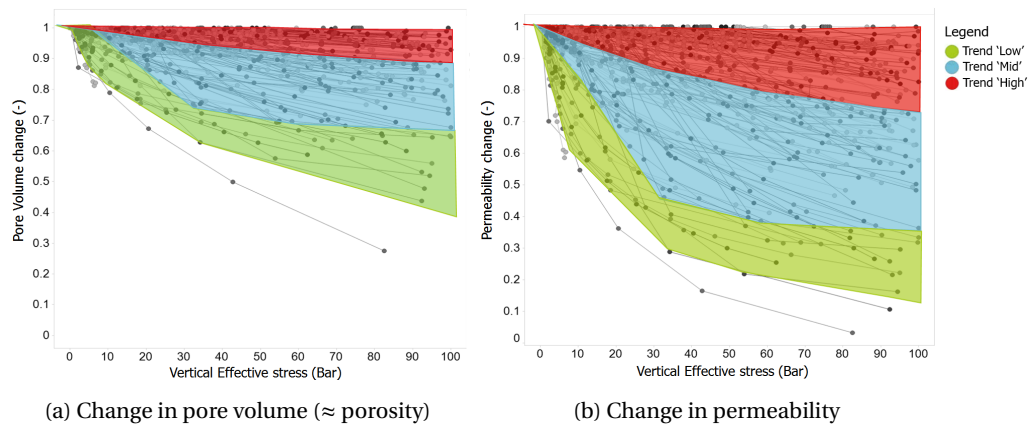
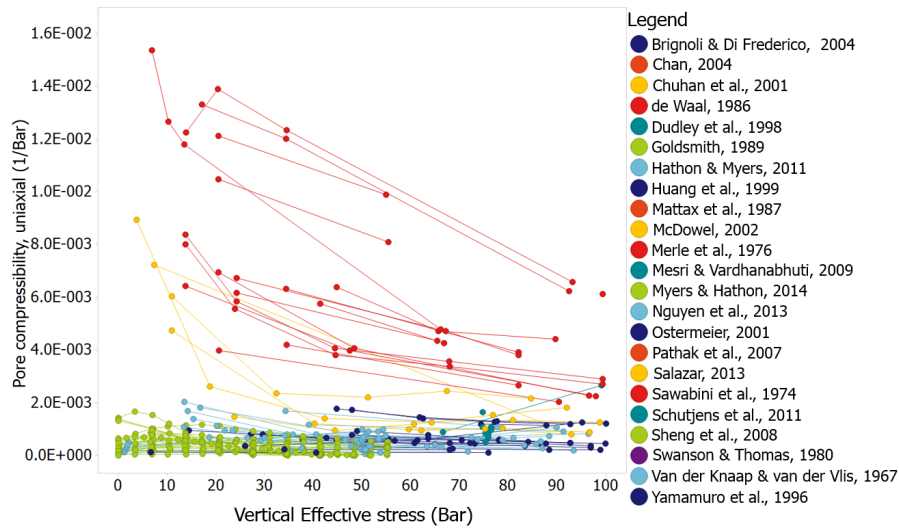
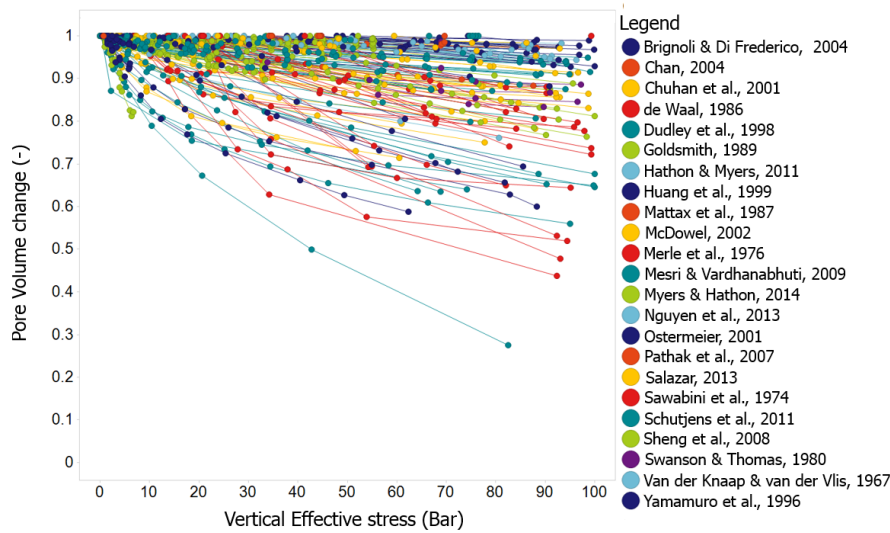


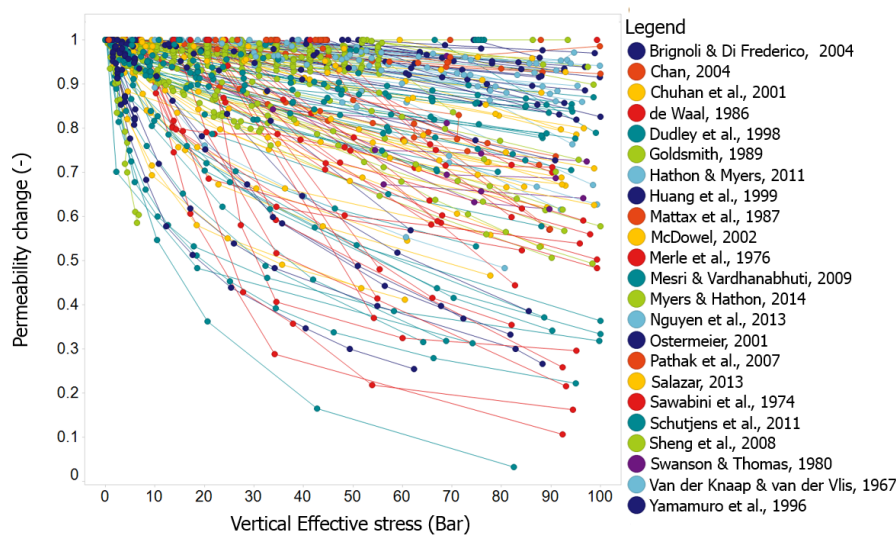
Figure 3.4: Three trends (low - mid - high) defined for the representation of the rock characteristics subject to compaction.



(a) Pore compressibility



(b) The compaction-induced change in pore volume (\approx porosity)



(c) The compaction-induced change in permeability

Figure 3.5: The complete data set constructed to represent the rock behaviour during compaction of weakly to unconsolidated sandstone. (a) Pore compressibility. (b) Variation in pore volume (\approx porosity). (c) Variation in permeability as reported and derived based on Carman-Kozeny.

3.2.2. IMPACT OF DATA CONVERSION: EXPERIMENTAL & CALCULATED DATA

For part of the samples the porosity reduction is measured and thus is the proportional pore volume reduction known. For the other samples the pore volume reduction is calculated based on the reported strain or the bulk or pore compressibility. There is a discrepancy between the calculated (predicted) and the measured results, as the measured pore volume reduction shows a curvature that is more flattened out for an increase in vertical effective stress (figure 3.6a). Furthermore most samples with a measured pore volume reduction (\approx porosity reduction) are within the upper half of the range of determined pore volume reductions.

Four articles, comprising 24 samples, have data both on permeability reduction and on rock compressibility or pore volume reduction. This allows for the comparison between the calculated permeability reduction and the measured permeability reduction. The known and permeability reduction (figure 3.6b) is less pronounced than the predicted permeability reduction. The discrepancy between the calculated and the measured permeability reduction increases with an increase in the vertical effective stress on the sample. The wider spread for the higher vertical effective stresses could be the offset for higher deviations with an increase in vertical effective stress outside the shallow gas reservoir stress regime (0-100 bar). The samples with the measured permeability reduction are mostly within the upper half of the range in possible permeability reduction. The samples of the four (Chan [6], Nguyen [7], Goldsmith [8] and Mattax [9]) are discussed in more detail. The plotted ranges are here from 0-300 Bar (in stead of the 0-100 Bar representative for the Dutch shallow gas fields), to increase the understanding of compaction-induced permeability changes as more rapid changes take place for these higher stresses.

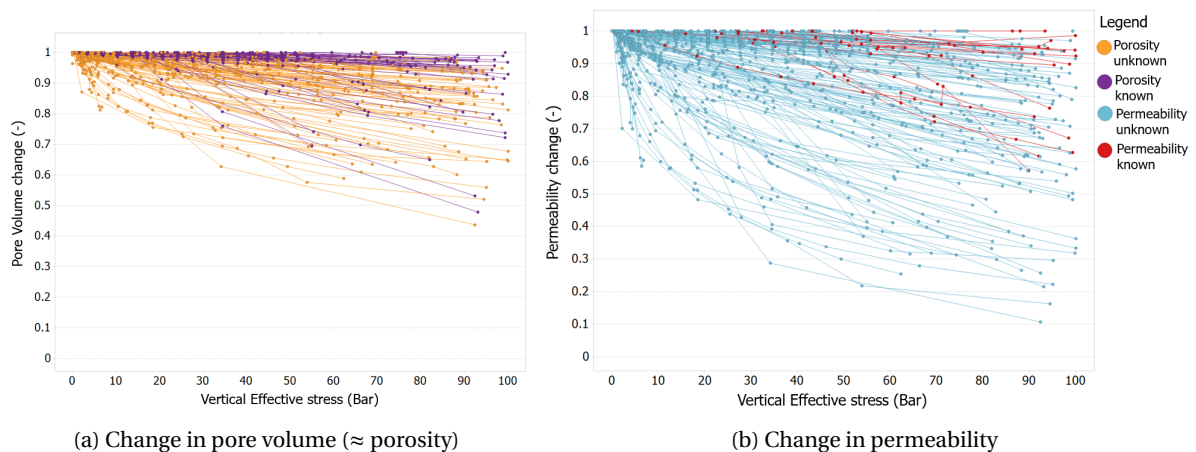


Figure 3.6: The differences between the measured rock characteristics and the calculated rock characteristics subject to compaction (i.e. pore volume and permeability) in weakly to unconsolidated sandstone.

CHAN

For the samples from the article of Chan [6] the permeability reduction and the porosity reduction are measured for all seven samples (figure 3.7). There is an immediate deviation between the measured and calculated dataset where the measured permeability is under-predicted by the calculated data.

NGUYEN

All five samples investigated by Nguyen [7] have data on the permeability reduction, the axial strain and the volumetric strain for an increase in (vertical effective) stress (figure 3.8). The highest deviation from the actual (measured) behaviour is found for the permeability reduction measured based on the axial strain data. The actual behaviour gives a more rapid decrease in permeability, where the calculated decrease is more gradual and flattened.

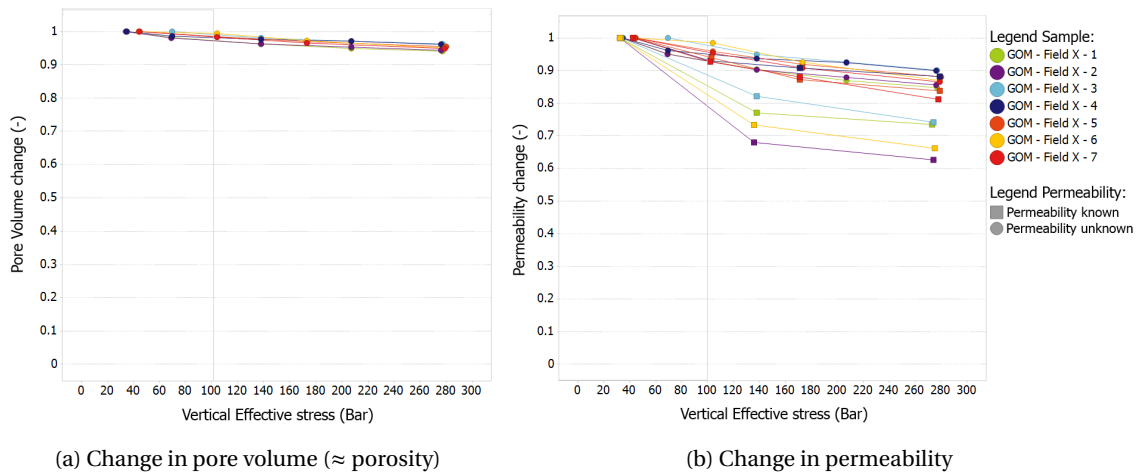


Figure 3.7: The change in the rock characteristics subject to compaction for the samples presented by Chan [6]. These samples have data both on the porosity and permeability variation and thus is possible to determine the discrepancies obtained by calculating the permeability variation based on the measured strain in stead of measuring the permeability variation. The valid stress range for the Dutch shallow gas fields is from 0-100 Bar.

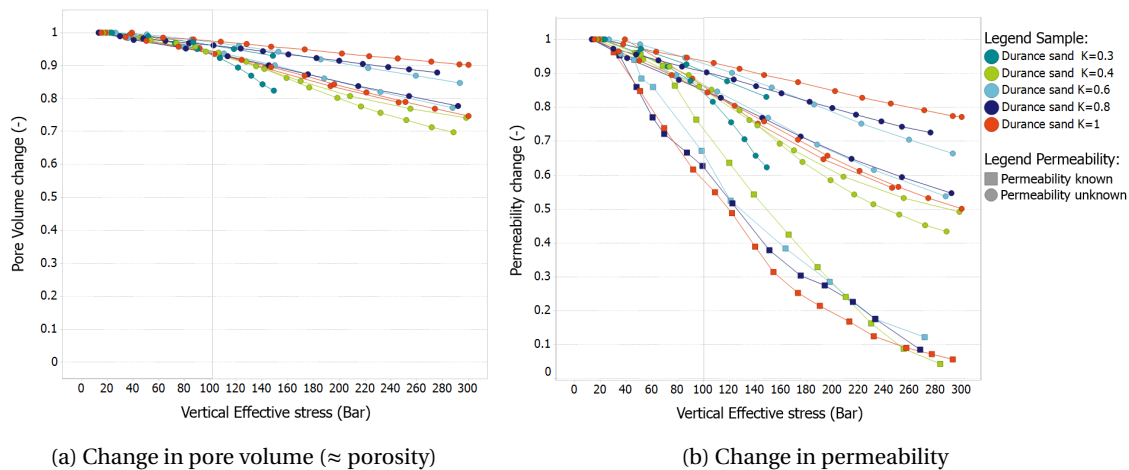


Figure 3.8: The change of the rock characteristics subject to compaction for the samples presented by Nguyen [7]. These samples have data both on the porosity and permeability variation. It is thus possible to determine the discrepancies obtained by calculating the permeability variation based on the measured strain in stead of measuring the permeability variation. The valid stress range for the Dutch shallow gas fields is from 0-100 Bar.

MATTAX

The data of the two samples as are presented in the article of Mattax [9] give a loading cycle in multiple stages. For the presented samples the permeability reduction and the porosity reduction are measured (figure 3.9). The deviation between the measured and the calculated data on pore volume reduction is limited.

GOLDSMITH

For the samples from the article of Goldsmith [8] the measured permeability reduction can be compared to the measured permeability reduction based on the compressibility and the porosity reduction (figure 3.10). Within the vertical effective stress reach of the Dutch shallow gas reservoirs (0 – 100 bar), onlu a small deviation can be detected between the measured and calculated permeability reduction. Though there are not enough data points within this range to make a comparison for all samples.

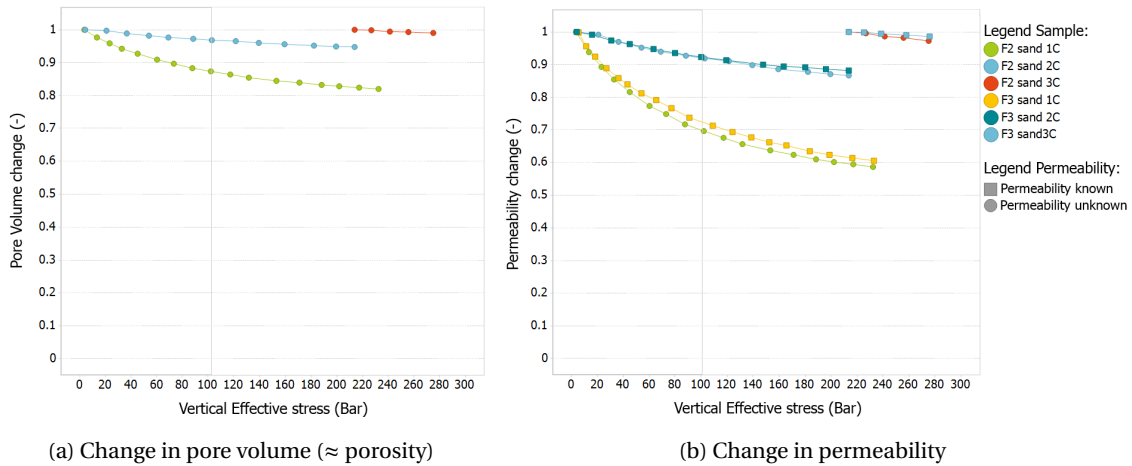


Figure 3.9: The change of the rock characteristics subject to compaction for the samples presented by Mattax [9]. These samples have data both on the porosity and permeability variation. It is thus possible to determine the discrepancies obtained by calculating the permeability variation based on the measured strain in stead of measuring the permeability variation. The valid stress range for the Dutch shallow gas fields is from 0-100 Bar.

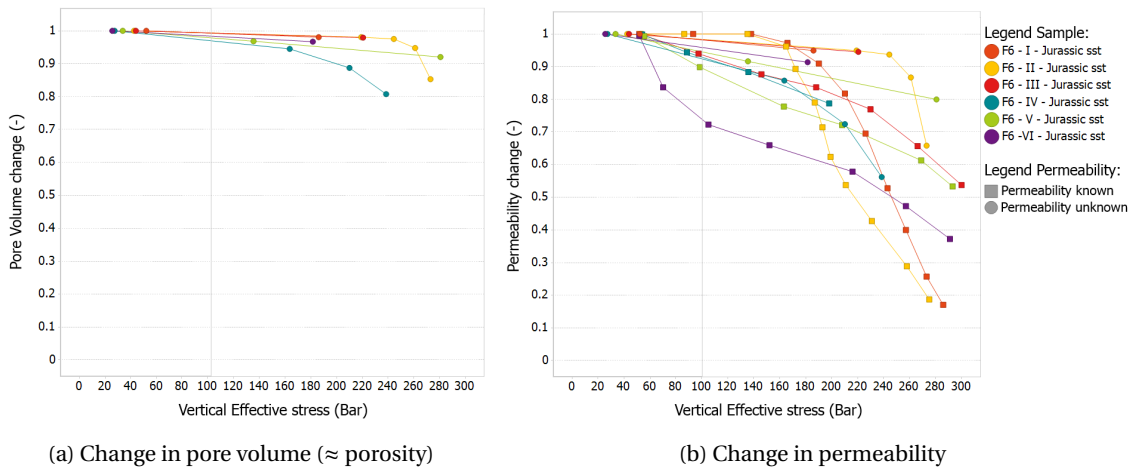


Figure 3.10: The change of the rock characteristics subject to compaction for the samples presented by Goldsmith [8]. These samples have data both on the porosity and permeability variation. It is thus possible to determine the discrepancies obtained by calculating the permeability variation based on the measured strain in stead of measuring the permeability variation. The valid stress range for the Dutch shallow gas fields is from 0-100 Bar.

3.2.3. TRENDS OBSERVED RELATED TO GEOLOGICAL CHARACTERISTICS

In order to assess the implications of variations in geological characteristics the data within the data set with data on a one of the geological characteristics is plotted. With this subsets the effects of geological characteristics on the compaction behaviour can be compared. Although here it is aimed to split up the behaviour for different effects, it should be taken into account that most geological characteristics are correlated. The compaction behaviour is related to a combination of the geological characteristics of the sample. The differences in the displayed compaction curves are thus not only caused by a specific quantity.

DEGREE OF CONSOLIDATION

There is only data of two articles [8] [7] in the dataset which are clearly stated as a weakly consolidated sample. The pore compressibility of the weakly consolidated samples is in the lower part of the range in pore compressibility (figure 3.11). The pore volume reduction is likewise minimal for the weakly consolidated samples, whereas the permeability reduction has a slightly wider spread. The decrease in pore volume and the reduction of the permeability is limited as well for the weakly consolidated samples and had spread of 2% and 16% respectively, where the total data set has spread of 70% and 95% respectively. The degree of consolidation

thus can have a significant impact on the compaction of the sample as there is a clear difference between the range of the unconsolidated and weakly consolidated samples.

PRE-CONSOLIDATION STRESS

The data on pre-consolidated stress is available from 4 articles [6] [4][43][44]. The range in variation in normalized pore volume reduction between the end-members is about 13% (figure 3.12), and the normalized permeability reduction has a variation of 40% at a VES of 100 bar. The data on pre-consolidation stress shows roughly that the higher the stresses are that the sample previously has experienced, the lower the compaction is. However not all samples confirm this trend as the samples with a pre-consolidation stress up to 100 bar are in the middle of the range. The pore compressibilities show a trend of a higher compressibility for a lower pre-consolidation stress, however the higher data ranges are missing here and thus cannot confirm this trend.

INITIAL POROSITY

The range in variation is for the normalized pore volume reduction is about 55% (figure 3.13), whereas the normalized permeability reduction has a variation of 0.9 at 100 bar of vertical effective stress. An increase in initial porosity increases the effects of compaction of the rock. The evidence is however only roughly detectable within the dataset. There are multiple samples that deviate from this trend, but mostly this trend is followed by the gross. The samples in the porosity class of 30-35% exhibit the widest range and has the most samples that deviate from the main trend. The samples in the porosity class of 35-40% show a higher reduction in pore volume and permeability than the 40-45% and 45-50% class. No clear trends could be observed regarding the role of initial porosity although there is a significant indication of an strong control of the initial porosity in the pore compressibility.

LITHOLOGY AND DEPOSITIONAL ENVIRONMENT

The data on samples other than 'sand' comes from 12 different samples from 2 authors [45][46]. From the various lithology's as are declared in the articles it is hard to differentiate clear trends (figure 3.14), as the naming of the various sands is rather sensitive to human interpretation. Furthermore, for most sands there has not been made a distinction about the composition of the sand. For the rock characteristics the whole range of data is covered by 'sand' samples, but with a denser coverage in the lower range. The order of the lithology's from low compaction to high compaction is quartz sand, lithic sand, arkosic sand and silty sand, in which the arkosic sand is including the ranges of the lithic and silty sand. The impact of the lithology on the pore compressibility deviates from the effect on the pore characteristics. The range covered by the 'sand' samples clearly lies in the lower range followed by the quartz sand, the lithic sand and with the highest compressibility's the arkosic sand.

GRAIN SIZE

From the data set it seems that the intermediate grain sizes (fine-medium) have the biggest impact on how much the samples compact (figure 3.15). The samples in this range come from 38 samples of 7 articles. If this sample set is left out the data set consists of 72 samples of 9 authors, where the least compressible grain size class is the medium sand, followed by the medium-coarse sand and the coarse grain size class is most affected by compaction. The fine sand class covers the whole ranges spanned by the medium and coarse grain size classes. The coarse silt is strongly affected by compaction, however since there are only two samples available the relevance is hard to determine.

GRAIN SHAPE

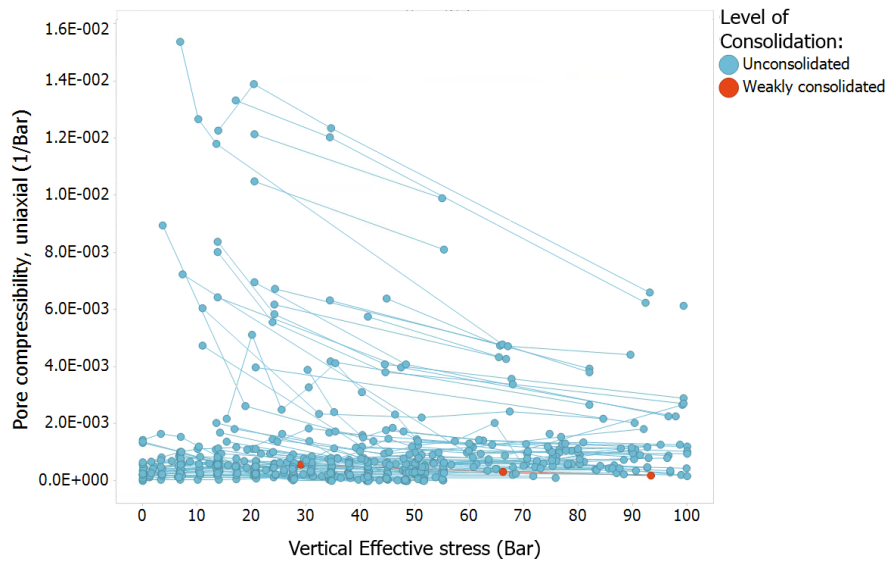
The defined grain shapes range from angular to rounded and are reported for 56 samples of 8 articles. The intermediate grain size classes (subangular to subrounded) are most affected by compaction (figure 3.16), but exhibit a wide range of potential pore volume variation (12% to 55%) and transmissibility (29% to 89%) reduction at an effective stress of 100 Bar. The various grain shape classes within this range are strongly overlapping and an order is hard to distinguish but could be defined as respectively subrounded, angular-subangular, rounded-subrounded, subangular-subrounded, and subangular, for least affected to most affected by compaction. The end-members, the rounded and angular grain size classes are least affected by compaction and have the lowest reduction in pore volume and permeability. There are a few outliers, which are not taken into account as they appear far out of the range of the other samples.

DUCTILE GRAINS

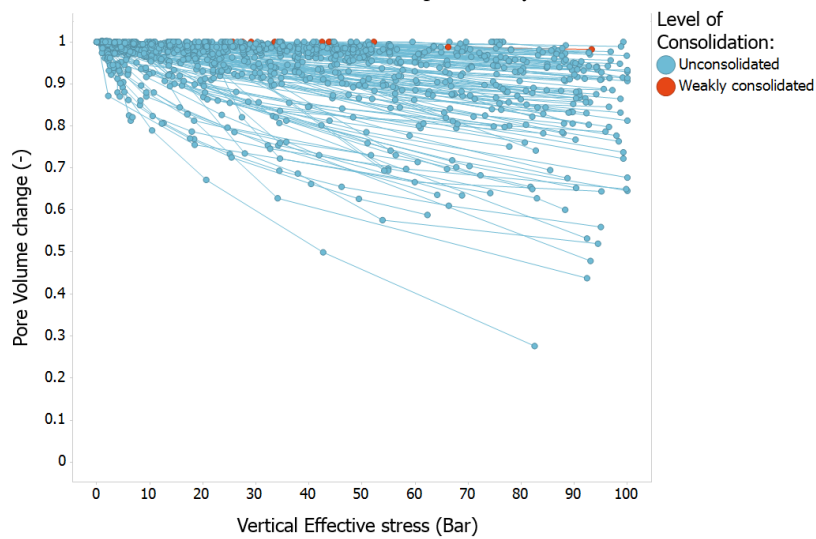
There is not enough data available on the samples comprising ductile grains to define trends in the pore volume and transmissibility reduction caused by rock compaction. For the pore compressibility's the data could direct towards a higher compressibility for a higher ductile grain content, but more samples are needed to be able to confirm this (figure 3.17).

FELDSPAR

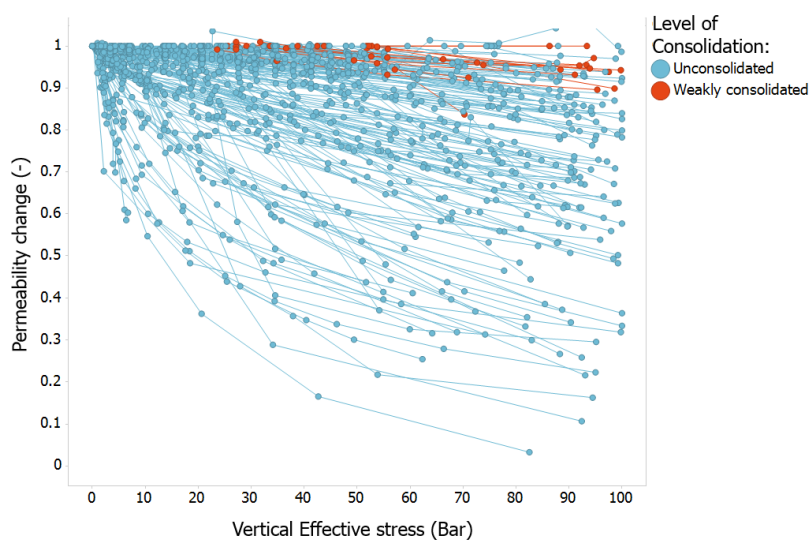
Within the full set of 37 samples from 6 articles which reported on the amount of feldspar, there is no clear distinction can be made on the effects of feldspar within the compaction processes (figure 3.18). When however the two lowest feldspar classes (light blue and dark blue) and compared to the rest of the decreasing pore volume and permeability data set, they can be classified as being in the lower part of the data set. However for the pore compressibility data there are multiple samples below these lowest feldspar classes. Within the samples of Hathon [4] where a comparison is made between two likewise samples a small variation based on the feldspar content can be detected, this effect is however not significant.



(a) Pore compressibility

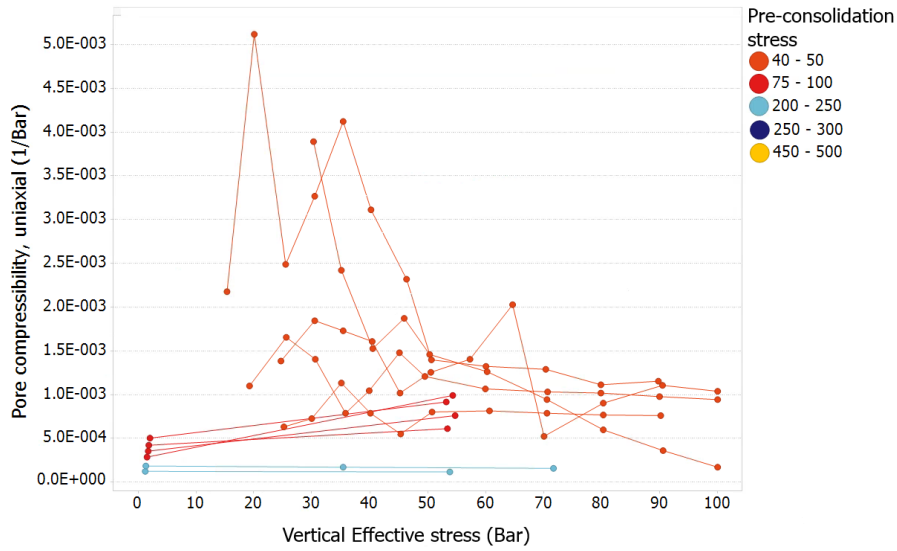


(b) Pore volume reduction

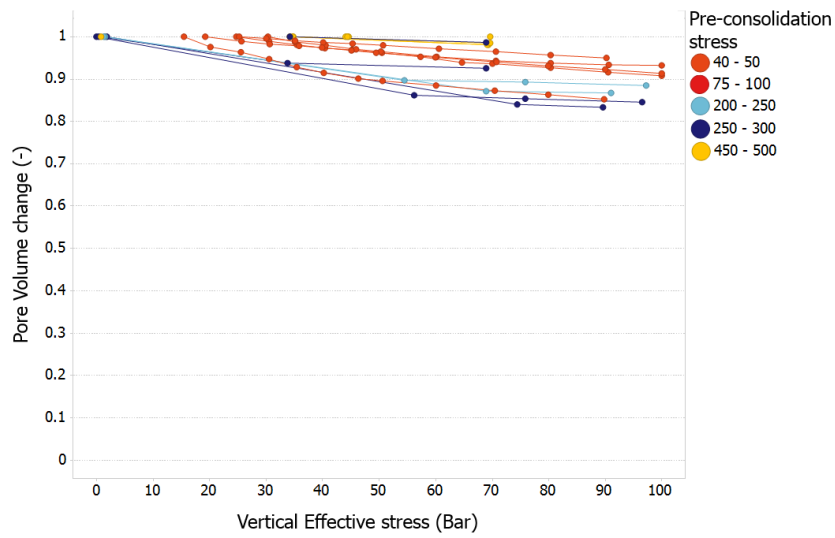


(c) Permeability reduction

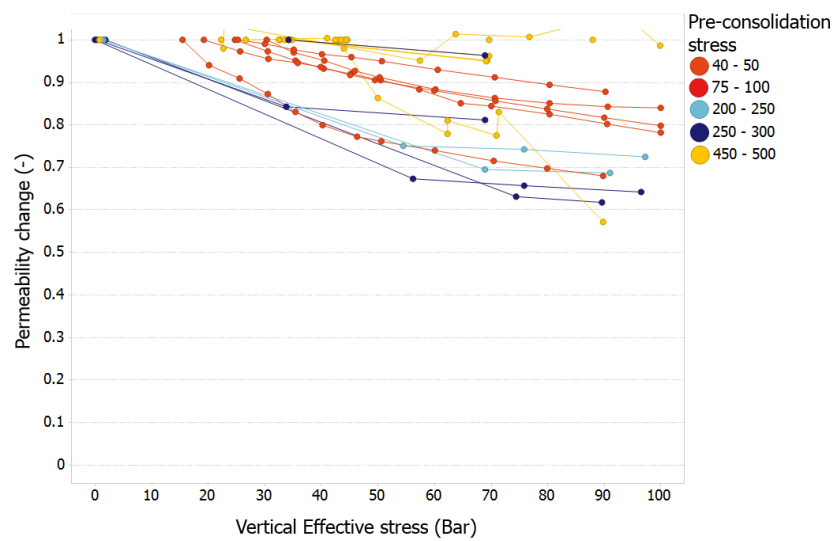
Figure 3.11: The change of the rock characteristics subject to compaction for the samples with data on the consolidation state of the sample. (a) Pore compressibility. (b) Variation in pore volume (\approx porosity). (c) Variation in permeability.



(a) Pore compressibility

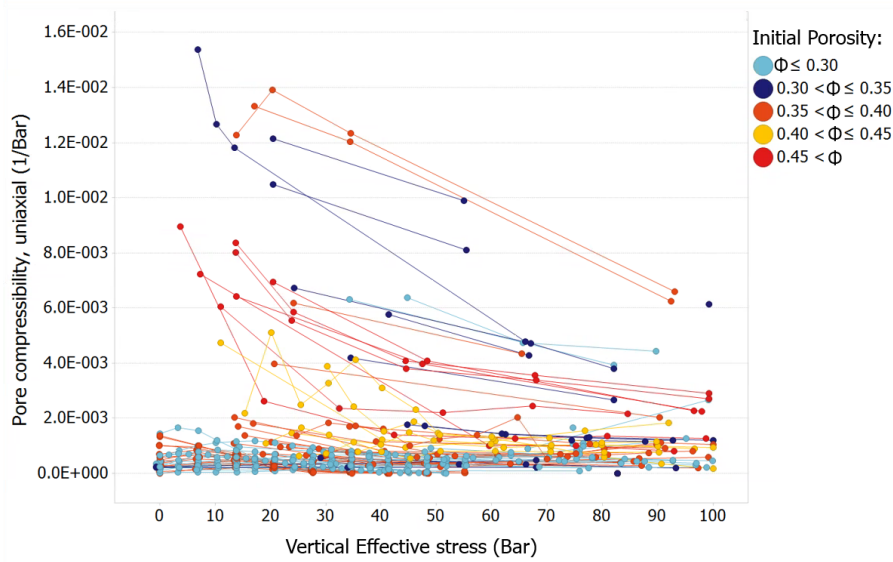


(b) Pore volume reduction

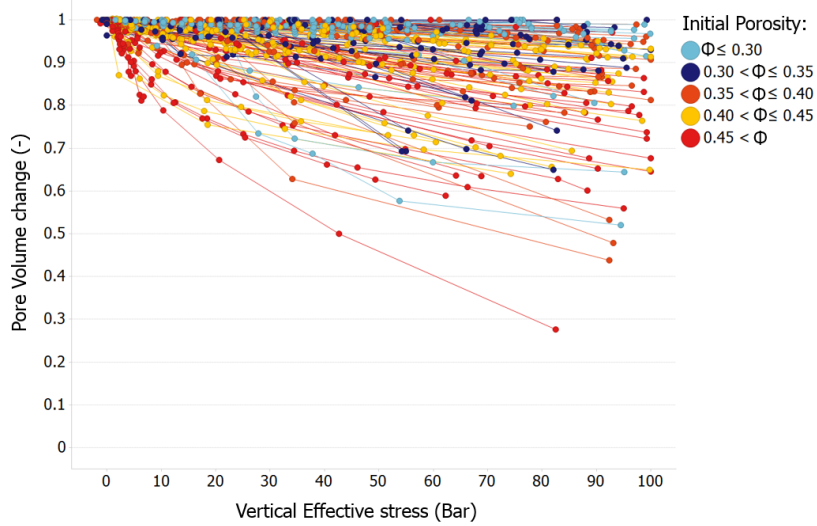


(c) Permeability reduction

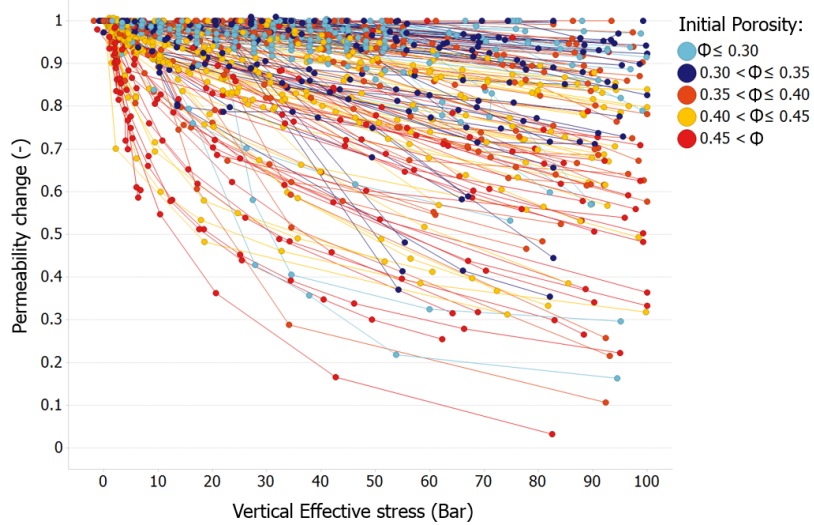
Figure 3.12: The change of the rock characteristics subject to compaction for the samples with data on the preconsolidation stress of the sample. (a) Pore compressibility. (b) Variation in pore volume (\approx porosity). (c) Variation in permeability.



(a) Pore compressibility for various initial porosities

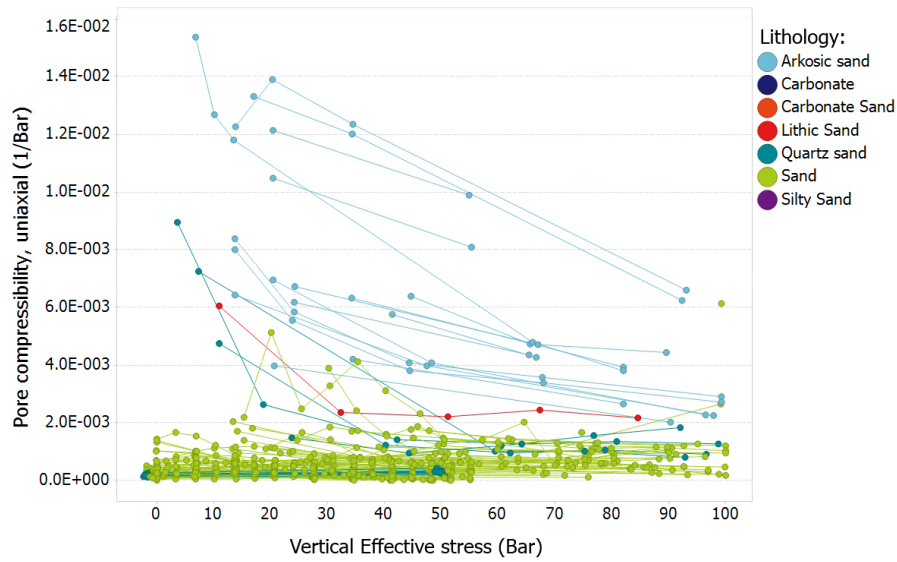


(b) Pore volume reduction

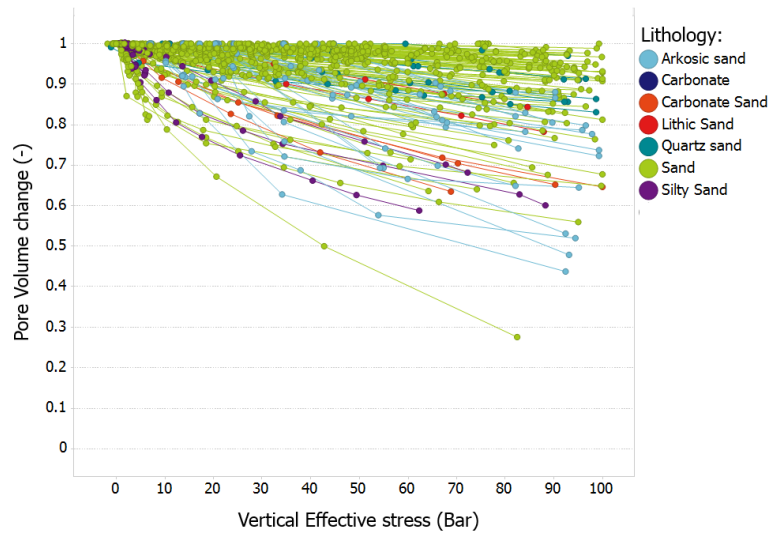


(c) Permeability reduction

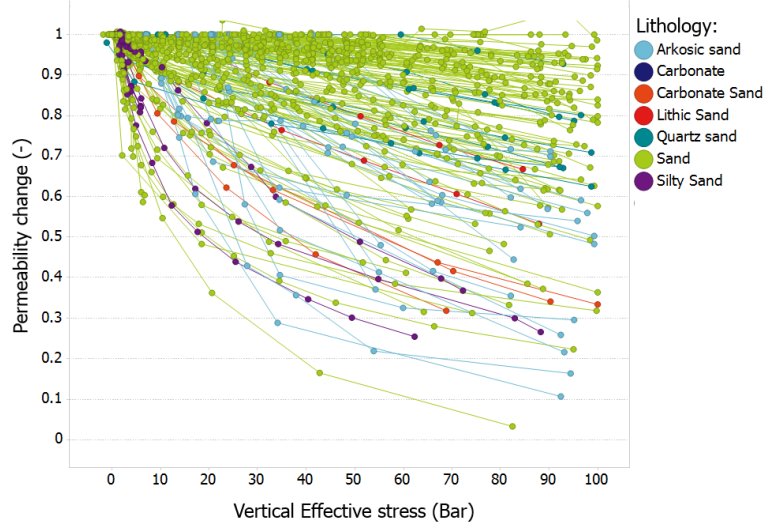
Figure 3.13: The change of the rock characteristics subject to compaction for the samples with data on the initial porosity of the sample. (a) Pore compressibility. (b) Variation in pore volume (\approx porosity). (c) Variation in permeability.



(a) Pore compressibility for various lithologies

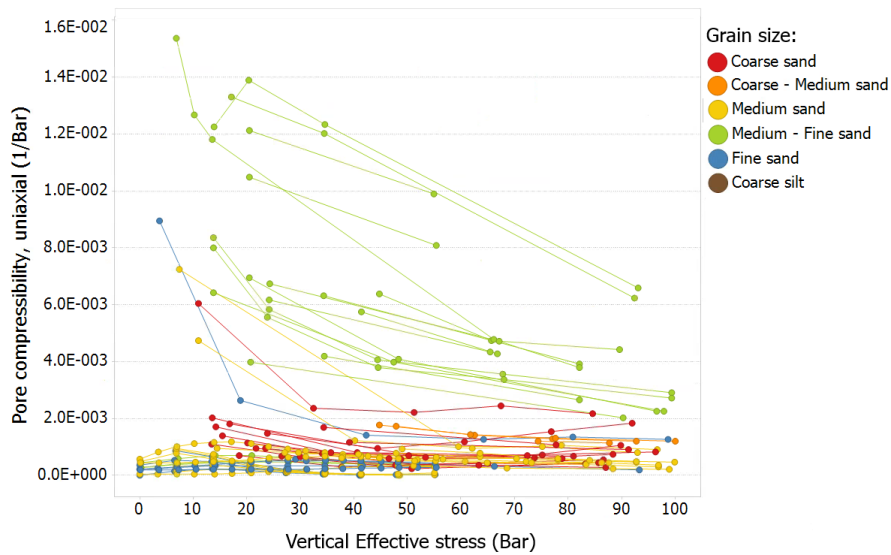


(b) Pore volume reduction

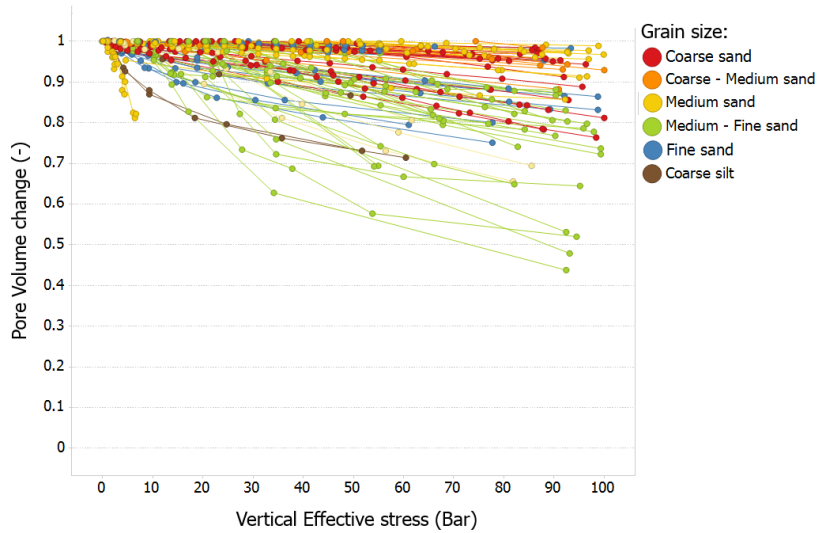


(c) Permeability reduction

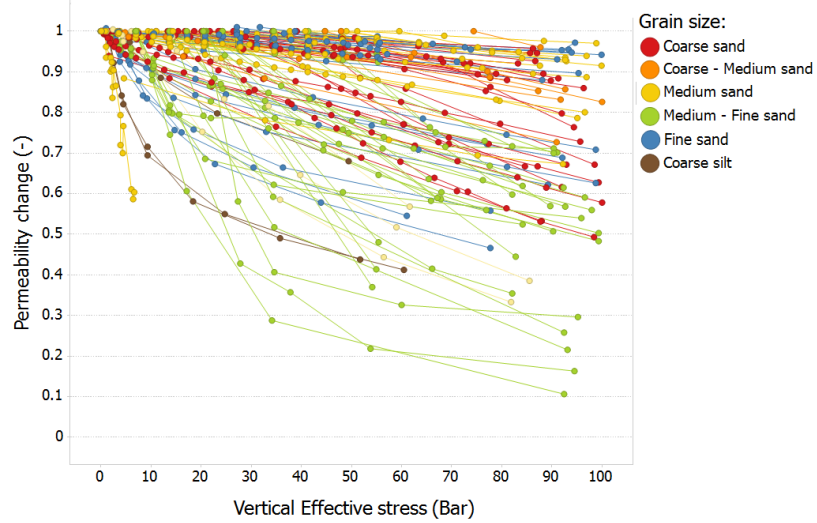
Figure 3.14: The change of the rock characteristics subject to compaction for the samples with data on the lithology of the sample. (a) Pore compressibility. (b) Variation in pore volume (\approx porosity). (c) Variation in permeability.



(a) Pore compressibility for various grain sizes

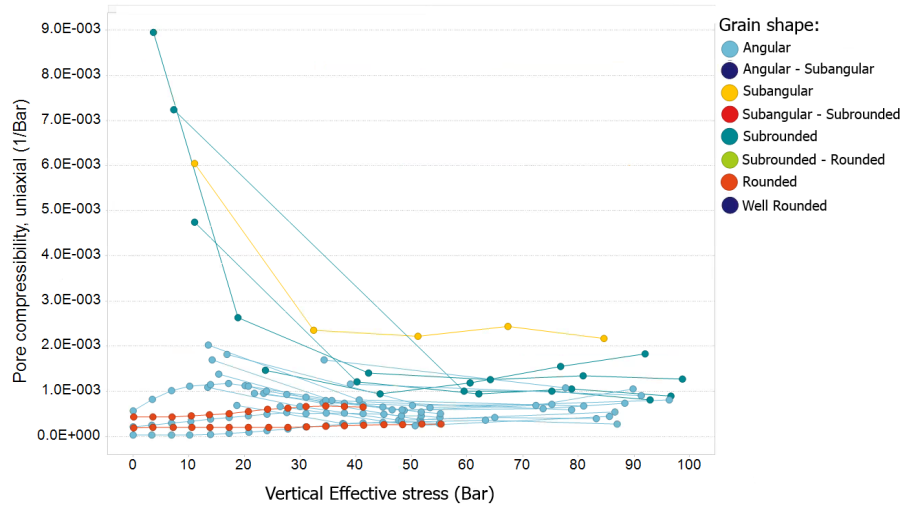


(b) Pore volume reduction

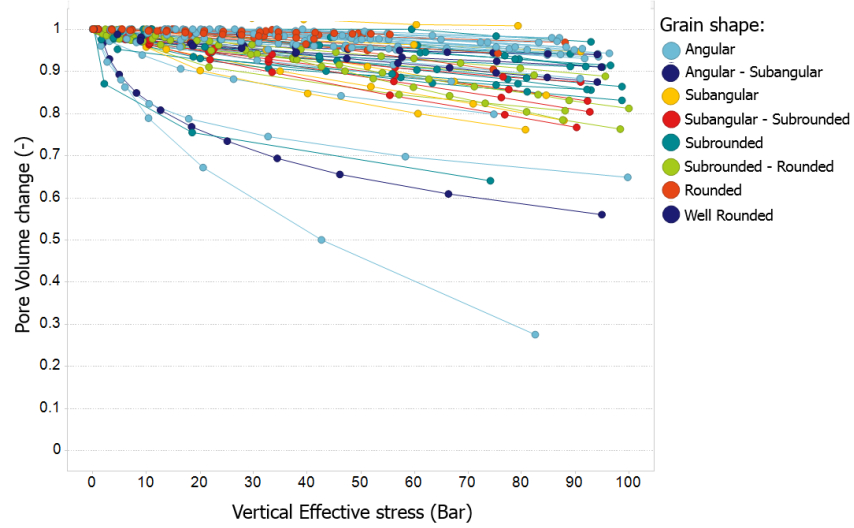


(c) Permeability reduction

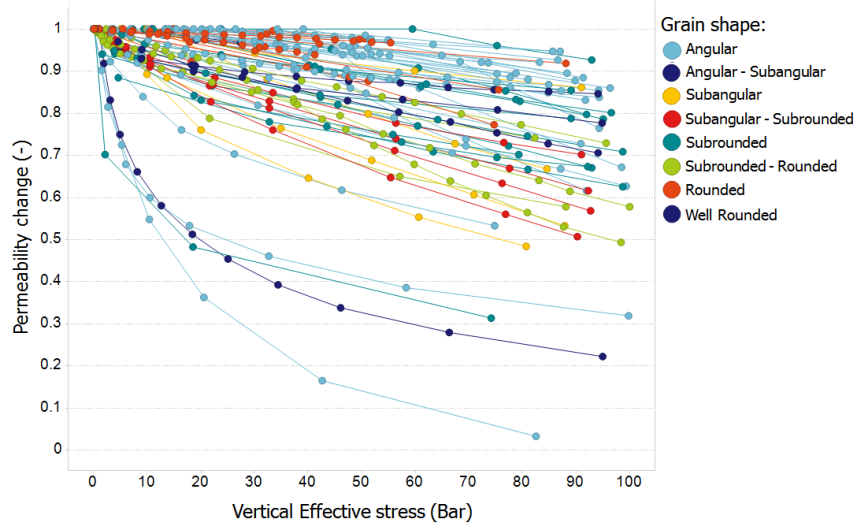
Figure 3.15: The change of the rock characteristics subject to compaction for the samples with data on the average grain size of the sample. (a) Pore compressibility. (b) Variation in pore volume (\approx porosity). (c) Variation in permeability.



(a) Pore compressibility for various grain shapes

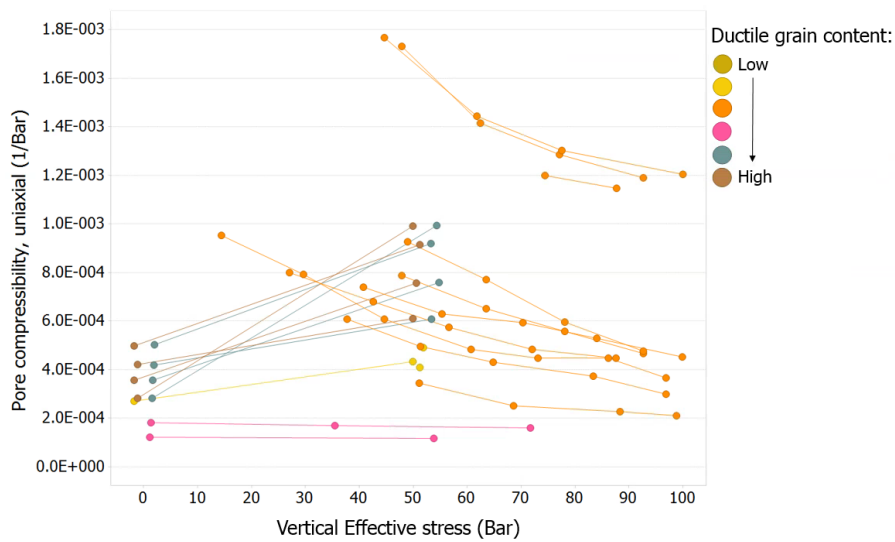


(b) Pore volume reduction

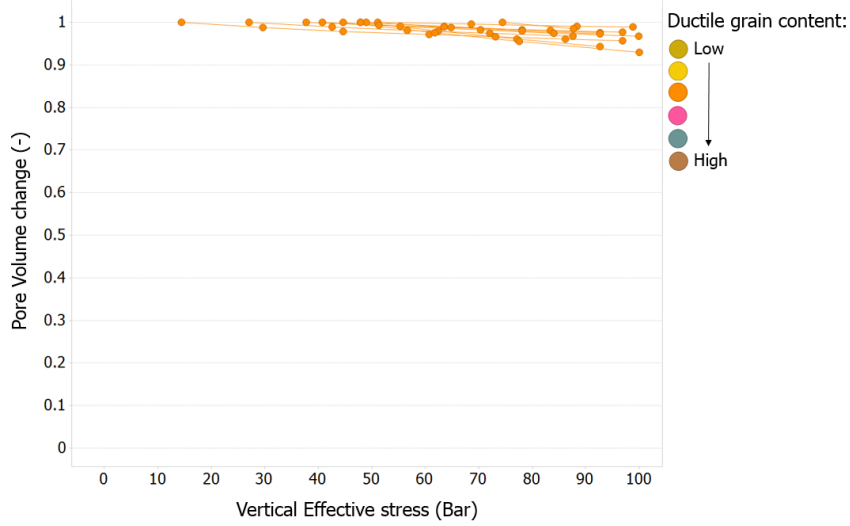


(c) Permeability reduction

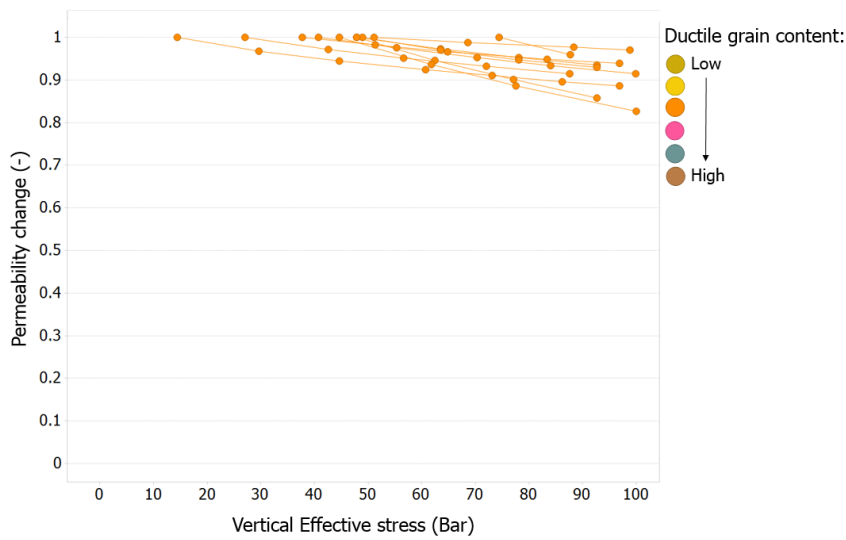
Figure 3.16: The change of the rock characteristics subject to compaction for the samples with data on the average grain shape of the sample. (a) Pore compressibility. (b) Variation in pore volume (\approx porosity). (c) Variation in permeability.



(a) Pore compressibility for various amounts of ductile grains

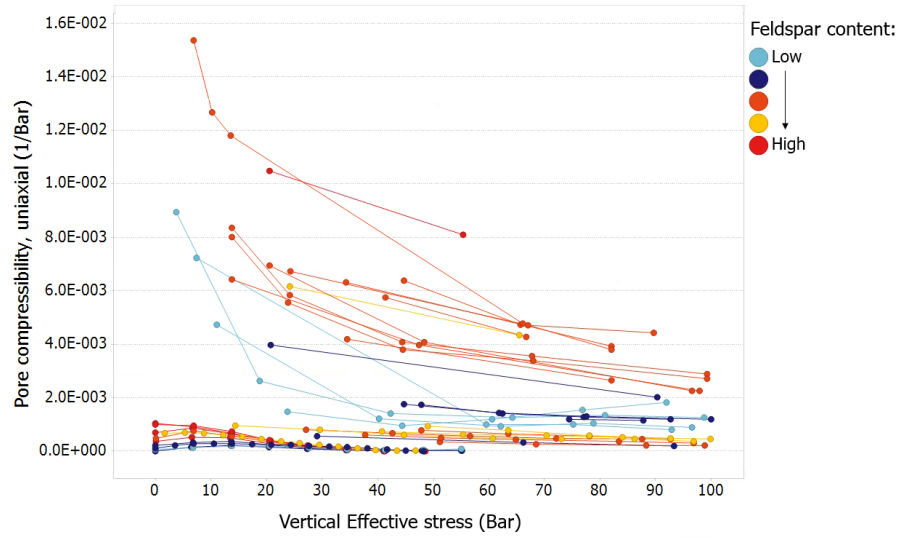


(b) Pore volume reduction

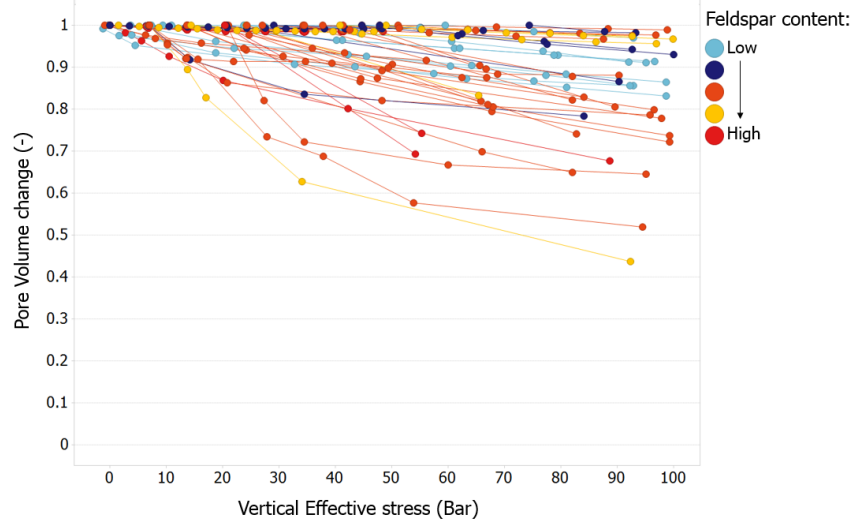


(c) Permeability reduction

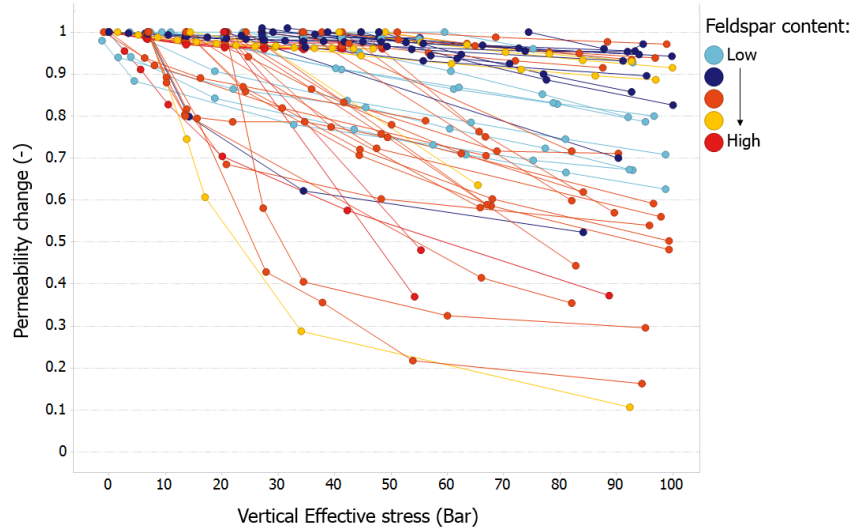
Figure 3.17: The change of the rock characteristics subject to compaction for the samples with data on the amount of ductile grains present in the sample. (a) Pore compressibility. (b) Variation in pore volume (\approx porosity). (c) Variation in permeability.



(a) Pore compressibility for various amounts of feldspar



(b) Pore volume reduction



(c) Permeability reduction

Figure 3.18: The change of the rock characteristics subject to compaction for the samples with data on the amount of feldspar present in the sample. (a) Pore compressibility. (b) Variation in pore volume (\approx porosity). (c) Variation in permeability.

3.3. DISCUSSION

To understand the impact of compaction on unconsolidated to weakly-consolidated sandstone, experimental literature data is used to form a database. Several limitations and uncertainties have been encountered as a result of the assumptions and methods applied.

DATA QUALITY

The available literature data on unconsolidated rock compaction experiments is of variable quality. Uncertainties that are difficult to assess are caused by the wide variety in nature of the samples (manufactured samples - core samples), the variable quality of the description on the sample characteristics, the core recovering method and the testing procedures causes uncertainties that are difficult to assess. The direct implication of the variability of the data is an error that cannot be avoided in the comparison of the data of different papers. Due to limited availability of sample descriptions for the presented experimental data in literature, it is often not possible to determine the cause and range of the error within the data set

The translation from experimental compaction data to in-situ reservoir compaction, an important aspect of the use of laboratory measurements, is not fully understood. Pauget [47] and Merle [48] attempted to assess the uncertainty related to unloading of the sample on the configuration and according compressibility of the sample. However the impact of the stress release during the recovering process of the sample is not taken into account in the comparison of the data within the dataset, as there is no standard approach available yet that accounts for this uncertainty.

Moreover prior to testing part of the samples is confined at in-situ reservoir pressure, and for part of the samples solely a change in vertical effective stress is assumed to be representative for reservoir compaction. These samples are tested without the initial confining pressure. As the exact testing conditions are often not described, it was not possible to correct for the impact of these differences on the stress path.

VALIDITY OF USED METHOD

Several assumptions are made to be able to normalize the data set to the defined standard quantities. These assumptions were necessary since there is not a consistent standard method in the literature to approach the data obtained for weakly to unconsolidated sandstone where compression is mostly associated with plastic deformation.

The assumption of deformation with solely uniaxial strain is a simplification of the deformational processes within a producing reservoir. Whereas in an producing reservoir the pressure depletion is not homogenous, neither is the resulting effective stress distribution. Near the well a zone with a large drawdown (i.e. the change in the near wellbore pressure with respect to the reservoir pressure) is situated, this will imply a variable stress path within the reservoir. Deformation processes will be affected by the aberrant impact of shear stress on the deformation.

The Biot-Willis constant (α) is approximated as one during the deformation of unconsolidated sandstone. This assumption is derived from the expected negligible grain compressibility. For the first period of deformation, where frictional forces dominate, this assumption is probably valid, but as the grains of the sample reconfigure and the sample stiffens, the importance of the grain compressibility cannot be neglected anymore. Brignoli [49] states that a wrong choice for the Biot-Willis constant affects the accuracy of the obtained results. It should thus be taken into account that in this study, the assumptions of a negligible grain compressibility is a limitation and could lead to an error by usage of the defined formula.

Creep is not measured in the gathered experimental compaction data and neglected in the determined set of equations. All experimental data is from samples tested with conventional compression tests, in which the measured time span is not sufficient to measure the response of creep in the deformation process. When one aims to compare the results of this study to rock compressibility as observed in the producing reservoir, it should be taken into account that creep could cause a deviation between the expected reservoir behaviour and the actual reservoir compaction behaviour.

ROCK COMPACTION TRENDS

A large range in compressibility's is found for weakly to unconsolidated samples, although the bulk of the data is within the range from 0 to $2 \cdot 10^{-3} \text{ bar}^{-1}$. This is in agreement with the type curves for weakly and unconsolidated sandstones as defined by Yale [19].

Three compaction behaviour trends representing the main behaviour observed in the datasets are defined. These trends are the 'end-members' of compaction behaviour in weakly to unconsolidated sandstone. The trends are solely based on the empirical behaviour and not on an understanding of the mechanisms causing the trends in the response. When no information is available on the compaction behaviour of the producing reservoir, it could be chosen to input one of these trends as a first hand approach.

IMPACT OF DATA CONVERSION: EXPERIMENTAL & CALCULATED DATA

There is not a consistent method in literature yet to approach the data obtained for weakly to unconsolidated sandstone, where compression is mostly associated with plastic deformation. With the defined assumptions a set of equations describing plastic deformation could be derived from the equations describing linear elastic compressibility. However, these equations with a linear elastic origin may not fully describe the deformational processes.

For part of the samples the porosity reduction is measured and reported (figure 3.20a), for the other samples the pore volume reduction is calculated based on the experimentally measured compressibility or strain. The deviation between the measured and predicted data could origin from the assumptions used to derive the set of equations. The set of equations derived from the equations describing linear elastic behaviour thus not fully describe the compaction behaviour in unconsolidated sandstone. However, regarding the lack of complete experimental measurements (i.e. pore volume and permeability reduction) for unconsolidated sandstone, the equations are a reasonable alternative in obtaining a full dataset.

The equations tend to over predict the effects of compaction compared to measured data. For an increasing vertical effective stress the measured pore volume levels off, whereas the calculated pore volume reduction has an ongoing decrease in pore volume reduction. The linear elastic origin of the equation assumes that a change in the compressibility gives a proportional decrease in pore volume, for plastic behaviour the grains reconfigure and a more optimal configuration is not necessarily represented by an equivalent decrease in pore volume.

Most samples with a measured pore volume and permeability reduction are within the upper half of the range of determined pore volume reductions (figure 3.19a 3.19b). This implicates that of the defined trends the low and mid trend are confirmed by measured data, whereas the high trend solely is based on predicted values. Part of the predicted range is thus not confirmed by measurements and gives need to a) more measurements to confirm the predicted behaviour and b) the relations used for the calculations must be adapted as the predicted results are not plausible.

The calculated permeability reduction likewise deviates from the measured permeability. The initial permeability decrease has a steep reduction and then gradually flattens out, where the measured permeability has an initially flatter reduction which for part of the samples rapidly decreases after a certain vertical effective stress. This effect is studied in more detail on the four articles comprising information on both permeability reduction and on the compressibility, strain or pore volume reduction. The samples from those four papers do not show, however, the same trend. The samples of the papers of Chan [6] and Nguyen [7] show a more rapid decrease in permeability for the measured data. An effect which is likewise described by Khan [36], where it is stated that if the critical pressure is exceeded (although the exact critical pressure is unknown for the studied samples) for a sample a large reduction in permeability can be observed.

The difference could be explained by the various data conversion steps. The first step is conversion from pore compressibility or strain data to pore volume reduction data, which results in an over prediction of the measured data (figure 3.20a). The second step is the conversion from data on the pore volume reduction to data on permeability reduction (figure 3.20b). The used simplified Carman-Kozeny equation cannot fully describe the permeability reduction as a result of compaction, as it tends to under predict the impact of compaction on the permeability.

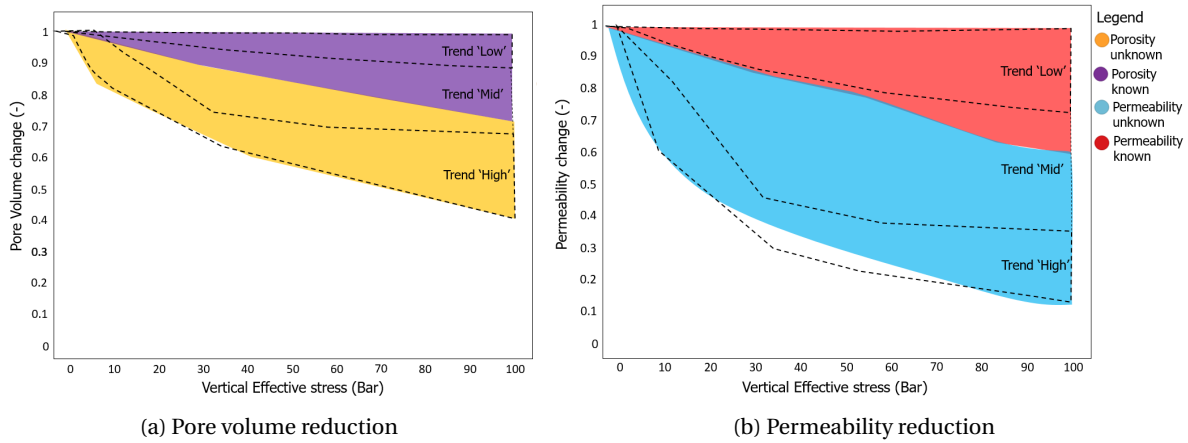


Figure 3.19: Link between the three defined trends and the differences in range between the measured and calculated rock compaction data. The high trend cannot be confirmed with the measured experimental data.

The observation that the measured permeability reductions are higher than predicted by the empirical relations could be explained by it not taking into account of the tortuosity changes within the simplified versions of Carman-Kozeny. The tortuosity is a measure for the deviation from a straight path that the fluid should encounter when flowing through the rock and is highly dependent of the size of the pore throats. Whereas grain shape, roundness, surface texture and grain orientation affect the shape of the pore throats [11]. Further studies should investigate the effect of the tortuosity compaction to be able to define a more accurate description of the impact of compaction on permeability.

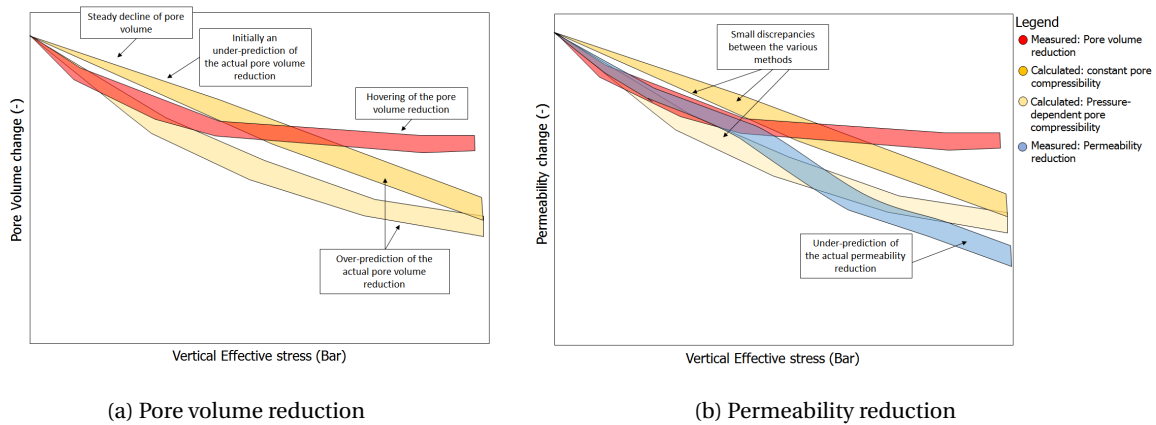


Figure 3.20: Simplified representation of the deviation between the measured and calculated rock compaction data.

TRENDS RELATED TO GEOLOGICAL CHARACTERISTICS

The description of the effect of geological characteristics on the compaction behaviour is limited by the lack of sufficient description on the literature-reported samples. The described trends on compaction behaviour, can as a result, only be seen as an indicator that a geological characteristics could have an impact of the deformational process.

Although here it is aimed to isolate the behaviour for different geological characteristics, it should be taken into account that most geological characteristics are correlated. The actual correlation between the various characteristics could only be tested with manufactured or manually adjusted samples in which only one of the characteristics is varied per test. This method is roughly the same as Hathon [4] used, however he lacked in describing the actual impact on the relevant rock characteristics for flow.

Degree of consolidation

The available data confirms the stiffening of the framework by the (minor) presence of cement. Very small volumes of overgrowth cements are thus sufficient to decrease the compressibility of a sands [4]. Where differences in behaviour within the weakly-consolidated class are a function of the compaction state of the sand at the onset of cement precipitation.

Pre-consolidation stress:

From the data for which the pre-consolidation stress is reported, it can be concluded that a higher pre-consolidation stress exhibits lower compaction and thus lower reduction of the related rock characteristics. The pre-consolidation stress (maximum burial depth) is by both Hathon [4] and Ashford [31] confirmed as an important control on the compressibility, whereas a lower pre-consolidation stress gives a higher compressibility.

Initial porosity

An increase in initial porosity increases the effects of compaction on the rock. The initial porosity is probably a representation of the optimal configuration that is obtained based on a certain depth (and according pre-consolidation stress), and the rock characteristics such as the grain size and grain shape. For porosities lower than 40% [34], the reduction is seems to be caused by an increase of cement present. Difference in behaviour within the weakly-consolidated class are a function of the compaction state of the san

Lithology

The lithology is correlated with the rock characteristics and describes the main mineralogy as present in the sample. However since the naming is highly dependent on the author and for most samples the lithology is qualified as the 'general' sand. No conclusions could be drawn regarding lithology.

Grain size

The grain size category covers two rock characteristics: 1) the main grain size present, but it is also a representation of 2) the sorting, where an increase in grain size gives an increase in the compressibility of the sample, a poorer sorting causes a decrease in the compressibility of the sample. However this effect should be evaluated in the context of pre-consolidation stress and the burial depth; these features determine how much chance the characteristics already had to influence the configuration.

The intermediate grain classes encountered in the database show the highest compressibility; this could be explained by the fact that for a manufactured sample a poorer sorting can lead to a further optimization of the configuration; by the smaller sand grains moving in between the open pore space. Where as for a buried sample this process already took place and the influence of the impact of the less compressible character of smaller grains increases and prevents further compression.

In literature no consistency is found on the impact of the grain size class on the rock compaction. Chuhan showed that the fine grains sand will have a higher porosity after compaction than its coarse grained counterpart [50]. This is most likely the result of a higher compressibility for the coarse grain size class [4]. Our results show a maximum compressibility for the intermediate grain size classes. Whereas Ashord states that a larger grain size improves the resistance to movement by the rock [31].

Grain shape

The grain shape (angularity) of the grains determines the optimal possible configuration. The intermediate grain shape classes (subangular - subrounded) seem to exhibit the highest compaction. This could be explained by the fact that an increase in angularity could increase the efficiency of the grain configuration. However, with an increase in angularity, the friction on the grain surface also increases. For low formation pressures, relevant for this study, this lowers the compressibility is lower. So an optimum is found and expected for the intermediate classes.

Ductile grains

Although there is not enough data available on the ductile grain content of the studied data, it can seen that an increase in ductile grains, increases the compressibility of the sample, which is in line with Hathon [4]. However the available data seems to indicate a lower impact than stated by Hathon. For the ductile grains samples it would be interesting to determine the exact effect on the pore volume and the permeability reduction. Since it could be possible that due to the effects of interbedding in the soft material and smearing

of the ductile material, the ductile grain related deformational processes affect the permeability reduction more than the pore volume reduction. Although pore throats could be blocked, porosity remains relatively unaffected

Feldspar

Since feldspar is a weak mineral, it could be expected that the sample compresses at a lower stress level. The frictional forces or grain breakage occur at a lower effective stress. However, this could not be confirmed by the literature data, since not enough information is available.

Proposed correlations

In the following an attempt is made to classify the importance of the different geological characteristics on compaction behaviour. This classification is based on the width of the range in rock characteristics and the ability to determine clear trends related to a certain geological characteristic, which are indications of a potential control on the rock compaction.

The impact of the geological characteristics on respectively a change in pore volume and a change in permeability are suggested by combining the observed trends in behaviour of the various geological characteristics with the mechanisms of deformation 2. Among others it is reasoned which geological characteristics could have the biggest impact on tortuosity changes and which rock characteristic could prevent further compression of the pore volume for a certain grain configuration.

An optimal combination of the geological characteristics that enhance the deformational process could cause the high deformation behaviour as reported, whereas the initial porosity seems to be the main controlling parameter. The initial porosity is, as stated, a representation of other geological characteristics such as the burial depth and pre-consolidation stress. In further studies it would be useful to determine whether initial porosity class a certain range in compressibility's can be determined.

A first attempt is done by linking the defined empirical relations to a certain area of geological characteristics, such that for a reservoir with a certain combination of reservoir characteristics, the according trend can be used as a first approximation in the reservoir analysis (figure 3.21 3.22).

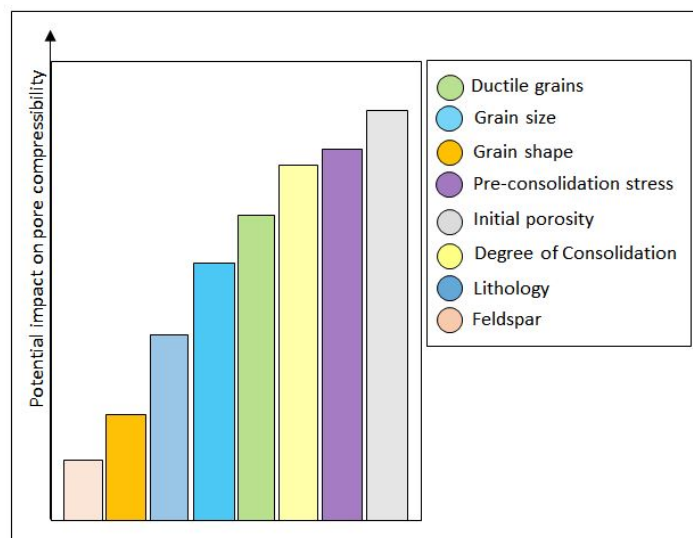


Figure 3.21: Indication of the importance of geological characteristic on the compaction of weakly to unconsolidated sandstone

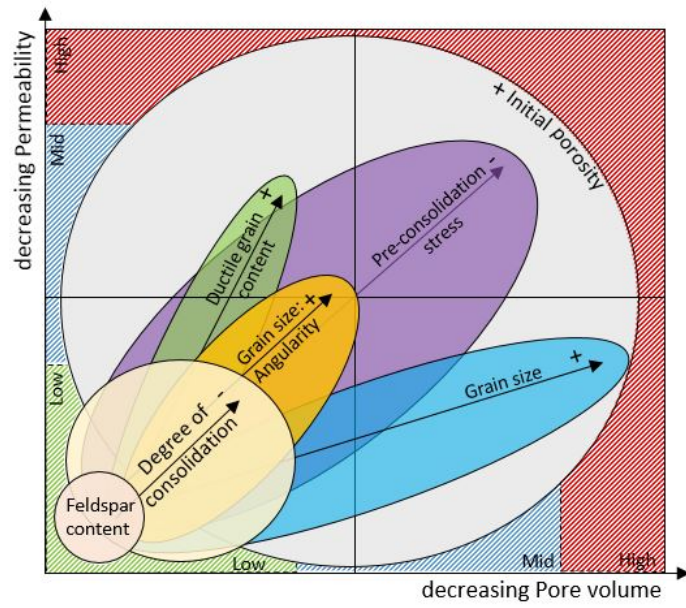


Figure 3.22: Indication of the influence of geological characteristic on the compaction of weakly to unconsolidated sandstone

4

RESERVOIR SIMULATIONS

4.1. METHODOLOGY

In the following the effect of rock compaction on the production behaviour of an unconsolidated shallow gas reservoir is studied with a numerical simulator. A generic model is established based on a simplified representation of an average Dutch shallow gas field. The skeleton of the generic model is filled with the reservoir characteristics as defined based on the simplified representation. Various simulations are initially performed to test the impact of the trends in the pressure-dependent rock characteristics (pore volume and permeability) during production-induced compaction on the reservoir productivity. Furthermore the impact of various uncertainties due to a lack of data or the data conversion is assessed by determining the possible span in the recovery factor.

4.1.1. RESERVOIR CHARACTERIZATION: DUTCH SHALLOW GAS FIELDS

The reservoir characteristics used in the simulations (table 4.1) are assumed to be representative of the Dutch shallow gas reservoirs situated in the Northern sector of the Dutch North Sea. The amount of data is limited and the quality is of varying nature, though the simplified reservoir model is considered to be valid for a typical unconsolidated shallow gas reservoir in the Netherlands.

The Dutch shallow gas reservoirs encounter top reservoir between 400 to 800 meter true vertical depth (TVD) below sea level (bsl). The gas column length detected within the reservoirs varies between 10 to 40 meter. The limited length of the gas column can be related to the strength of the seal in this relative young and shallow setting [42]. The temperature at the reservoir depth can be calculated based on the temperature gradient. The temperature is approximated by 32 °C.

Most of the Dutch shallow gas reservoirs have a three or four way dip closure occasionally bounded by a fault, surrounded by sealing clay layers. These are part of a system of westward prograding shallow marine sands and shales deposited by the Eridanos delta [51]. The reservoir lithology comprises relatively immature bioturbated glauconite sands deposited in a lower shoreface setting [42]. These are fine grained, poorly to unconsolidated with a variable clay content. Diagenesis appears to be minimal with grains in point contact or floating which suggests very little effect from compaction due to burial [42]. For none of the reservoir the presence of an aquifer is proved.

Simplified reservoir characteristics		
Parameter (Initial)	Unit	Value
Porosity	0.3	-
Permeability	200	mD
N/G	0.95	-
Relative Permeability Water at $S_w = 1$		-
Relative Permeability Water at $S_g = S_{gr}$		-
Relative Permeability Gas at $S_w = S_{w,min}$		-
Irreducible water saturation	0.2	-
Critical water saturation	0.22	-
Critical gas saturation	0.05	-
Corey coefficient (water)	4	-
Corey coefficient (gas)	2	-
Gas gravity	0.5594	kg/m ³
Reservoir temperature	28	°C

Table 4.1: The simplified reservoir characteristics used for the reservoir simulations

4.1.2. MODEL DEFINITION

RESERVOIR MODEL

The reservoir model is constructed using the simple grid tool in Petrel. The reservoir is approximated by a homogeneous tank model, with no-flow boundaries. The skeleton of the generic model (table 4.2) is filled with the defined representative reservoir characteristics (table 4.1). This simplification is necessary to allow comparison between various scenarios. The model is homogenous with a vertical-to-horizontal isotropy. A heterogeneous or layered reservoir with an anticlinal structure and faults would have been a more realistic representation, but would make the quantitative comparison of the impact of reservoir compaction more complicated.

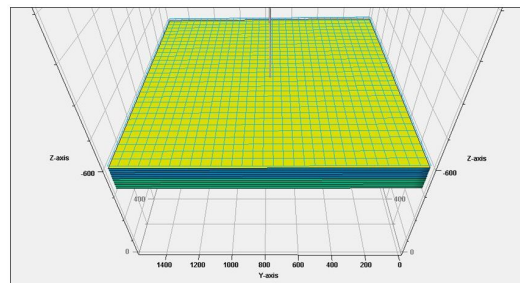


Figure 4.1: Reservoir model as used for the simulations

For modeling purposes, the top of the reservoir is set at 600 meter TVD, the GWC at 630 meter TVD. The gas initially in place (GIIP) of the reservoir is 1 Bcm, which results in a reservoir size of 1530 by 1530 meter. For the simulations the grid size is set as 50x50, and is in the vertical direction represented in 10 layers. The right balance between accuracy and grid size was determined during the preliminary runs.

The reservoir is simulated with an unrestricted flow condition and a constant bottom hole pressure (BHP) of 30 bar. It was chosen to produce with an unrestricted flow condition such that the effect of compaction could be tested. The constant BHP is based on the assumption of a 15 bar inlet of the compressor at surface and loss is pressure due to well bore friction of about 15 bar. The perforations are applied through the entire reservoir thickness.

Due to the lack of reliable capillary pressure data it is decided to use the assumption that the gas water contact is equal to the free water level. This equality means that there is no transition zone and that the gas zone above the GWC is at irreducible water saturation. This is in line with the general statement that in a high porosity medium low capillary forces exist and thus a lower water saturation.

Input parameters Simulation - Base Case model		
Parameter	Unit	Value
BHP	30	Bar
Nr of Grid cells	50 x 50	-
Number of layers	10	-
Reservoir thickness	30	m
Reservoir size	1530 x 1530	m
Reservoir pressure	63	Bar

Table 4.2: The model properties as used for the base case model.

To summarize, the following assumptions have been made:

- The reservoir is homogenous and can be represented by a square tank model with no-flow boundaries.
- The reservoir is produced with an unrestricted flow condition and a constant bottom hole pressure of 30 bar.
- The gas water contact is equal to the free water level.
- The reservoir deformation comprises only uniaxial strain.
- The impact of compaction on the reservoir can be quantified as a change in the pore volume and transmissibility.

4.1.3. SIMULATION

Preliminary runs were carried out to assess the effect of the reservoir model variables (grid size, etc) on the output. The results are used to define the optimal model characteristics used to test the impact of various trends on the compaction behaviour. The reservoir parameters are then kept constant.

SIMULATION SETUP

To test the effects of reservoir compaction on the reservoir simulations Eclipse 100 is used. The Eclipse keyword ROCKTAB gives the possibility to account for the effects of compaction. The effects of compaction can be expressed in the reduction of pore volume (porosity) and the decrease of transmissibility (permeability) as function of the production related change in the stress field. This is done by incorporating a pressure-dependent pore volume multiplier (Pvm) and transmissibility multiplier (Tm) (table 4.3), which range from one (100% of the original characteristic is intact) to zero (0% of the original characteristic is intact). The pore volume multiplier (Pvm) is equal to the change in pore volume. The transmissibility multiplier is equal to the change in transmissibility, which can be approximated by the permeability reduction (equation 3.52).

Quantity	Eclipse reservoir simulator input
Relative change in Pore Volume	Pore Volume Multiplier (Pvm)
Relative change in Permeability	Transmissibility Multiplier (Tm) height

Table 4.3: Conversion as is necessary to incorporate the relative change in pore volume and permeability within the reservoir simulations.

The use of the Eclipse keyword (figure 4.2) differs from the standard Petrel input, in which the permeability reduction is neglected. The change in pore volume (initial depended on volume, porosity and net-to-gross) not automatically linked to a subsequent change in the transmissibility (initially depended on permeability, area, net-to-gross and length). The standard input requires a constant pore volume compressibility during production. The usage of the ROCKTAB keyword gives the possibility to use the manually calculated pore volume reduction and permeability reduction coefficients. This manual input allows the input of a varying pore volume compressibility for the calculations.

The reservoir characteristics affected by the depletion-induced compaction of the reservoir are adjusted based on the new stress distribution. The modification of the pore volume and transmissibility is treated explicitly: it only affects the subsequent time step. The ROCKTAB keyword is used in combination with related keywords for the reservoir simulations. The compaction is assumed to be irreversible and not induced by water (ROCKCOMP). The compaction tables can be entered as function of the effective stress (ROCKOPTS). This calculation requires the input of the overburden (vertical) stress (OVERBURD).

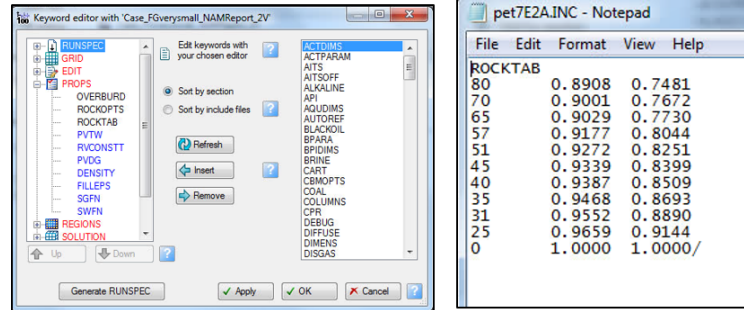


Figure 4.2: Usage of the Petrel interface to incorporate the ROCKTAB keyword in Eclipse100

OUTPUT

The impact of reservoir compaction on the performance of the reservoir can be described by several parameters. The effect on the production rate is easiest detected in the cumulative production curve. Whereas the recovery factor, a measure of the cumulative production under certain restriction scaled to the initial gas in place, gives the performance of the reservoir.

The recovery factor is calculated with the following equation:

$$RF = \frac{G_p \text{ (by a BHP of 30 bar)}}{GIIP}$$

To be able to recognize the potential effects of compaction during production, the MBE is used in the form of a P/Z-plot. The P/Z plot as could be plotted at the end of field life, is plotted with the help of Eclipse. Note that this is a P/Z plot which is not corrected for the effects of rock and water compressibility [52].

PRELIMINARY RUNS

To investigate the optimal modeling characteristics, preliminary runs are performed. The scenario's presented in table 4.4 have been analyzed. The effect of several model characteristics are investigated and accounted for and used to optimize the base characteristics of the model.

In the sensitivity analysis the effect of using different reservoir model characteristics is tested under the constraint of unchanged model properties. Furthermore the simulation time and reporting frequency are unchanged for every simulation.

The results of the pre-liminary runs show that the impact of the grid characteristics (number of grid cells, figure 4.3) has negligible impact. For the reservoir characteristics only the presence of anisotropy or heterogeneity within the reservoir model could severely impact the prediction of the ultimate recovery. An anisotropy with a horizontal to vertical permeability ratio of 0.1 can lower the recovery factor for the high trend up to 36.6%. A heterogeneous reservoir encounters for the high trend, with respect to the base case, a variation on the recovery factor up to 50%. Due to the heterogeneity lower production rates are obtained within the reservoir. A variation in the gas initially in place (GIIP) mostly affects the recovery factor if the GIIP of the reservoir model is increased. The variation has a negligible maximum of 0.5%, but it should be considered that this amount increases for a further increase of the GIIP. The flow rate affects the recovery factor only for the flow rate of 100 000 m³/day. The restriction of flow in combination with a production period of 30 years, cuts off the production while the reservoir is not yet at a BHP of 30 bar.

Preliminary runs				
	Parameter	Value of simplified reservoir characteristic	Unit	Note
Reservoir volume	GIIP	0.5	Bcm	1080m x 1080m
		1	Bcm	1530m x 1530m
		2	Bcm	2165m x 2165m
		3	Bcm	2650m x 2650m
	Thickness/Width	30	m	Base case model
		45	m	0.5 Bcm, 1 Bcm, 2 Bcm, 3 Bcm
Reservoir structure	Square model	-	-	-
	Anticline	-	-	-
	Layered	10	-	Base case model
		25	-	-
Nr of Gridcells	25 x 25	-	-	
	50 x 50	-	Base case model	
	100 x 100	-	-	
Operating parameters	Homogeneous	-	-	-
	Heterogeneous	KxyKz = 0.1	-	-
		Por = Normal(0.32,0.03) Perm = 10 ^{28.302·φ-8.0656}	-	-
	Flow rate	Unrestricted flow	[mD]	-
100 000		sm ³ /day	-	-
200 000		sm ³ /day	-	-
400 000		sm ³ /day	-	-

Table 4.4: The parameters varied during the pre-liminary runs.

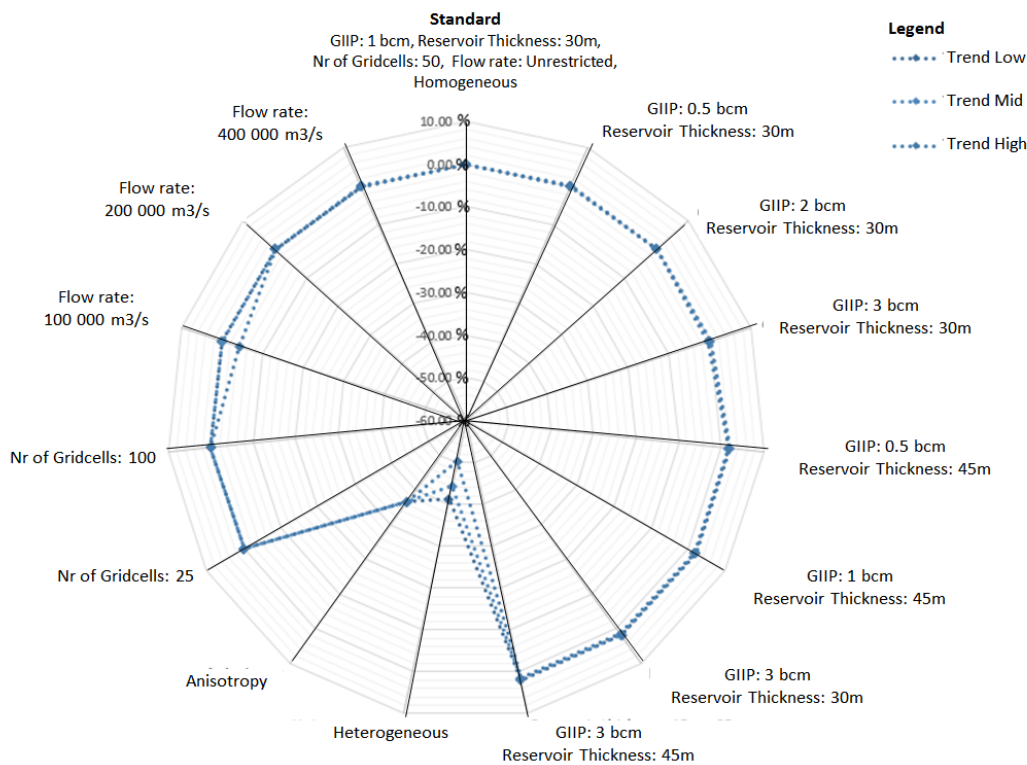


Figure 4.3: Results of the preliminary runs; the results are given as the deviation (in %) with respect to the base case model

SIMULATION SCENARIOS

Multiple scenarios have been tested by combining the reservoir model with a compaction-behaviour trend based on rock compaction trends defined in chapter 3. A trend is here defined as a characteristic development of the compaction related reservoir characteristics (here: pore volume and permeability). To investigate the impact of compaction on the performance of the reservoir the following scenarios are proposed as input for the generic model, related to: 1) trends of compaction behaviour, 2) uncertainty related to data conversion, 3) the effect of pressure-dependent pore compressibility and 4) geological trends in compaction.

The trends defined based on the characteristic development of the compaction related reservoir characteristics are used to study the effect of reservoir compaction in shallow unconsolidated gas reservoirs. Per trend are furthermore three simulations performed, to investigate into detail the separate effects of pore volume and permeability reduction in reservoir simulation. First both the pore volume and the permeability are assumed to reduce. In the standard scenario both permeability and porosity loss will contribute to the estimated cumulative production of the conceptual reservoir. The impact of the pore volume reduction is assessed by neglecting potential loss of permeability during simulation. Only the pore volume change as a function of depletion and stress reduction is taken into account. The impact of permeability reduction on the estimated cumulative production is demonstrated by using only the permeability variation in the simulations.

Permeability reduction due to compaction is often a not measured quantity during compressional experiments. The compaction-induced permeability reduction then only can be predicted with the help of an empirical relation. The empirical relations describing the relation between porosity and permeability (equation 3.50 & 3.51) are only a valid approximation under certain circumstances. The uncertainty related to this simplification is assessed by comparing the calculated permeability variation with a measured permeability variation for the samples with information on both the compressibility and the permeability variation.

The conventional input for a reservoir simulator is a constant pore compressibility over the production period. The reservoir simulator calculates for this pore compressibility, the according pore volume (and transmissibility) variation. The impact of the assumption of a constant (pressure-independent) pore compressibility is tested with the defined end-member trends. This is done by comparing the pore volume and transmissibility variation based on a constant pore compressibility with the pore volume and transmissibility variation calculated based on a pressure-dependent pore compressibility. The calculations are done with the formula presented in chapter 3.

The geological trends as defined in chapter 3 are the basis of the simulations used to determine the uncertainty related to a lack of geological data. The defined geological end-members give a span in possible recovery factors. An uncertainty range is defined, which represents the maximum error made when the reservoir compaction is defined based on a non-valid geological trend.

4.2. RESULTS

4.2.1. ROCK COMPACTION TRENDS

The three trends (defined in chapter 3) (figure 4.4 4.5) represent the main behaviour of pore volume and permeability reduction as can be found for weakly to unconsolidated sandstone. With these trends the impact of compaction on an unconsolidated gas reservoir is studied.

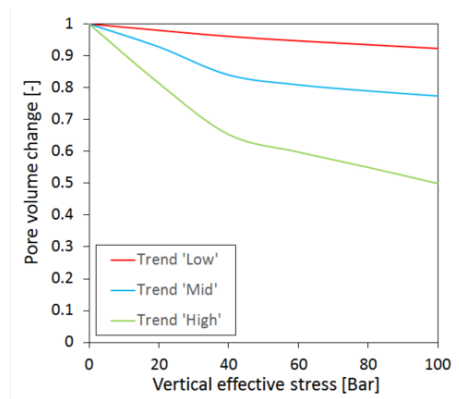


Figure 4.4: The change in pore volume for the three trends.

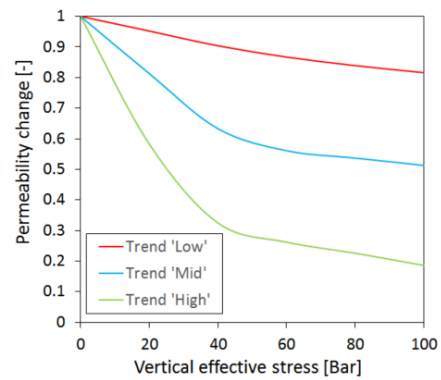


Figure 4.5: The change in permeability for the three trends.

The reservoir simulations for the three trend show clear differences in production behaviour and recovery. The cumulative gas production (i.e. the recovery) is significantly higher for the high trend, whereas the 'low' trend shows a significantly lower cumulative gas production. For the gas production rate and the reservoir pressure, the main differences are detected within the first 2000 days.

The 'high' trend (scenario) has initial the highest gas rate, but the gas rate decreases rapidly and becomes, although only with a small difference, the lowest (figure 4.7). After about 1/60 of the production time, the gas rate of the 'low' trend has a slightly higher decline in gas rate than the other scenarios and obtains the lowest production rate. None of the in the gas rate detected variations is covered in the reservoir pressure (figure 4.33). For all three scenarios the reservoir pressure has a substantial fall but obtains with ongoing production a more gradual decrease. The recovery factor varies about 20% between the 'low' and the 'high' scenario (figure 4.10).

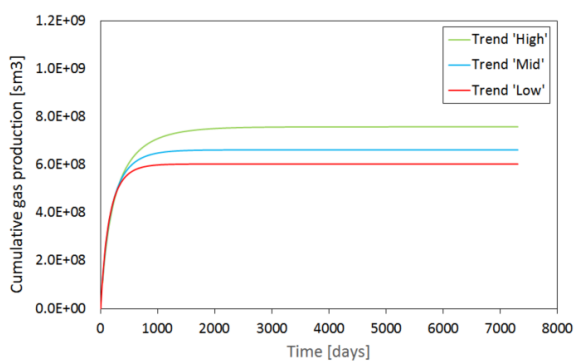


Figure 4.6: Cumulative gas production resulting from the reservoir simulations with the defined rock compaction trends.

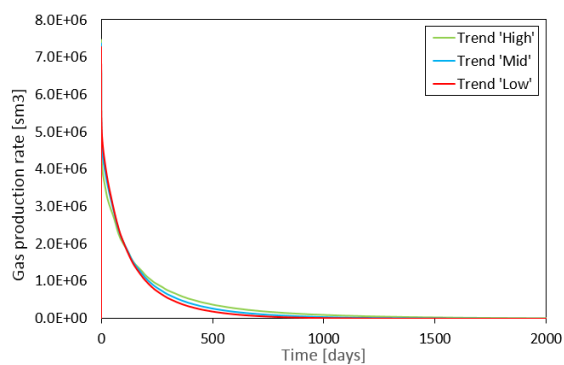


Figure 4.7: Gas production rate resulting from the reservoir simulations with the defined rock compaction trends. The time covered by this graph is only 1/4 of the total production period.

The P/Z-plot shows a clear distinction in the behaviour for the 'low', 'medium' and 'high' trend (figure 4.9). The 'low' trend is given by a straight line with the rapidest decrease. The medium trend decreases less than the 'low' trend, but shows a slight bending with increasing cumulative production. The 'high' trend starts with a straight P/Z-line but clearly starts bending for an increasing cumulative production.

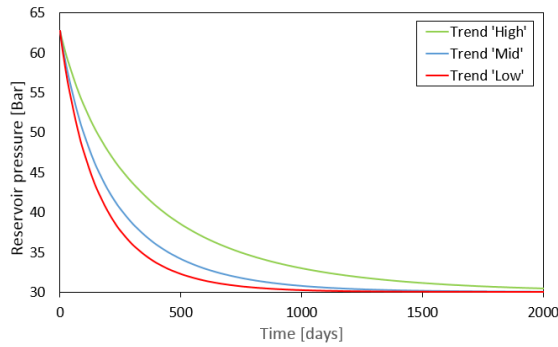


Figure 4.8: Reservoir pressure resulting from the reservoir simulations with the defined rock compaction trends. The time covered by this graph is only 1/4 of the total production period.

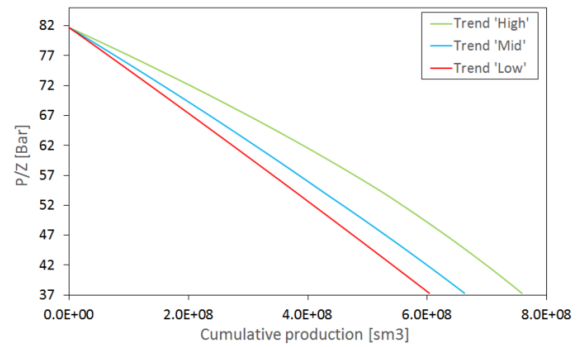


Figure 4.9: P/Z-plot resulting from the reservoir simulations with the defined rock compaction trends.



Figure 4.10: Recovery factor resulting from the reservoir simulations with the defined rock compaction trends.

The production-induced reservoir depletion induces a change in the pore volume and permeability within the reservoir. The impact of drawdown on compaction is visualized by plotting the distribution in the relative change in the pore volume and permeability (figure 4.11 & 4.12). The pore volume and permeability decrease the most near the well and this effect diffuses with on-going production.

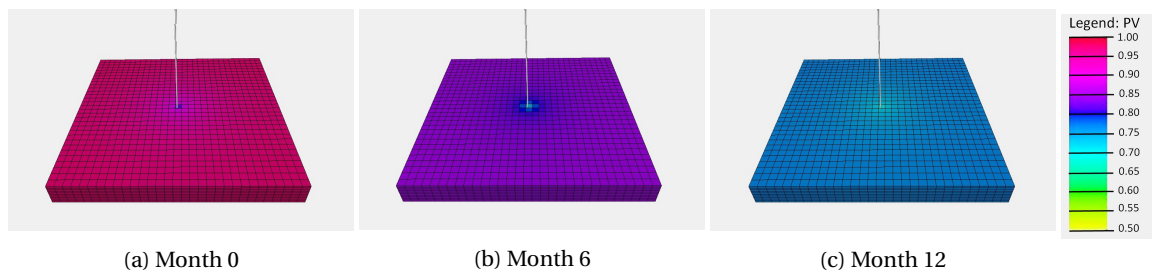


Figure 4.11: Pore volume reduction during the first year of production for the 'high' trend.

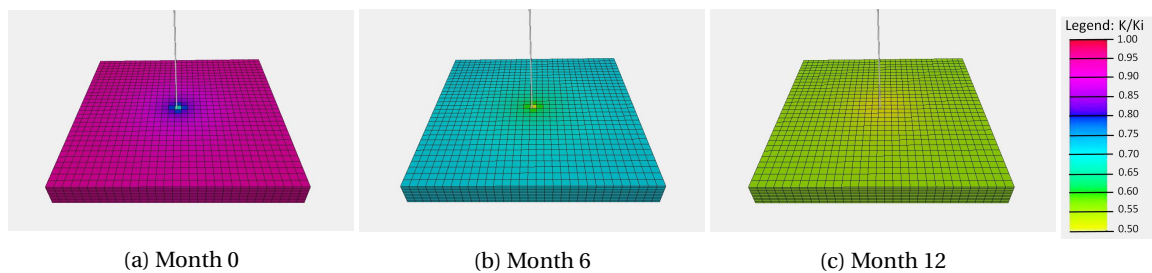


Figure 4.12: Permeability reduction during the first year of production for the 'high' trend.

Impact of Pore volume and Permeability loss on reservoir production

Three simulations are performed per trend, to investigate the separate effects of pore volume and permeability reduction in reservoir simulation. The 'low' trend is in the middle of the range validated by measured data 3, but the differences between the various scenarios are minimal. The 'mid' trend represents approximately the boundary of the measured pore volume and permeability variations found for the gathered samples. The results of the 'high' pore volume reduction scenario show the clearest deviation and thus are discussed here in detail (figure 4.13 & 4.14). The results of the simulations using the 'mid'- and 'low'- trend can be found in Appendix D.

The lowest cumulative gas production is found for the scenario with only permeability reduction (figure 4.15) whereas the highest cumulative production is found for the scenario with only pore volume reduction. For the gas production rate (figure 4.16) initially the same order can be found. Whereas the standard scenario (both decrease of pore volume and permeability) has initially the highest gas rate. But with ongoing production the decline of the standard and the scenario with only permeability reduction (PR) have a more rapid decline in gas rate than the scenario with only pore volume reduction (PV). After 360 days of production PV scenario has with respect to the other scenarios a more pronounced decrease in gas rate. After 655 days of production the gas rate of the pore-volume reduction scenario is less than the gas rate of both other scenarios. The reservoir pressure (figure 4.17) shows initially the most dramatic fall for the permeability-reduction scenario, however as production continues the decrease in reservoir pressure levels off. The PV scenario shows a longer period of rapid decrease in the reservoir pressure before gradual decline is obtained. As a result, after day 305, the reservoir pressure of the PV scenario is lowered the most. The recovery factors (figure 4.19) for the various scenarios confirm the results from the cumulative production plot. It is found that the recovery for the PV scenario and standard scenario are equal. For the scenario with only a permeability reduction the recovery factor is about 20% lower.

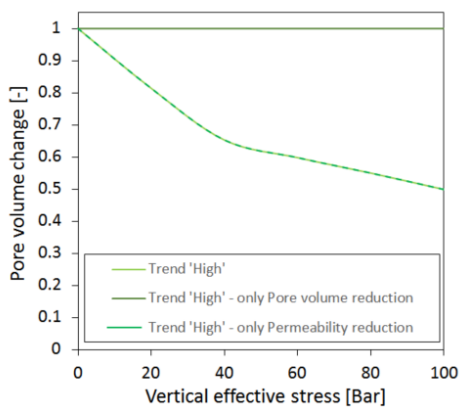


Figure 4.13: The change in pore volume for the three input scenario's of the 'high' trend.

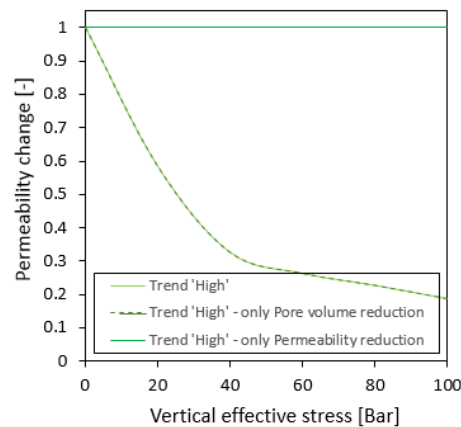


Figure 4.14: The change in permeability for the three input scenario's of the 'high' trend.

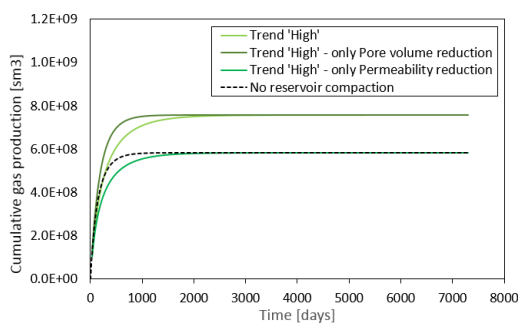


Figure 4.15: Cumulative gas production resulting from the reservoir simulation with the defined 'high' rock compaction trend.

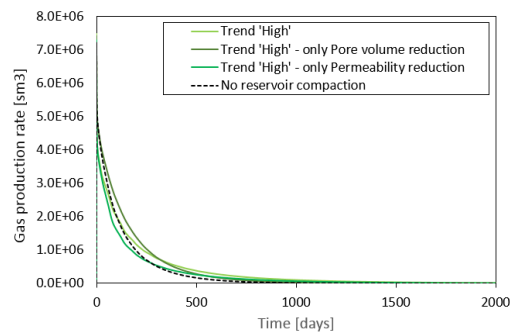


Figure 4.16: Gas production rate resulting from the reservoir simulation with the defined 'high' rock compaction trend. The time covered by this graph is 1/4 of the total production period.

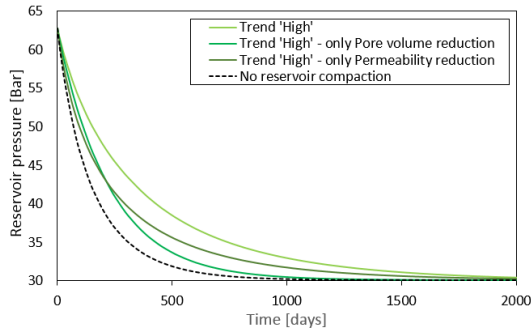


Figure 4.17: Reservoir pressure resulting from the reservoir simulation with the defined 'high' rock compaction trend. The time covered by this graph is only 1/4 of the total production period.

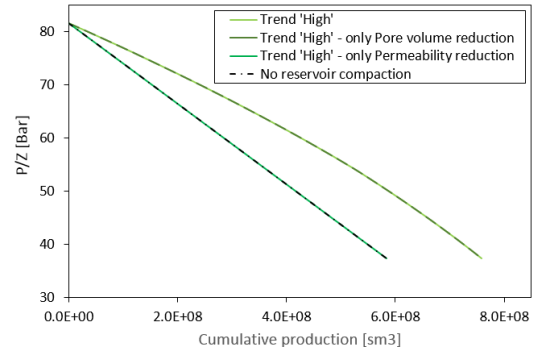


Figure 4.18: P/Z-plot resulting from the reservoir simulation with the defined 'high' rock compaction trend.

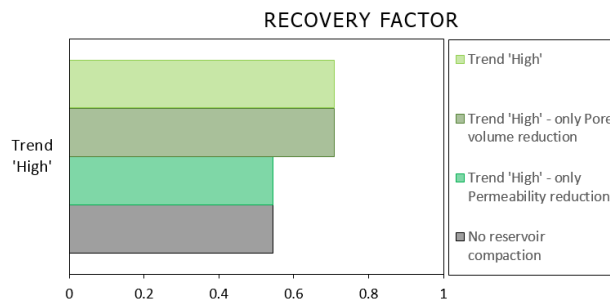


Figure 4.19: Recovery factor resulting from the reservoir simulation with the defined 'high' rock compaction trend.

4.2.2. IMPACT OF DATA CONVERSION: EXPERIMENTAL & CALCULATED DATA

Four papers, comprising 24 samples, have data both on permeability reduction and on rock compressibility or pore volume reduction. The predicted permeability variation based on calculations and the measured permeability reduction with their according (equal) pore volume reduction are used as scenarios for the reservoir simulations to determine the uncertainty related to the lack of measured data.

CHAN

The difference between the calculated and the experimental data on the loss of permeability is marginal and has a maximum of 0.0014% (figure 4.20).

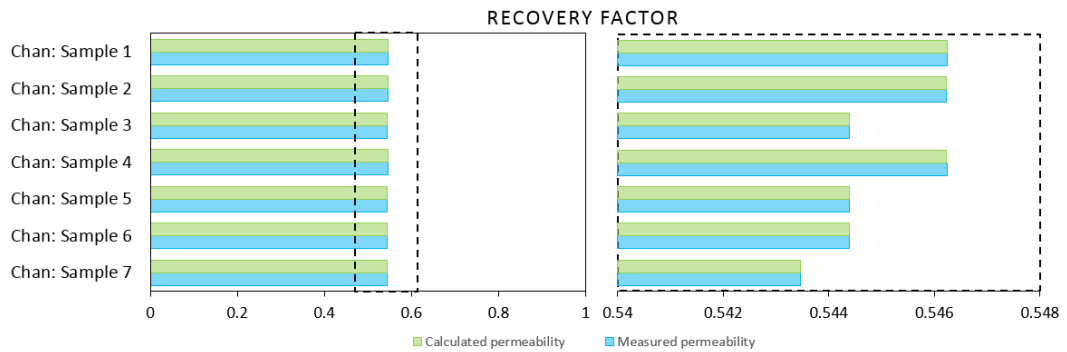


Figure 4.20: Recovery factors as found for the calculated and measured permeability reduction data for the samples presented by Chan [6].

NGUYEN

For the four samples as are presented by Nguyen [7] the maximum deviation between the provided permeability reduction data and the calculated permeability reduction based on the axial strain is maximum 0.018% (figure 4.21). The error between the experimental permeability reduction data and the volumetric-strain based permeability reduction calculation has a maximum of 1,4% for the four samples.

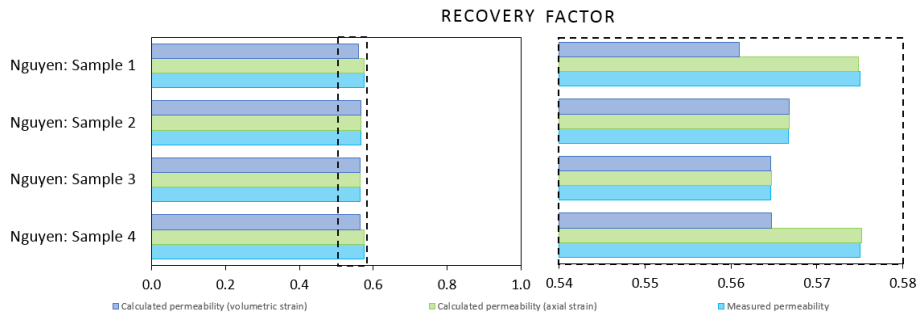


Figure 4.21: Recovery factors as found for the calculated and measured permeability reduction data for the samples presented by Nguyen [7].

GOLDSMITH

Three of the six samples as are presented by Goldsmith [8] show no deviation between the measured and the calculated permeability reduction. The range in uncertainty caused by the assumptions as done in the calculations to determine the permeability reduction has a minimum of 0.0007% and a marginal maximum of 0.0018% (figure 4.22).

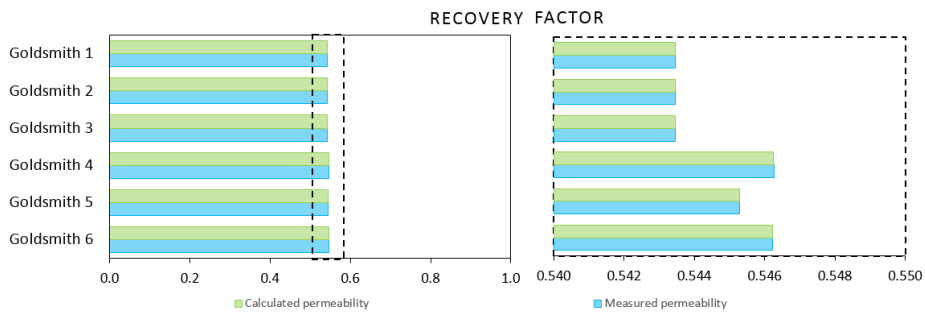


Figure 4.22: Recovery factors as found for the calculated and measured permeability reduction data for the samples presented by Goldsmith [8].

MATTAX

For the three samples of Mattax [9] a maximum error of 0.009% is found (figure 4.23).

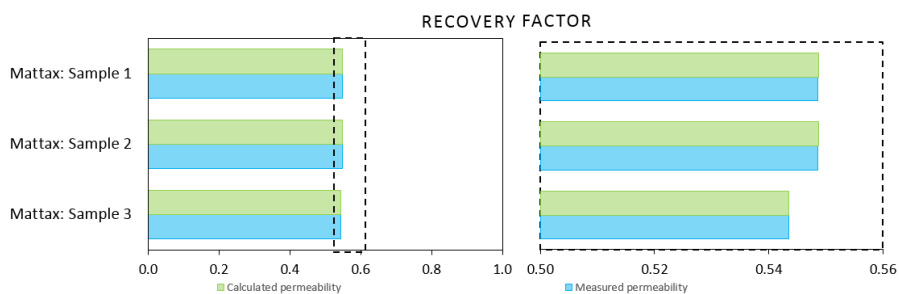


Figure 4.23: Recovery factors as found for the calculated and measured permeability reduction data for the samples presented by Mattax [9].

4.2.3. PRESSURE-DEPENDENT PORE COMPRESSIBILITY

A variation of 9.6% can be found depending on the choice of using in the model a pressure-dependent pore compressibility or a constant pore compressibility (figure 4.24).

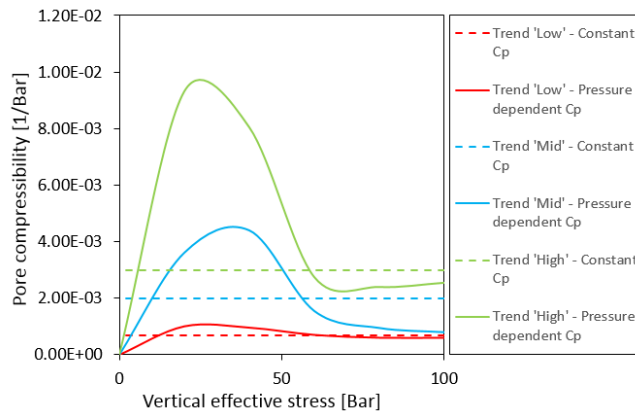


Figure 4.24: Difference between a constant and a pressure-dependent pore compressibility for the defined trends in compaction behaviour of unconsolidated sandstones

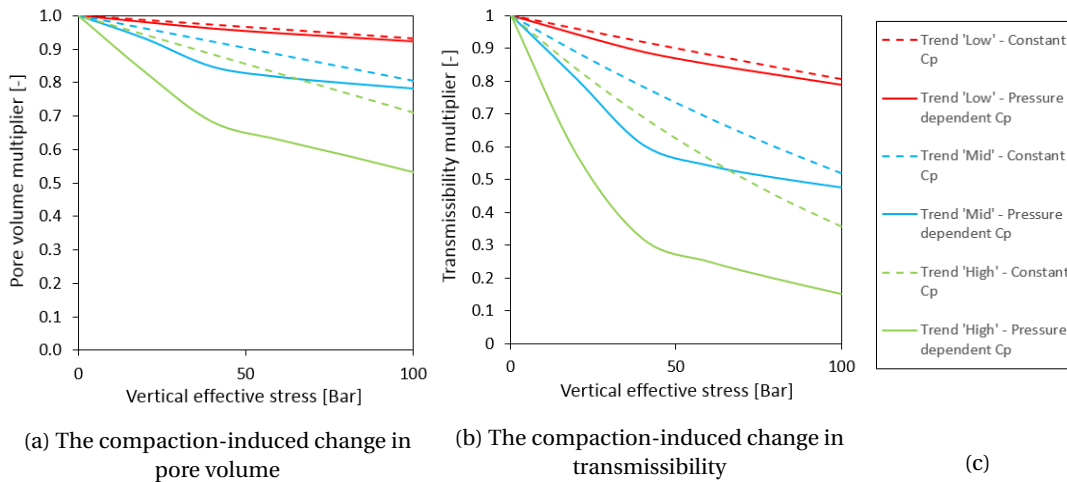


Figure 4.25: Discrepancy between the calculated change in pore volume and transmissibility caused by the choice of a constant or a pressure-dependent pore compressibility for the defined trends in compaction behaviour of unconsolidated sandstones.

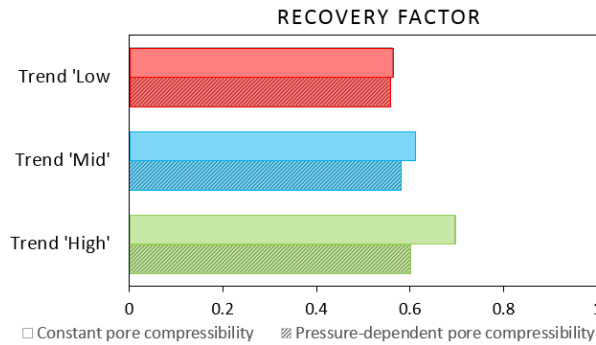


Figure 4.26: Recovery factors as found by the reservoir simulations with a constant or a pressure-dependent pore compressibility for the defined trends in compaction behaviour of unconsolidated sandstones.

4.2.4. TRENDS RELATED TO GEOLOGICAL CHARACTERISTICS

The geological trends as defined in chapter 2 are the basis of the simulations used to determine the uncertainty related to a lack of geological data. The defined geological end-members give after simulation a span in possible recovery factors. An uncertainty range can be / is defined, which represents the maximum error made when the reservoir compaction is defined based on a non-valid geological trend.

DEGREE OF CONSOLIDATION

Based on the recovery factors as found for the geological end-members, related to the consolidation state of the rock, an uncertainty range of 3% is found (figure 4.27).

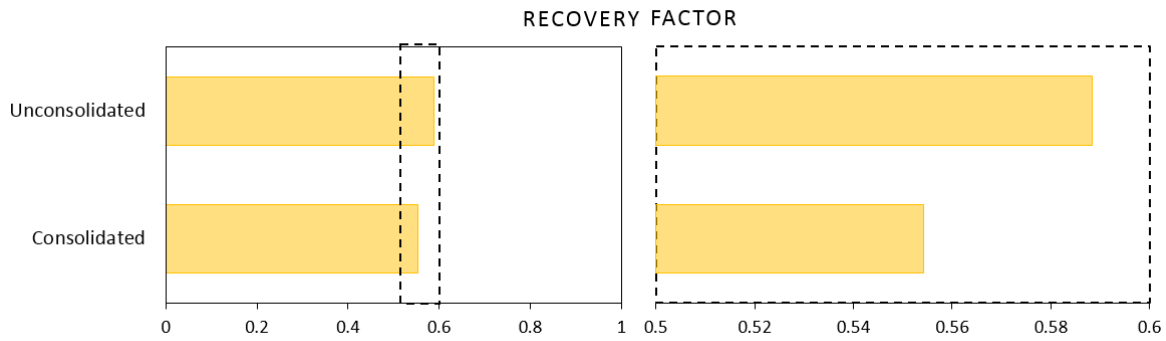


Figure 4.27: Recovery factors with the compaction trends based on the consolidation state of the reservoir.

INITIAL POROSITY

For the initial porosity the recovery factor is determined per porosity class. The recovery increases with an increase of the initial porosity. The uncertainty range as is given by the range of possible recovery factors for the various initial porosity classes is 8% (figure 4.28).

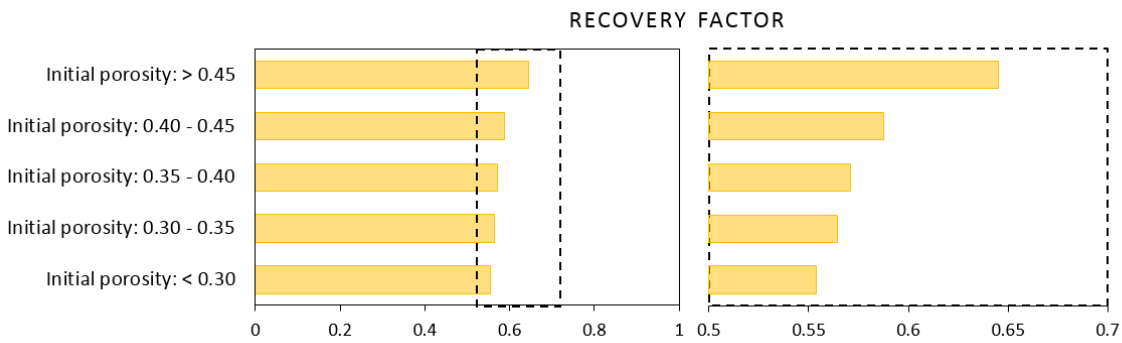


Figure 4.28: Recovery factors with the compaction trends based on the initial porosity of the reservoir.

GRAIN SIZE

The recovery factors as defined by simulation show an optimum for the fine to medium grain size class. The recovery for this grain size class is almost 5% higher than for the up following fine grain size class (figure 4.29). The uncertainty in recovery factors for the various grain size classes has a range of 8%.

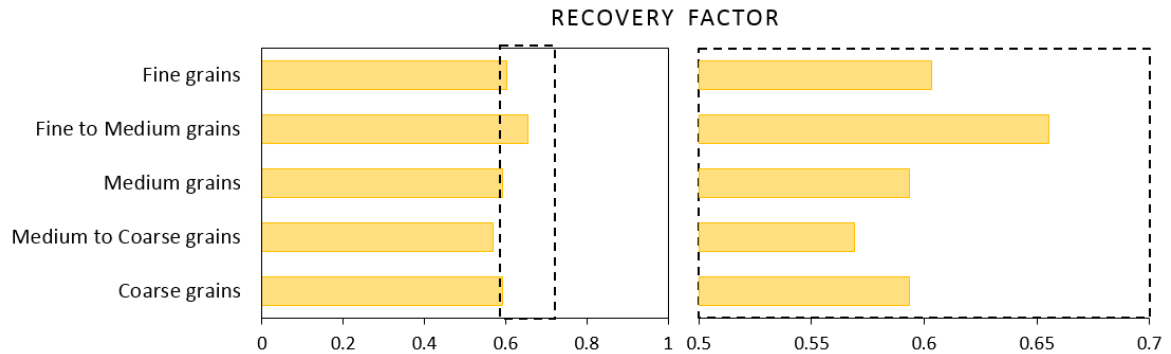


Figure 4.29: Recovery factors with the compaction trends based on the average grain size of the reservoir.

GRAIN SHAPE

Based on the data as provided from the database the subangular grain shape class has the highest recovery factor. The lowest recovery factor is found for the subrounded to subangular grain size class. The span in recovery factors has a range of about 5.5% (figure 4.30).

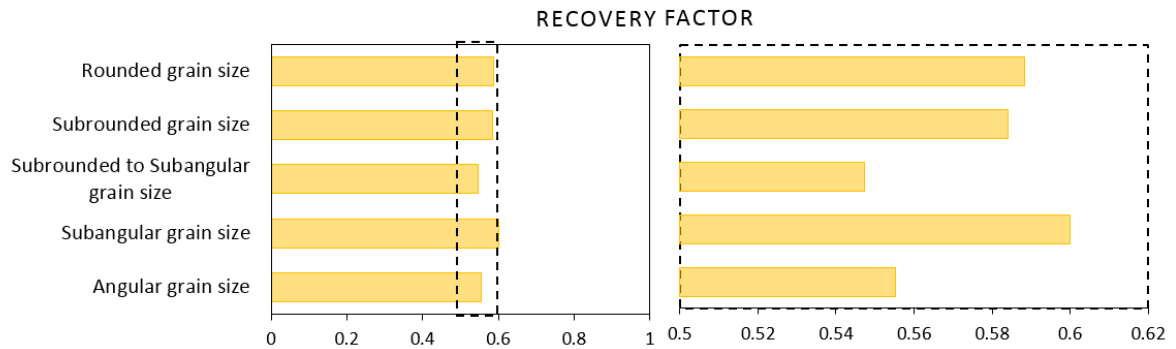


Figure 4.30: Recovery factors with the compaction trends based on the average grain shape of the reservoir.

4.3. DISCUSSION

In the following the reservoir model and the simulation results are reviewed.

RESERVOIR MODEL

The reservoir is approximated by a homogeneous tank model with no flow boundaries. Although the simplified reservoir model is considered to be a valid simplification for a typical shallow gas reservoir in the Netherlands. This homogenous model should be compared to its heterogeneous counterpart, where a spread and a vertical-to-horizontal anisotropy in reservoir characteristics are incorporated within the model. The coupling between fluid flow and reservoir compaction within a heterogeneous model can be optimized by using different compaction curves for the various ranges in reservoir characteristics such as the porosity classes. Due to a variation in the impact of compaction on the various reservoir characteristics classes, the impact of compaction on low permeable zones may induce non-producing areas. These processes could cause limitations in the reservoir development, as the flow might be bounded to certain flow paths.

A sensitivity study with varying reservoir characteristics (such as the porosity and fluid saturation) should be carried out to verify the found results for a broader range of reservoir characteristics. However, as the impact of the geological reservoir characteristics, as studied in chapter 3, is not yet fully understood, it will be a challenge to accurately implement the effect of varying geological characteristics with the according compaction curves.

Another simplification is the use of all no-flow boundaries in the model. In reality, many gas reservoir are not completely closed but subject to some water influx from an aquifer. Water breakthrough would have an impact on the recovery factor. This effect combined with porosity and permeability reduction, as a result of compaction, was not tested in the simulations. However, it could be postulated that if compaction occurs and leads to a significant permeability reduction it would also directly affect the water relative permeability and probably retard water breakthrough as water flow through the compacted pores would be more hindered than gas flow. Additional simulations are required to test the effects of reservoir compaction in gas reservoirs with an active aquifer.

In addition, the effect of drawdown on compaction near the well needs to be investigated into more detail to understand the effects on the flow paths near the well. A significant impact of compaction is observed in this region, due to the higher differences in initial pressure and the reservoir pressure during production. The relation between the initial drawdown, the pore volume and permeability reduction and the following development of drawdown could strongly affects the near well bore flow. However, the standard Petrel module is not valid to study this relation since the effects cannot be controlled into detail.

ROCK COMPACTION TRENDS

The reservoir simulations for the three compaction trends show a clear differentiation in production behaviour and recovery. The 'high' trend (highest pore volume and permeability reduction) has the highest recovery, whereas the 'low' trend has a significantly lower recovery (figure 4.31).

The 'high' trend (scenario) has initial the highest gas rate, but the gas rate decreases rapidly and becomes, although only with a small difference, the lowest (figure 4.32). After about 1/60 of the production time, the gas rate of the Low trend has a slightly higher decline in gas rate than the other scenarios and obtains the lowest production rate. The variations in gas rates for the three trends can be explained by an impact of the permeability reduction on the gas rate. The higher initial flow rate of the 'high' scenario induces a higher drawdown, which leads to a higher compaction-induced decrease in permeability and subsequent production rate. As production continues the impact of the drawdown diminishes. There are multiple ways explain this phenomena 1) the reservoir pressure lowers and the drawdown decreases, 2) due to the obtained higher gas rate within the 'low' scenario the higher drawdown implies a permeability reduction which strongly impacts the gas rate, 3) the impact of the pore volume reduction for the 'high' scenario counteracts for the impact of the permeability reduction.

The power-like shape of the gas rate curves and their respective order with respect to rock compressibility are likewise found by Geilikman [53]. Geilikman linked the shape of the gas rate curve to the ratio of fluid

compressibility and rock compressibility. In this study the (initial) gas compressibility is kept constant and thus depends the ratio of fluid compressibility and rock compressibility, only on the rock compressibility. The ratio-dependent variation of the production rates with respect to each other, as found by Geilikman, is equal to the variation in the gas rates obtained in this study and confirms the dependency of the depletion time and production rates on the rock compressibility.

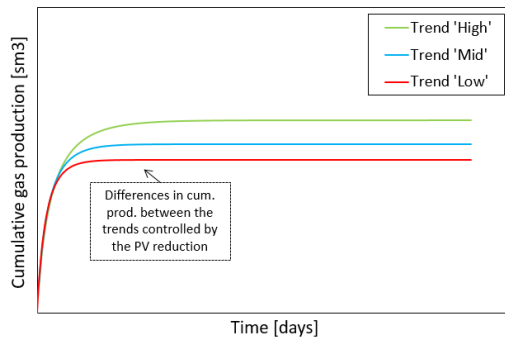


Figure 4.31: Simplified graph of the cumulative gas production resulting from the reservoir simulations with the defined rock compaction trends.

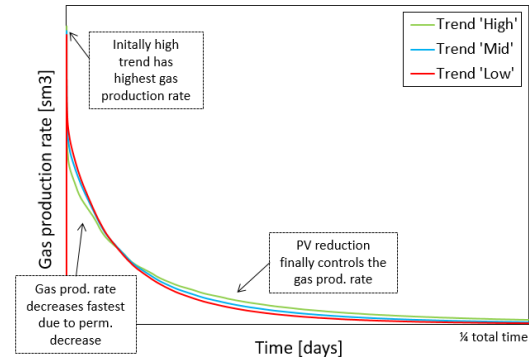


Figure 4.32: Simplified graph of the gas production rate resulting from the reservoir simulations with the defined rock compaction trends. Note: The time covered by this graph is only 1/4 of the total production period.

None of the in the gas rate detected variations is covered in the reservoir pressure (figure 4.33). For all three scenarios the reservoir pressure has a substantial fall but obtains with ongoing production a more gradual decrease. What stands out from the graph is that the 'high' trend has an overall higher reservoir pressure, whereas the low trend on the whole has the lowest reservoir pressure. This indicates a potential positive effect of compaction on the reservoir pressure.

Considerable trends are likewise seen in the solution of the mass balance equation (the P/Z plot). From the shape of the P/Z plot drive mechanisms can be identified. From the shape of the P/Z plot drive mechanisms can be identified. The shape of the P/Z plot for the low trend is almost a straight line which is usually an indication of volumetric depletion, i.e. the drive mechanism is gas expansion. Deviations from the straight line typically indicate other (internal or external) energy sources. The 'mid' and 'high' trend show a deviation from the straight line. The general trend is downward, however the slope becomes shallower (bowshape trend) i.e. the decline is more gradual. The downward bending of the line an initial pressure support which is decreasing with on-going production. When compaction occurs the formation compressibility and pore volume do not stay constant anymore. The higher the pore volume reduction, the more pronounced is the bending of the P/Z-line if the pressure support loses its drive energy.

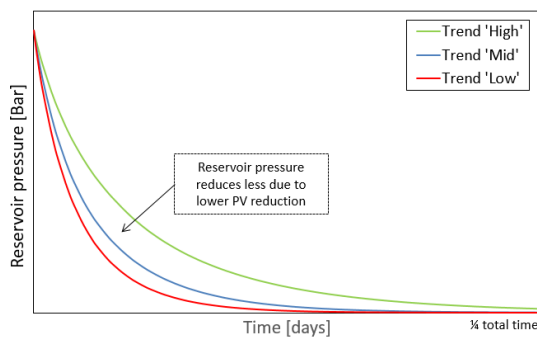


Figure 4.33: Simplified graph of the reservoir pressure resulting from the reservoir simulations with the defined rock compaction trends. Note: The time covered by this graph is only 1/4 of the total production period.

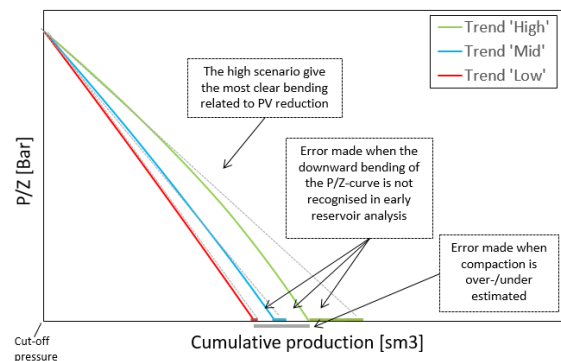


Figure 4.34: Simplified graph of the P/Z-plot resulting from the reservoir simulations with the defined rock compaction trends.

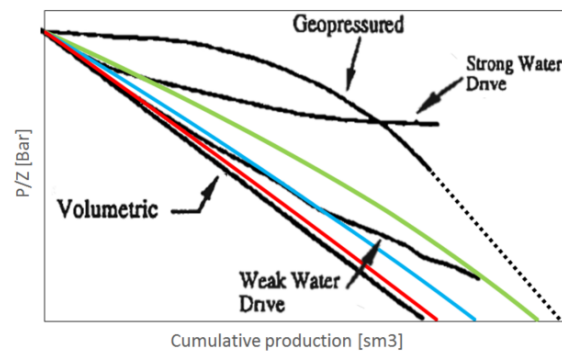


Figure 4.35: Shapes of P/Z plots for various drive mechanisms compared to the simplified graph of the P/Z plot for the in this study defined empirical trends in compaction. Adjusted from [10].

If during the initial stage of production the rock compaction is determined to be lower than valid, the ultimate recovery will be underestimated. Figure 4.33 shows an potential underestimation of 15% between the low and 'high' trend. This means that for a 1 Bcm reservoir an underestimation of 0.15 Bcm could be made. This can have a significant impact on the development decisions for the small Dutch shallow gas fields. If during later stages of production, the downward bending of the P/Z curve is not taken into account the ultimate recovery will be overestimated. For the 'high' scenario this can lead to an overestimation of 27% of the dynamic GIIP.

A comparison is made with the impact of other potential drive energies on the shape of the P/Z plot (figure 4.35). For the Dutch shallow gas reservoir the driving mechanism could likewise be water drive. The current absence of water production, is not in itself a proof of a pure depletion mechanism [52]. The difference between the two driving mechanism is hard to recognize as a varying combination of rock compaction and water expansion from a small water aquifer could provide the same performance effects to the reservoir [19]. However a strong water drive has a significant upward bending, which does strongly deviates from the found downward bending of the P/Z shape for a high pore volume reduction.

The shape of the P/Z plot of an compacting reservoir is comparable with that of a geo-pressured gas reservoir [52]. The produced gas volume is determined by the total compaction of the reservoir, comprising the gas and formation compressibility. Where in a unconsolidated reservoir the gas compressibility is roughly equal to the pore compressibility due to the high formation compressibility, is in an geo-pressured reservoir the gas compressibility lower and is the gas compressibility roughly equal to the formation compressibility.

Impact of Pore volume and Permeability loss on reservoir production

To illustrate the impact of pore volume and permeability decrease during production the effects of reservoir compaction, i.e. pore volume reduction and transmissibility decrease were tested separately and linked to each other using the 'high' trend.

The standard scenario (both decrease of pore volume and permeability) has initially the highest gas rate (figure 4.38). But with ongoing production the decline of the standard and the scenario with only permeability reduction (PR) have a more rapid decline in gas rate than the scenario with only pore volume reduction (PV). After 1/5th of the time covered by the graph, PV case has with respect to the other scenarios a more pronounced decrease in gas rate. These differences can be explained by linking the obtained gas rates to the reservoir pressure. Where the scenario with only pore volume reduction has the most substantial fall in reservoir pressure. Although pressure stays high due to compaction permeability is not hindered and higher rates are possible (figure 4.37). The reservoir then depletes faster with respect to the other scenarios. The impact of a decrease in the potential drive energy of the reservoir the gas rate diminishes.

To determine the recovery, for all scenarios a restriction was set at a limit of 30 bar BHP. When comparing the cumulative production of all scenarios it can be seen that the permeability reduction only scenario produces significantly less than the other scenarios (figure 4.36). A permeability reduction implies that flow rates would be hindered and a higher drawdown would be needed to maintain the gas rates. The reservoir pressure limit of 30 bar BHP is quickly reached leading to less gas produced cumulative and lower recovery.

In reality pore volume reduction coupled with permeability reduction are expected to occur in a compacting reservoir. The standard scenario, with both pore volume and permeability reduction incorporated, has on the whole the most gradual decrease in reservoir pressure and subsequent the highest reservoir pressure. This can be explained by a combination of a lower production rate due to permeability reduction (lower pressure decrease) and a decrease in pore volume, which levels up the decrease in reservoir pressure.

The P/Z plot shows no deviation from the straight line for the scenario with only permeability reduction (figure 4.39). Whereas the shape of the P/Z line is equal for the scenarioe with only pore volume reduction and the standard scenario. This indicates that solely a reduction in pore volume is of influence on the shape a of the P/Z-plot as discussed before. The impact of permeability reduction cannot be detected in the solution of the mass balance equation.

Chan incorporated both depletion-induced pore volume and permeability reduction into reservoir simulations of an unconsolidated oil reservoir and confirms the results found in this study. Although Chan found a more pronounced difference between the scenario with only pore volume reduction and the standard scenario caused by the lower relative permeability of the reservoir fluid (oil).

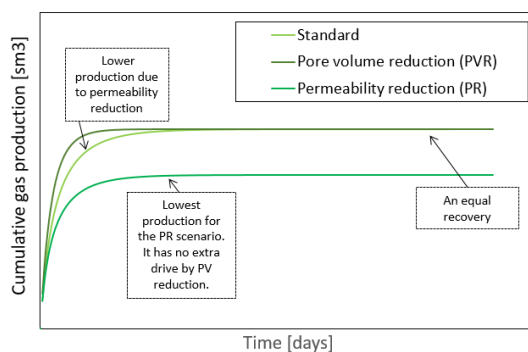


Figure 4.36: Simplified graph of the cumulative gas production resulting from the reservoir simulations with the defined rock compaction trends.

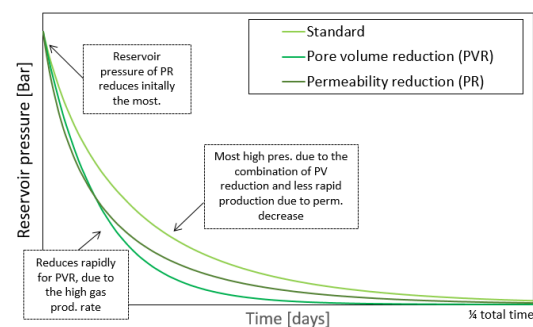


Figure 4.37: Simplified graph of the reservoir pressure resulting from the reservoir simulations with the defined rock compaction trends. Note: The time covered by this graph is only 1/4 of the total production period.

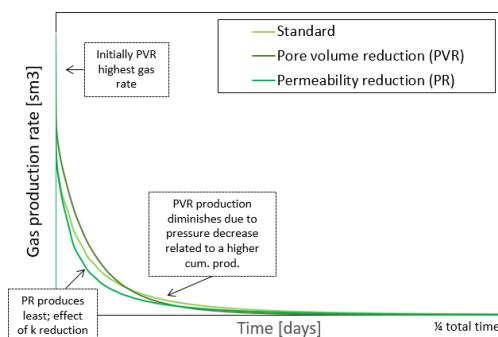


Figure 4.38: Simplified graph of the gas production rate resulting from the reservoir simulations with the defined rock compaction trends. Note: The time covered by this graph is only 1/4 of the total production period.

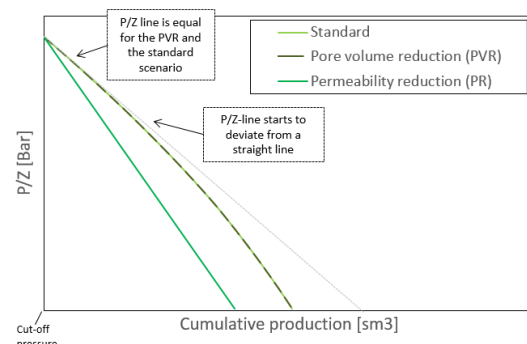


Figure 4.39: Simplified graph of the P/Z-plot resulting from the reservoir simulations with the defined rock compaction trends.

IMPACT OF DATA CONVERSION: EXPERIMENTAL & CALCULATED DATA

The impact of the usage of the various empirical relations is negligible and as a result the simplest relation can be used to calculate the permeability reduction subsequent to the pore volume reduction (for the stress range of the Dutch shallow gas reservoirs). The negligible impact is mainly controlled by the minor impact of a decreasing permeability on the recovery factor. Nevertheless it is necessary to perform more research as the discussion of chapter 3 implies that the studied samples do not fully cover the range in reduction of pore volume and permeability. A careful and well-planned laboratory study are the key to reducing the uncertainties associated with porosity, permeability and compaction prediction [6].

PRESSURE DEPENDENT PORE COMPRESSIBILITY

When using a reservoir simulator there are two ways of incorporating the reservoir compressibility within the simulation model. The first and often used option is the use of a constant compressibility with the help of calculated pore volume and transmissibility reduction. The second option is a pressure dependent pore compressibility. Whereas the second option is according to literature most valid option since the assumption of a constant compressibility does not fully cover the behaviour of weakly to unconsolidated sandstones.

The obtained results are strongly dependent on interpretation of the experimental rock compaction data. Here it is chosen to define the representative compressibility independent of the peak compressibility, since the peak compressibility is often interpreted as partly the result of unloading of the sample.

The deviation between the recovery factors found for the various methods has a maximum of about 10 %. The assumption of a constant rock compressibility thus may be suitable but will not fully capture the reservoir compaction effects on shallow gas.

Yale states that one of the main reasons that formation compressibility has been underestimated in reservoir analysis is that it has been assumed that pore compressibility is fairly constant with stress and of the same order of magnitude as the compressibility of water [19]. Incorporation of pressure-dependent rock compressibilities in reservoir simulations will allow for the correct determination of drive energies and the prediction of the ultimate recovery, which can aid in the most efficient development of the reservoir [19].

TRENDS RELATED TO GEOLOGICAL CHARACTERISTICS

For each of the geological trends it is aimed to determine an uncertainty range which represents the possible error as could have been made when one takes into account the wrong geological characteristic.

For the geological characteristics a variation in the recovery factor of around 5-8% is found. The uncertainty range is only determined for the geological characteristics for which a clear trends based on the geological characteristics could be defined. An interesting point is that the easiness to define clearly deviating trends is strongly impacted by the behaviour of the geological characteristics for a change in character of the characteristic. For the characteristics that hardly impact the rock characteristics, no deviation could be found, whereas would have given a narrower range in the recovery factor. So the found uncertainty ranges are high, but it should be considered that they represent the maximum uncertainty related to a lack of knowledge on the geological reservoir characteristics.

Since most rock characteristics are inter-correlated with other characteristics, it would be best to say that the two-end members in behaviour (clean sand to clay) have an uncertainty range of 8%. All the combinations within this predictions give a small variation within this range.

5

RECOMMENDATIONS

Unconsolidated sands have some unique poorly understood characteristics, some of which have been clarified during this study. However this study also implies potential further research questions to increase the understanding and to assess the assumptions and simplifications as used in this study.

Coring program

As the laboratory measurements are strongly affected by the grain configuration of the sample it is necessary to do further research on the effect of sample disturbance due to drilling and sample recovery. Furthermore the effect of drilling on the in-situ sample configuration needs to be considered. Due to the drawdown the compaction has the highest impact near the well-bore, within the same area that is affected by drilling; this impact should be considered.

Data acquisition

Improving the conversion from experimental compaction data to in-situ compaction can be done by incorporating various monitoring methods to determine the actual compaction within the reservoir. The possible options are: 1) 4D seismics, to monitor variation in the acoustic velocities caused by the compacting rock, 2) sand property determination from logs [55] [56] and 3) the usage of radio-active bullets to measure strain.

Experimental

More research is necessary to determine the correlation between the various rock characteristics as the derived equations describing plastic unconsolidated compaction tend to over-predict the experimental results. The least understood is the variation in permeability as a result of rock compaction; an experimental research is recommended to understand the effects of compaction on the pore throats (tortuosity) of the sample. The ideal research would comprise monitored sand compaction under known conditions and with known rock characteristics. One is then able to determine the impact of the various rock characteristics on the tortuosity development.

Furthermore is it necessary to confirm the applicability of the high rock compaction trend, as there is no experimental data from core samples available yet to confirm this relationship which is only based on manufactured samples.

Reservoir modeling

The simplified reservoir model can be improved in several ways by incorporating the characteristics that, based on this compaction study, impact the production. First the impact of flow restriction needs to be tested, especially in relation with the found impact of the drawdown region; can it be counteracted or prevented? Further the impact of a variation in lithology with varying compaction curves per zone should be tested. As resulting distribution of potential flow paths can lead to non-producing zones or expelling water from neighbouring water bearing shale's.

In addition to this study, the effects of compaction on unconsolidated shallow gas reservoirs can be studied by analysing the production rate and reservoir pressure by rate transient analysis and pressure transient anal-

ysis. As a first step this could be done for the theoretical production data as found for this study. As second step the model could be applied to the actual production behaviour. The end-member trends as defined in this study can be used to investigate the production behaviour for the ultimate characteristics of the rock.

Furthermore compaction drive and aquifer pressure support show a similar impact on the production behaviour. It is recommended to define how one can distinguish the difference between these two driving mechanisms in production behaviour.

6

CONCLUSIONS

Rock compaction data base

- The variation of the compaction-related rock characteristics, such as pore volume and permeability, cannot be fully predicted based on the pore compressibility.
- The compaction-induced permeability reduction in unconsolidated samples cannot be fully reproduced with empirical relations such as the simplified Carman-Kozeny (equation 3.50), since it does not take into account the effects of the various geological rock characteristics on the new grain configuration and according variations in the tortuosity.
- The pore volume reduction based on the rock compressibility, as determined by the equations derived from the linear elastic behaviour, tend to overestimate the porosity reduction when compared to experimental data.
- The initial porosity, the pre-consolidation stress and degree of consolidation of the formation have the strongest influence on the rock compressibility of an unconsolidated sandstone.

Reservoir simulation

- Pore volume reduction has a positive influence on the production rate.
- Permeability reduction, and subsequent transmissibility reduction, has a negative influence on the obtained production rate.
- The recovery factor is only influenced by the amount of pore volume reduction during reservoir compaction. Changes in transmissibility (hence permeability reduction) have negligible impact on the recovery factor.
- Two effects of pore volume reduction are visible in the P/Z-plots (mass balance plots) of compaction-sensitive gas reservoirs, 1) the P/Z-line stays longer up than expected, 2) the straight line bends downwards. This translates for a shallow gas reservoir of 1 Bcm to a potential underestimation of 0.25 Bcm on the GIIP.
- The effect of permeability reduction, and subsequent transmissibility reduction cannot be detected in the mass balance plot of the reservoir (P/Z-plot).
- The error made due to the use of empirical relations to estimate the development of rock characteristics during compaction is negligible.
- The assumption of a constant rock compressibility is not a suitable and realistic assumption when taking into account the reservoir compaction effects on shallow gas.
- Uncertainties in the geological characteristics of the reservoir rock lead to an impact of +/- 10% on the recovery factor.

A

APPENDIX: GLOSSARY

Nomenclature

α	= Biot-Willis constant (-)
ϵ	= Strain (-)
ϕ	= Porosity (-)
γ	= Average stress path (-)
μ	= Viscosity (Pa·s)
ν	= Poissons ratio (-)
ρ	= Density (kg/m ³)
σ	= Effective stress (Bar)
A	= Surface (m ²)
C	= Compressibility (1/Bar)
e	= Void ratio (-)
g	= Gravitational constant (m ³ /kg·s ²)
h	= Height (m)
k	= Permeability (mD)
K	= Stress ratio (-)
L	= Length (m)
n	= Substance of gas (-)
P	= Gas pressure (Bar)
R	= Universal gas constant (J · mol · K ⁻¹)
S	= Stress (Bar)
T	= Absolute temperature (K)
V	= Volume (m ³)
T	= Transmissibility (-)
z	= Compressibility factor (-)

Subscripts

0	= Initial
b	= Bulk
f	= Fluid
g	= Gas
h	= Horizontal (1)
H	= Horizontal (2)
H	= Hydrostatic
k	= Uniaxial
p	= Pore
prod	= Produced at reservoir conditions
ref	= Reference state
s	= Grain
t	= Total
v	= Vertical
w	= Water
m	= Mean

B

APPENDIX: ROCK COMPACTION DATABASE

Reference	Sand/Sandstone	Test	Stress Path	Loading rate	Porosity	Permeability
Brignoli & Di Federico, 2004 [49]	W	Isotropic compression	1	1 Mpa/min	0.275	86
		Anisotropic compression	0.5 and 0.7	1 Mpa/min	0.275	86
	X	Isotropic compression	1	1 Mpa/min	0.25 - 0.3	160
		Anisotropic compression	0.5 and 0.7	1 Mpa/min	0.25 - 0.3	160
	Y	Isotropic compression	1	1 Mpa/min	>0.3	1417
		Anisotropic compression	0.5 and 0.7	1 Mpa/min	>0.3	1417
Chan, 2004 [6]	GOM - Field X 1	Confining Pressure	-	-	0.31	1350
	GOM - Field X - 2	Confining Pressure	-	-	0.30	1260
	GOM - Field X - 3	Confining Pressure	-	-	0.30	655
	GOM - Field X - 4	Confining Pressure	-	-	0.29	518
	GOM - Field X - 5	Confining Pressure	-	-	0.27	148
	GOM - Field X - 6	Confining Pressure	-	-	0.24	120
	GOM - Field X - 7	Confining Pressure	-	-	0.23	80
	GOM - F2.11	Confining Pressure	-	-	0.31	-
	GOM - Field Z Well A	Confining Pressure	-	-	0.30	143
	GOM - Field Z Well B	Confining Pressure	-	-	0.30	342
	GOM - Field Z Well C	Confining Pressure	-	-	0.30	453
Chuhan et al., 2001 [50]	Sample A	Uniaxial compression	-	1 Mpa/90 s	0.46	-
	Sample B	Uniaxial compression	-	1 Mpa/90 s	0.45	-
	Sample C	Uniaxial compression	-	1 Mpa/90 s	0.45	-
	Sample D	Uniaxial compression	-	1 Mpa/90 s	0.46	-
	Sample E	Uniaxial compression	-	1 Mpa/90 s	0.49	-
de Waal, 1986 [16]	F9 - Sand	Oedometer	-	-	-	-
	BCS	Uniaxial compression	-	-	-	-
Dudley et al., 1998 [57]	Brazos River sand	Uniaxial compaction	-	0.5 to 2 psi/s	-	-
	GOM A	Uniaxial compaction	-	0.5 to 2 psi/s	-	-
	GOM B	Uniaxial compaction	-	0.5 to 2 psi/s	-	-
	GOM C	Uniaxial compaction	-	0.5 to 2 psi/s	-	-
Ghafhazi, 2014 Goldsmith, 1989 [8]	Fraser River Sand	Triaxial compression	-	-	0.50	-
	F6 - I - Jurassic sst	Uniaxial compaction	-	-	0.40	-
	F6 - II - Jurassic sst	Uniaxial compaction	-	-	0.38	-
	F6 - III - Jurassic sst	Uniaxial compaction	-	-	0.36	-
	F6 - IV - Jurassic sst	Uniaxial compaction	-	-	0.32	-
	F6 - V - Jurassic sst	Uniaxial compaction	-	-	0.31	-
	F6 - VI - Jurassic sst	Uniaxial compaction	-	-	0.30	-
Hagin, 2004	Wilmington sand	Hydrostatic compression	-	-	-	-
Hathon & Myers, 2011 [4]	Mars Basin - GOM A	Uniaxial compaction	-	-	-	-
	Mars Basin - GOM B	Uniaxial compaction	-	-	-	-
	Sand C	Uniaxial compaction	-	-	-	-
	Sand D	Uniaxial compaction	-	-	-	-
	GOM E	Uniaxial compaction	-	-	-	-
	GOM F	Uniaxial compaction	-	-	-	-
	West Africa Qtz sand	Uniaxial compaction	-	-	-	-
	Mai-Liao Sand Dr50	Isotropic Consolidation	-	-	0.45	-
Huang et al., 1999 [58]	Mai-Liao Sand Dr50 -II	Isotropic Consolidation	-	-	0.43	-
	Mai-Liao Sand Dr60	Isotropic Consolidation	-	-	0.43	-
	Mai-Liao Sand Dr60 - II	Isotropic Consolidation	-	-	0.42	-
	Mai-Liao Sand Dr70	Isotropic Consolidation	-	-	0.42	-
	Mai-Liao Sand Dr70 - II	Isotropic Consolidation	-	-	0.40	-
	Mai-Liao Sand Dr85	Isotropic Consolidation	-	-	0.39	-
	Mai-Liao Sand Dr85 - II	Isotropic Consolidation	-	-	0.38	-
	Mai-Liao Sand Dr24	Isotropic Consolidation	-	-	0.48	-
	Mai-Liao Sand Dr38	Isotropic Consolidation	-	-	0.47	-
	Mai-Liao Sand Dr62	Isotropic Consolidation	-	-	0.43	-
	F2 sand 1C	Triaxial test	-	-	0.33	1271

Reference	Sand/Sandstone	Test	Stress Path	Loading rate	Porosity	Permeability	
Mattax et al., 1987 [9]	F2 sand 1U	Triaxial test	-	-	0.33	1271	
	F2 sand 2C	Triaxial test	-	-	0.33	1271	
	F2 sand 3C	Triaxial test	-	-	0.33	1271	
	F2 sand 2U	Triaxial test	-	-	0.33	1271	
	F2 sand 3U	Triaxial test	-	-	0.33	1271	
	F3 sand 1C	Triaxial test	-	-	0.33	751	
	F3 sand 1U	Triaxial test	-	-	0.33	509	
	F3 sand 2C	Triaxial test	-	-	0.33	509	
	F3 sand3C	Triaxial test	-	-	0.33	449	
	F3 sand 2U	Triaxial test	-	-	0.33	444	
	F3 sand 3U	Triaxial test	-	-	0.33	501	
	McDowel, 2002 [59]	Leighton Buzzard sand 1	One-dimensional compression	-	-	0.35	-
		Leighton Buzzard sand 2	One-dimensional compression	-	-	0.35	-
Leighton Buzzard sand 3		One-dimensional compression	-	-	0.36	-	
Merle et al., 1976 [48]	Bachaquero sand	One-dimensional compression	-	-	(0.3-0.4)	(500-3500)	
	Clay	One-dimensional compression	-	-	-	-	
Mesri & Vardhanabhuti, 2009 [60]	Ottawa sand F2	Ansotropic compression	-	-	0.37	-	
	Ottawa sand F3	Ansotropic compression	-	-	0.33	-	
	Toyoura sand Dr43	Ansotropic compression	-	-	0.45	-	
	Toyoura sand Dr80	Ansotropic compression	-	-	0.41	-	
	Toyoura sand Dr98	Ansotropic compression	-	-	0.38	-	
	Ottawa sand Dr5	Ansotropic compression	-	-	0.45	-	
	Ottawa sand Dr85	Ansotropic compression	-	-	0.40	-	
	Mono-quartz sand C1	Ansotropic compression	-	-	0.45	-	
	Mono-quartz sand C20	Ansotropic compression	-	-	0.45	-	
	Silica, Quartz Dr47	Ansotropic compression	-	-	0.40	-	
	Silica, Quartz Dr100	Ansotropic compression	-	-	0.30	-	
	Ganga sand Dr25	Ansotropic compression	-	-	0.40	-	
	Ganga sand Dr65	Ansotropic compression	-	-	0.30	-	
	Wabash River Sand Dr5	Ansotropic compression	-	-	0.40	-	
	Wabash River Sand Dr71	Ansotropic compression	-	-	0.34	-	
	Mol sand	Ansotropic compression	-	-	0.39	-	
	Feldspar sand	Ansotropic compression	-	-	0.52	-	
	Quiou sand Dr48	Ansotropic compression	-	-	0.51	-	
	Quiou sand Dr88	Ansotropic compression	-	-	0.45	-	
	Carbonate sand D60-0.19	Ansotropic compression	-	-	0.54	-	
	Carbonate sand D60-0.38	Ansotropic compression	-	-	0.54	-	
	Carbonate sand D60-1.48	Ansotropic compression	-	-	0.54	-	
	Silty sand (FC 13%)	Ansotropic compression	-	-	0.48	-	
	Mono Quartz sand (FC 10%) Dr5	Ansotropic compression	-	-	0.48	-	
	Mono Quartz sand (FC 10%) Dr86	Ansotropic compression	-	-	0.43	-	
	Ganga sand	Ansotropic compression	-	-	0.49	-	
	Silica Dr22 (FC 30%)	Ansotropic compression	-	-	0.40	-	
	Silica Dr100 (FC 30%)	Ansotropic compression	-	-	0.22	-	
	Toyoura sand Dr46	Ansotropic compression	-	-	0.46	-	
	Toyoura sand Dr54	Ansotropic compression	-	-	0.44	-	
	Toyoura sand Dr80	Ansotropic compression	-	-	0.40	-	
	Silica sand Dr37	Ansotropic compression	-	-	0.45	-	
	Silica sand Dr52	Ansotropic compression	-	-	0.43	-	
	Silica sand Dr77	Ansotropic compression	-	-	0.40	-	
	Wabash river sand	Ansotropic compression	0.44	-	0.00	-	
	Wabash river sand, Quartz	Ansotropic compression	0.41	-	0.00	-	
	Pennsylvania sand Dr63	Ansotropic compression	0.42 - 0.52	-	0.41	-	
	Pennsylvania sand Dr70	Ansotropic compression	0.41 - 0.52	-	0.40	-	
	Minnesota sand	Ansotropic compression	0.34	-	0.32	-	
	Myers & Hathon, 2014 [30]	F10 - 300A	Confined / Uniaxial compression	-	-	0.30	-
		F10 - 150A	Confined / Uniaxial compression	-	-	0.30	-
		F10 - 450A	Confined / Uniaxial compression	-	-	0.30	-
		F11 - 150R	Confined / Uniaxial compression	-	-	0.30	-
		F11 - 300R	Confined / Uniaxial compression	-	-	0.30	-
		F13 - 7030K	Confined / Uniaxial compression	-	-	0.30	-
		F13 - 8515K	Confined / Uniaxial compression	-	-	0.30	-
		F15 - 15C	Confined / Uniaxial compression	-	-	0.30	-
		F15 - 10C	Confined / Uniaxial compression	-	-	0.30	-
		F15 - 7.5C	Confined / Uniaxial compression	-	-	0.30	-
		F27 - 25P	Confined / Uniaxial compression	-	-	0.40	-
		F27 - 12.5P	Confined / Uniaxial compression	-	-	0.40	-
		F27 - 6.25P	Confined / Uniaxial compression	-	-	0.40	-
		F29 - 5050/150300	Confined / Uniaxial compression	-	-	0.40	-
		F29 - 25/75150300450	Confined / Uniaxial compression	-	-	0.40	-
		F29 - 1238/75150300450	Confined / Uniaxial compression	-	-	0.40	-
		F29 - 50/75450	Confined / Uniaxial compression	-	-	0.40	-
F31 - 100Fi		Confined / Uniaxial compression	-	-	0.40	-	

Reference	Sand/Sandstone	Test	Stress Path	Loading rate	Porosity	Permeability
	F31 - 50Fi	Confined / Uniaxial compression	-	-	0.40	-
	F31 - 12.5Fi	Confined / Uniaxial compression	-	-	0.40	-
	F33 - 100K	Confined / Uniaxial compression	-	-	0.40	-
	F33 - 50K	Confined / Uniaxial compression	-	-	0.40	-
	F33 - 25K	Confined / Uniaxial compression	-	-	0.40	-
	F33 - 12.5K	Confined / Uniaxial compression	-	-	0.40	-
	F33 - 6.25K	Confined / Uniaxial compression	-	-	0.40	-
Nguyen et al., 2013 [7]	Sherwood Sandstone K=0	0	0	0.1 Mpa/min	0.335	164
	Sherwood Sandstone K=0.2	Deviatoric / Uniaxial compaction	0.2	0.1 Mpa/min	0.31	222
	Sherwood Sandstone K=0.3	Deviatoric / Uniaxial compaction	0.3	0.1 Mpa/min	0.32	150
	Sherwood Sandstone K=0.4	Deviatoric / Uniaxial compaction	0.4	0.1 Mpa/min	0.334	185
	Sherwood Sandstone K=0.6	Deviatoric / Uniaxial compaction	0.6	0.1 Mpa/min	0.337	258
	Sherwood Sandstone K=0.8	Deviatoric / Uniaxial compaction	0.8	0.1 Mpa/min	0.31	215
	Sherwood Sandstone K=1	Isotropic compression	1	0.1 Mpa/min	0.341	200
	Durance sand K=0.2	Deviatoric / Uniaxial compaction	0.2	0.1 Mpa/min	0.386	620
	Durance sand K=0.3	Deviatoric / Uniaxial compaction	0.3	0.1 Mpa/min	0.389	600
	Durance sand K=0.4	Deviatoric / Uniaxial compaction	0.4	0.1 Mpa/min	0.385	605
	Durance sand K=0.6	Deviatoric / Uniaxial compaction	0.6	0.1 Mpa/min	0.387	610
	Durance sand K=0.8	Deviatoric / Uniaxial compaction	0.8	0.1 Mpa/min	0.382	614
	Durance sand K=1	Isotropic compression	1	0.1 Mpa/min	0.39	627
	Durance sand - Dg:0506mm	Isotropic compression	1	0.1 Mpa/min	0.39	627
Ostermeier, 2001 [11]	GOM A - QE2	Isostatic	-	-	(0.25-0.33)	1240
	GOM B - CJ31	Isostatic	-	-	(0.3-0.35)	3000
	GOM C - TA2	Isostatic	-	-	(0.29-0.33)	2180
	GOM D - BP2	Isostatic	-	-	(0.25-0.265)	558
Pathak, 2007	NSO Gas field A	Hydrostatic depletion	-	-	0.345	-
	NSO Gas field B	Hydrostatic depletion	-	-	0.381	-
	NSO Gas field C	Hydrostatic depletion	-	-	0.17	-
Salazar, 2013 [61]	F19 - 100N	One-dimensional	-	-	0.42	-
	F19 - 90N10S	One-dimensional	-	-	0.41	-
	F19 - 80N20S	One-dimensional	-	-	0.41	-
	F19 - 65N35S	One-dimensional	-	-	0.39	-
	F19 - 50N50S	One-dimensional	-	-	0.37	-
	F19 - 100S	One-dimensional	-	-	0.41	-
	F11 - 100N Vibrated	One-dimensional	-	-	0.33	-
	F11-100S Slurry	One-dimensional	-	-	0.33	-
Sawabini et al., 1974 [46]	Arkosic sand	Hydrostatic	-	-	-	-
	Arkosic sand - R12	Hydrostatic	-	-	0.31	-
	Arkosic sand - R14	Hydrostatic	-	-	0.33	-
	Arkosic sand - R15	Hydrostatic	-	-	0.23	-
	Arkosic sand - R16	Hydrostatic	-	-	0.46	-
	Arkosic sand - R19	Hydrostatic	-	-	0.46	-
	Arkosic sand - R20	Hydrostatic	-	-	0.39	-
	Arkosic sand - R21	Hydrostatic	-	-	0.38	-
	Arkosic sand - R22	Hydrostatic	-	-	0.33	-
	Arkosic sand - R23	Hydrostatic	-	-	0.33	-
	Arkosic sand - R24	Hydrostatic	-	-	0.29	-
	Arkosic sand - R9	Hydrostatic	-	-	0.27	-
Shutjens et al., 2011 [38]	F2 - X	Uniaxial compression	-	-	(0.25-0.30)	-
Sheng et al., 2008 [62]	Sacramento River sand 1	isotropic compression	-	-	0.47	-
	Sacramento River sand 2	isotropic compression	-	-	0.44	-
	Sacramento River sand 3	isotropic compression	-	-	0.42	-
	Sacramento River sand 4	isotropic compression	-	-	0.38	-
	Cambria sand 1	isotropic/triaxial compression	-	-	0.41	-
	Cambria sand 2	isotropic compression	-	-	0.38	-
	Cambria sand 3	isotropic compression	-	-	0.34	-
	Toyourea sand	isotropic compression	-	-	0.44	-
	Tung-Chung sand	isotropic compression	-	-	0.46	-
Swanson, 1980 [44]	SPB27 nr 68 - 7990ft	Confining pressure	-	-	0.31	-
	SPB27 nr 71 - 7434ft: 300psi/day	Confining pressure	-	-	0.37	-
	SPB27 nr 71 - 7439ft	Confining pressure	-	-	0.38	-
	SPB24 nr 79A - 7925ft: 300psi/day	Confining pressure	-	-	0.38	-
	SPB24 nr 79A - 7925ft: 300psi/day	Confining pressure	-	-	0.37	-
	SPB27 nr 68 - 7990ft	Confining pressure	-	-	0.33	-
van der Knaap & van der Vlis, 1967 [63]	BCS 1	Anisotropic, confined compression	-	-	0.37	-
	BCS 2	Anisotropic Unloading	-	-	0.26	-
	BCS 3	Anisotropic, confined compression	-	-	0.27	-
	Clay	Anisotropic, confined compression	-	-	0.20	-
	Illite	Anisotropic, confined compression	-	-	0.49	-
	Kaolinite	Anisotropic, confined compression	-	-	0.39	-
Yamamuro et al., 1996 [64]	Quartz sand 1	Confined compression	-	-	(0.4-0.52)	-
	Quartz sand 2	Confined compression	-	-	(0.4-0.52)	-
	Quartz sand 3	Confined compression	-	-	(0.4-0.52)	-
	Cambria sand 1	Confined compression	-	-	(0.33-0.44)	-
	Cambria sand 2	Confined compression	-	-	(0.33-0.44)	-
	Cambria sand 3	Confined compression	-	-	(0.33-0.44)	-
	Gypsum sand 1	Confined compression	-	-	(0.41-0.49)	-
	Gypsum sand 2	Confined compression	-	-	(0.41-0.49)	-
	Gypsum sand 3	Confined compression	-	-	(0.41-0.49)	-

C

APPENDIX: UNIT CONVERSION

Input parameters Simulation			
Parameter	Original Unit	New unit	Conversion factor
Pressure	MPa	Bar	10
	Psi	Bar	0.06895
Compressibility	1/MPa	1/Bar	0.1
	1/Psi	1/Bar	14.504
Porosity	%	-	0.01
Strain	%	-	0.01
Permeability			

Table C.1: The unit conversions as used to convert the data to the defined 'standard' units

D

APPENDIX: RESERVOIR SIMULATION: TREND DETAIL

Trend detail: 'Mid'

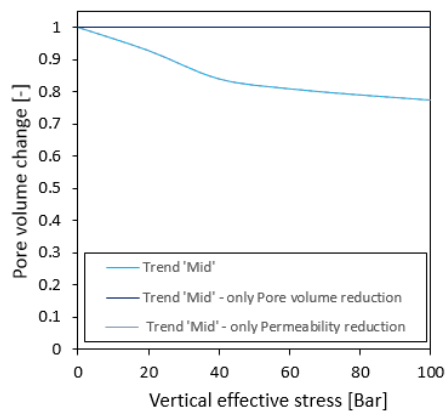


Figure D.1: The compaction-induced change in pore volume reduction for the three input scenario's for the 'mid' trend.

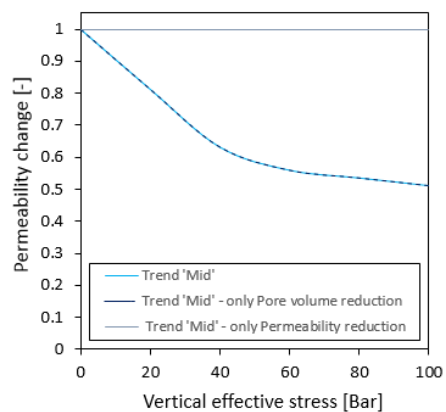


Figure D.2: The compaction-induced change in transmissibility reduction for the three input scenario's for the 'mid' trend.

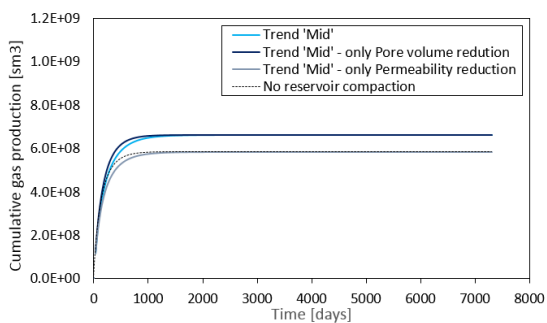


Figure D.3: Cumulative gas production resulting from the reservoir simulation with the defined 'mid' rock compaction trend.

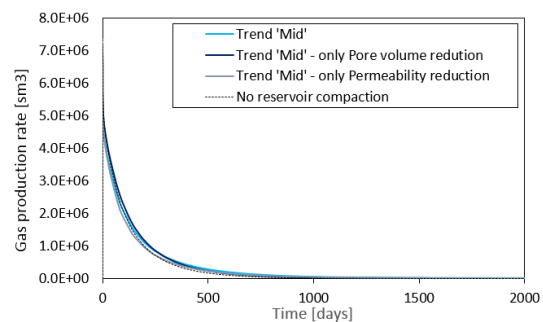


Figure D.4: Gas production rate resulting from the reservoir simulation with the defined 'mid' rock compaction trend. Note: The time covered by this graph is only 1/4 of the total production period.

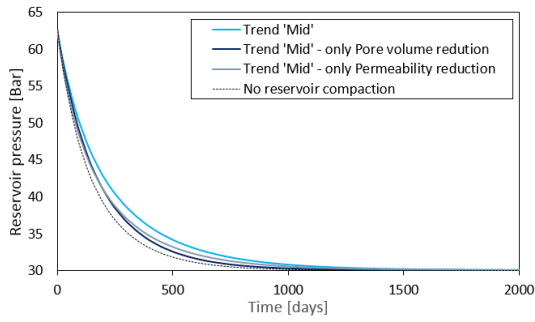


Figure D.5: Reservoir pressure resulting from the reservoir simulation with the defined 'mid' rock compaction trend. Note: The time covered by this graph is only 1/4 of the total production period.

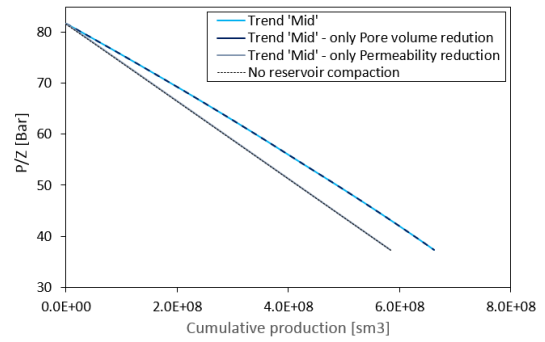


Figure D.6: P/Z-plot resulting from the reservoir simulation with the defined 'mid' rock compaction trend.

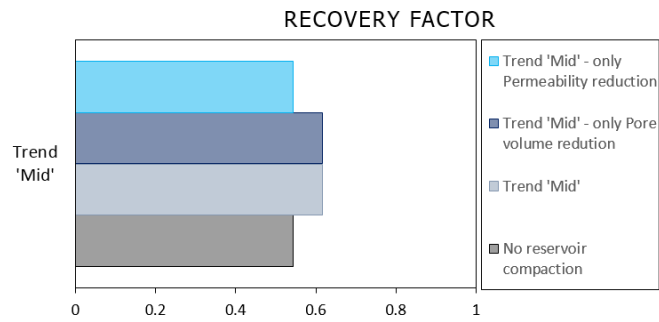


Figure D.7: Recovery factor resulting from the reservoir simulation with the defined 'mid' rock compaction trend.

Trend detail: 'Low'

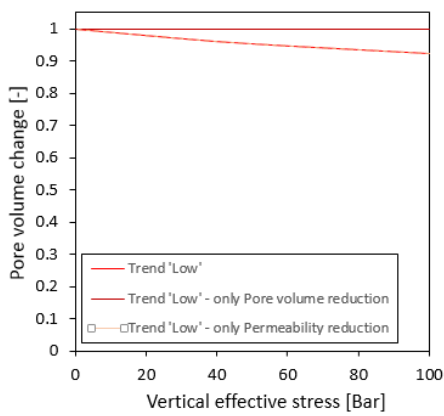


Figure D.8: The compaction-induced change in pore volume reduction for the three input scenario's for the 'low' trend.

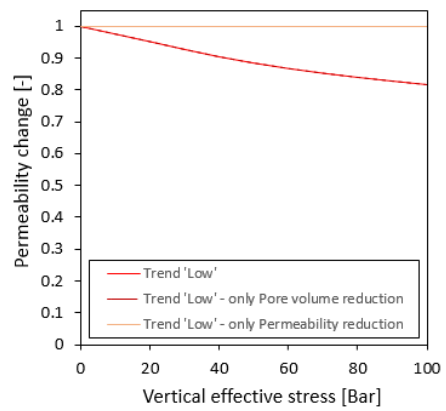


Figure D.9: The compaction-induced change in transmissibility reduction for the three input scenario's for the 'low' trend.

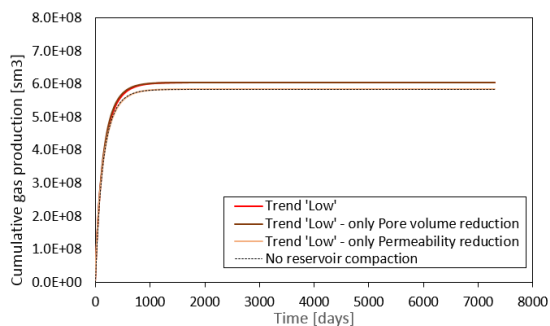


Figure D.10: Cumulative gas production resulting from the reservoir simulation with the defined 'low' rock compaction trend.

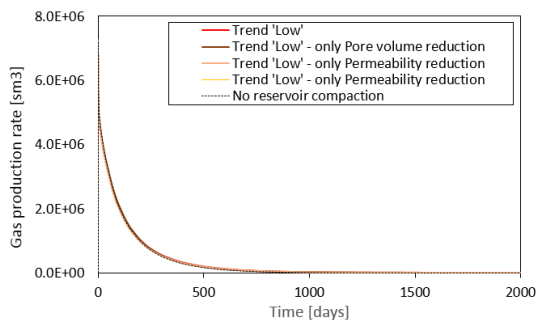


Figure D.11: Gas production rate resulting from the reservoir simulation with the defined 'low' rock compaction trend. Note: The time covered by this graph is only 1/4 of the total production period.

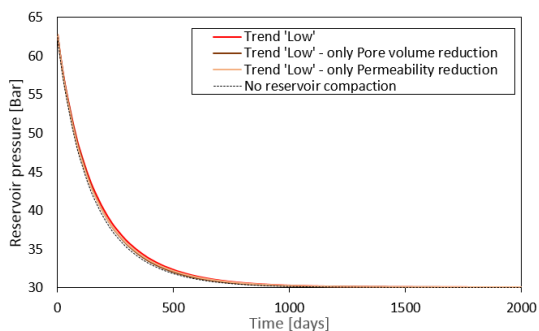


Figure D.12: Reservoir pressure resulting from the reservoir simulation with the defined 'low' rock compaction trend. Note: The time covered by this graph is only 1/4 of the total production period.

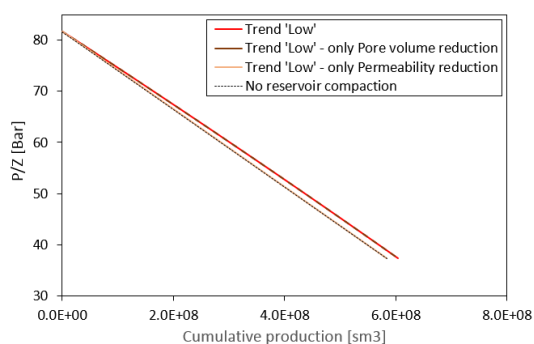


Figure D.13: P/Z-plot resulting from the reservoir simulation with the defined 'low' rock compaction trend.

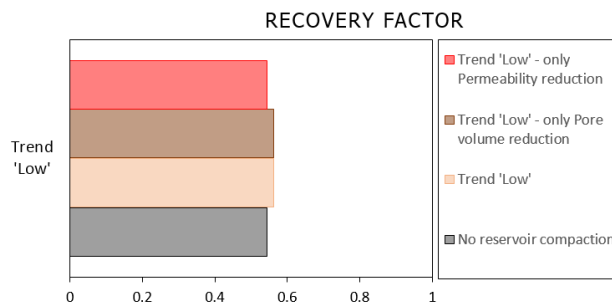


Figure D.14: Recovery factor resulting from the reservoir simulation with the defined 'low' rock compaction trend.

BIBLIOGRAPHY

- [1] *Focus on Dutch oil and gas* (EBN B.V., 2015).
- [2] M. Jones, M. Leddra, A. Goldsmith, and D. Edwards, *The geomechanical characteristics of reservoirs and reservoir rocks*, Tech. Rep. (The health and safety executive, 1992).
- [3] D. Yale, *Couples geomechanics fluid flow modeling: Effects of plasticity and permeability alteration*, SPE Annual Technical Conference and Exhibition, New Orleans, Louisiana, 30 September - 3 October 2001 (2002).
- [4] L. Hathon and M. Myers, *A survey of the production time scale compaction behavior of unconsolidated sands*, 45th Rock mechanics/Geomechanics Symposium, San Fransisco, CA, June 26-29 (2011).
- [5] M. Zoback, *Reservoir geomechanics* (Camebridge University Press, 2007).
- [6] A. Chan, *Production induced reservoir compaction, permeability loss and land surface subsidence*, Ph.D. thesis, Standford University (2004).
- [7] V. Nguyen, N. Gland, J. Datriat, C. David, J. Wassermann, and J. Guelard, *Compaction, permeability evolution and stress path effects in unconsolidated and weakly consilidated sandstone*, International journal of rock mechanics & mining Sciences **67**, 226 (2013).
- [8] A. Goldsmith, *Permeability decline and compressibility in sandstone reservoir rrock*, Rock at Great depth (1989).
- [9] C. Mattax, R. McKinley, and A. Clothier, *Core analysis of unconsolidated and friable sands*, SPE-AIME 49th Annual fall meeting, Houston, October 6-9 1974 (1975).
- [10] J. Lee and R. Wattenbarger, *Gas Reservoir Engineering* (SPE Textbook series volume 5, 1996).
- [11] R. Ostermeier, *Compaction effetcs on porosity and permeability: Deepwater gulf of mexico turbidites*, Society of Petroleum Engineers: Distinguished author series (2001).
- [12] S. Schutjens, C. van Dijk, F. Marcelis, S. Pruno, J. Martin, and R. van den Oord, *Compaction of poorly consolidated quartz-rich reservoir sandstone: Experiments for the prognosis of compaction drive*, The sixth international symposium on land subsidence (2000).
- [13] J. Geertsma, *Land subsidence above compacting oil and gas reservoirs*, Journal of Petroleum Technology (1973).
- [14] P. Schutjens, T. Hanssen, M. Hetteema, J. Merour, J. de Bree, J. Coremans, and G. Helliesen, *Compaction induced porosity/permeability reduction in sandstone reservoirs: Data and model for elasticity-dominated deformation*, SPE Annual Technical Conference and Exhibition held in New Orleans, Louisiana, 30 September - 3 October 2001. (2001).
- [15] O. Adeyanju and O. Olafuyi, *Experimental studies of sand production from unconsolidated petroleum reservoirs in niger-delta*, Nigerian Journal of Technology **30** (2011).
- [16] J. de Waal, *On the rate type compaction behaviour of sandstone reservoir rock*, Ph.D. thesis, Technical University Delft (1986).
- [17] L. Dake, *Fundamentals of Reservoir Engineering* (Elsevier, 1998).
- [18] A. Settari, *How to approximate effects of geomechanics in conventional reservoir simulation*, Society of Petroleum Engineers: Distinguished author series (2005).

- [19] D. Yale, G. Nabor, J. Russell, H. Pham, and M. Yosef, *Application of variable formation compressibility for improved reservoir analysis*, 68th Annual conference and exhibition of the Society of Petroleum Engineers, Houston, Texas, 3-6 October, 1993 (1993).
- [20] M. Guitierrez and H. Hansteen, *Fully coupled analysis of reservoir compaction and subsidence*, European petroleum conference, London, U.K., 25-27 October, 1994 (1994).
- [21] H. Beggs, *Gas Production Operations* (OGCI Publications, 1985).
- [22] *Advanced Gas Reservoir Engineering* (Edinburgh Petroleum Services Limited, 2002).
- [23] A. Settari, *Reservoir compaction*, (2002).
- [24] A. Revil, D. Grauls, and O. Brevart, *Mechanical compaction of sand/clay mixtures*, Journal of geophysical research **170**, 2293 (2002).
- [25] R. Zimmerman, *Compressibility of Sandstones* (Elsevier, 1991).
- [26] B. Crawford and D. Yale, *Constitutive modeling of deformation and permeability: relationships between critical state and micromechanics*, SPE/ISRM Rock Mechanics Conference, Irving, Texas, 20-23 October 2002 (2002).
- [27] R. Sulak, L. Thomas, and R. Boade, *3d reservoir simulation of ekofisk compaction drive*, Society of Petroleum Engineers (1991).
- [28] B. Crawford, M. Gooch, and D. Webb, *Textural controls on constitutive behavior in unconsolidated sands: Micromechanics and cap plasticity*, 6th North America Rock Mechanics Symposium (NARMS): Rock Mechanics Across Borders and Disciplines, Houston, Texas, June 5-9, 2004 (2004).
- [29] J. Zhang, T. Wond, and D. Davis, *Micromechanics of pressure-induced grain crushing in porous rocks*, Journal of geophysical research **95**, 341 (1990).
- [30] L. Myers, M.T. Hathon, *Compaction: Models for prediction from thin section data*, 48th US Rock Mechanics / Geomechanics Symposium, Minneapolis, MN, USA, 1-4 June 2014 (2014).
- [31] F. Ashford and Y. Ghoniem, *Preliminary evaluations applicable to predicting the probability of occurrence for compaction and subsidence resulting from fluid withdrawal in unconsolidated shallow sands*, Section VI. Recovery.
- [32] I. Fatt, *Compressibility of sandstones at low to moderate pressures*, Bulletin of the American Association of petroleum geologists **42**, 1924 (1958).
- [33] J. Dvorkin and A. Nur, *Pore fluid: Attenuation, permeability, compress*, Gas Research Institute (1997).
- [34] G. Weltje and L. Alberts, *Packing states of ideal reservoir sands: Insights from simulation of porosity reduction by grain rearrangement*, Sedimentary Geology (2011).
- [35] J. Dong, J. Hsu, W. Wu, T. Shimamoto, J. Huand, and E. Yeh, *Stress-dependence of the permeability and porosity of sandstone and shale tcdp hole-a*, International Journal of Rock Mechanics and Mining Sciences (2010).
- [36] M. Khan and L. Teufel, *The effect of geological and geomechanical parameters on reservoir stress path and its importance in studying permeability anisotropy*, SPE Annual Technical Conference and Exhibition, Denver, Colorado, 6-9 October (2000).
- [37] Fjaer, Holt, Horsrud, Raaen, and Risnes, *Petroleum related Rock mechanics* (Else, 2008).
- [38] P. Schutjens, K. Hindriks, and M. Myers, *Depletion induced reservoir compaction: Two geomechanical models and their application in the planning of subsidence monitoring*, 42nd US Rock Mechanics Symposium and 2nd U.S.-Canada Rock Mechanics Symposium, San Francisco, June 29-July 2, 2008. (2011).
- [39] A. Rohatgi, [Webplot digitizer](#), (2016).

- [40] M. Hettema, *Design and interpretation of laboratory experiments to determine the pore volume compressibility of sandstone*, 47th US Rock Mechanics / Geomechanics symposium, San Fransisco, CA, USA, 23 - 26 June (2013).
- [41] A. Schofield and P. Wroth, *Critical state soil mechanics* (Camebridge University Press, 1968).
- [42] E. B.V., Tech. Rep.
- [43] *An experimental investigation into the compaction behaviour of core material from well B13-3 (NAM, offshore the Netherlands)*, Tech. Rep. (NAM, 1993).
- [44] B. Swanson and E. Thomas, *The measurement of petrophysical properties of unconsolidated sand cores*, The Log analyst (1980).
- [45] P. Pathak, S. Wirya, M. Catanzano, H. Prickett, and D. Mangunsong, *Impact of rock compaction of nso gas field performance*, International petroleum technology conference, Dubai, U.A.E, 4-6 December, 2007 (2007).
- [46] C. Sawabini, G. Chilingar, and D. Allen, *Compressibility of unconsolidated, arkosic oil sands*, SPE-AIME 47th Annual Dall Meeting, San Antonio, Texas, October 9-11 (1974).
- [47] L. Pauget, F. Specia, and A. Boubazine, *Reliability of laboratory porosity and pore compressibility obtained on unconsolidated deep-off shore and heavy-oil reservoirs*, SPE Aannual Technical Conference and Exhibition, San Antonio, Texas, 29 September - 2 October (2002).
- [48] H. Merle, C. Kentie, G. van Opstal, and G. Schneider, *The bachaquero study - a composite analysis of the behavior of a compaction drive/solution gas drive reservoir*, Society of Petroleum Engineers (1976).
- [49] M. Brignoli and A. Di Federico, *Compaction of unconsolidated sand and stress path effects: Laboratory evidence*, 6th North America Rock Mechanics Symposium (NARMS): Rock Mechanics Across Borders and Disciplines, Houston, Texas, June 5-9, 2004 (2004).
- [50] E. Chuhan, A. Kjeldstad, K. Bjorlykke, and K. Hoeg, *Porosity loss in sand by grain crushing - experimental evidence and relevance to reservoir quality*, Marine and Petroleum Geology **19**, 39 (2002).
- [51] I. Overeem, G. Weltje, C. Bishop-Kay, and S. Kroonenberg, *The late cenozoic eridasos delta system in the southern north sea basin: a climate signal in sediment supply?* Basin research **13**, 293 (2001).
- [52] W. Bernard, *Reserves estimation and performance prediction for geopressed gas reservoirs*, Journal of Petroleum Science and Engineering, volume 1, 15-21 (1987).
- [53] M. Geilikman and S. Wong, *Oil and gas reservoir compaction -induced production decline- influence of rock parameters*, 11th Congress of the International Society for Rock Mechanics (2007).
- [54] G. Leich, *Shallow gas reserve and rate prediction from type curve interpretation*, 6th Petroleum Conference of the South Saskatchewan section, The petroleum society of CIM, Regina, October 16-18, 1995 (1995).
- [55] X. Luo, P. Were, J. Liu, and Z. Hou, *Estimation of biot's effective stress coefficient from well logs*, Environmental Earth Science (2014).
- [56] A. Khatchikian, *Deriving reservoir pore-volume compressibility from well logs*, SPE Advanced Technology series (1995).
- [57] J. Dudley, M. Myers, R. Shew, and M. Arateh, *Measurins compaction and compressibilities in unconsolidated reservoir materials by time-scaling creep*, SPE/ISRM Rock Mechanics Conference, Delft, The Netherlands, 29-31 August (1998).
- [58] A. Huang, H. Hsu, and J. Chang, *The behavior of a compressible silty fine sand*, Canadian Geotechnical Journey **36**, 88 (1998).
- [59] G. McDowel, *On the yielding and plastic compression of sand*, Soils and Foundations **42**, 139 (2002).

-
- [60] G. Mesri and B. Vardhanabhuti, *Compression of granular materials*, Canadian Geotechnical Journey **46**, 369 (2009).
- [61] S. Salazar, *One dimensional compressibility of intermediate non plastic soil mixtures*, Ph.D. thesis, University of Arkansas (2013).
- [62] D. Sheng, Y. Yao, and J. Carter, *A volume stress model for sands under isotropic and critical stress states*, Canadian Geotechnical Journey **45**, 1639 (2008).
- [63] W. van der Knaap and A. van der Vlis, *On the cause of subsidence in oil-producing areas*, Rock Mechanics in Oijeld Geology Drilling and Production (1967).
- [64] J. Yamamuro, P. Bopp, and P. Lade, *One-dimensional compression of sands at high-pressures*, Journal of geotechnical engineering **122**, 147 (1996).